Doctoral Thesis

Lightpath Provisioning in Elastic Optical Networks

Kenta TAKEDA

Graduate School of Informatics, Kyoto University

March 2024

Preface

The rapid growth in worldwide communications and the rapid adoption of the Internet have led to a growth in the amount of communication traffic every year. An optical network can potentially support the continuously increasing demands for communications. Therefore, researchers focus on new technologies for high-speed, flexible, and scalable optical networks. Elastic optical networks (EONs) are regarded as promising techniques to achieve flexible utilization of spectrum resources in optical networks. In EONs, lightpaths are provisioned for traffic demands. In lightpath provisioning, it needs to use spectrum resources efficiently. This thesis studies three specific problems with lightpath provisioning in EONs. Each problem corresponds to lightpath failure, inter-core crosstalk (XT) and intra-core physical layer impairments (PLIs), and spectrum fragmentation due to inter-core XT, respectively.

Firstly, this thesis proposes a multipath provisioning (MPP) scheme that allows allocating the different numbers of spectrum slots and different amounts of transmission capacity to each path to minimize required spectrum resources in EONs. To minimize the required spectrum resources, two optimization problems in the proposed scheme are presented. One problem considers that the route of link-disjoint paths for a traffic demand is given, and the other determines the routes of link-disjoint paths and the number of spectrum slots allocated to each path simultaneously. The transmission capacity allocated to each path is determined by solving each optimization problem. The optimization problems are formulated as an integer linear programming (ILP) problem. Numerical results show that the proposed scheme, compared to the conventional scheme, reduces the required spectrum resources in several cases. It is also observed that the required spectrum resources can be reduced by considering the routing of link-disjoint paths in the proposed scheme at the

expense of more computation time.

Secondly, this thesis proposes a routing, modulation, spectrum, and core allocation (RMSCA) model that jointly considers inter-core XT and intra-core PLIs for spectrally-spatially EONs (SS-EONs) by considering the aspect of the optical signal to noise ratio (OSNR) penalty, which is the value of decreasing amount of OSNR due to inter-core XT. The proposed model sets multiple XT thresholds and their corresponding transmission reaches. The transmission reach corresponding to each XT threshold is set so that the optical signal deteriorated by inter-core XT and intra-core PLIs can be delivered to the destination node while maintaining the signal quality. The proposed model relaxes the XT threshold when the transmission reach becomes short as the intra-core PLIs are less due to the shorter transmission reach. On the other hand, the XT threshold becomes severe with the increasing transmission reach. Thus, the proposed model allows a small XT value for long-distance transmission and a larger XT value for shorter-distance transmission, and hence it enhances spectrum efficiency. To minimize the maximum allocated spectrum slot index, an optimization problem based on the proposed model is presented. The optimization problem is formulated as an ILP problem. A heuristic algorithm for the proposed RMSCA model is presented when the ILP problem is not tractable. The performances of the proposed model are evaluated, in terms of the maximum allocated spectrum slot index and the computation time, and compare the proposed model to a benchmark model. The numerical results show that the proposed model enhances resource utilization compared to the benchmark model.

Thirdly, this thesis proposes a fragmentation-aware lightpath provisioning model to suppress both fragmentation caused by allocating spectrum slots to lightpaths and due to inter-core XT in SS-EONs. To suppress the fragmentation due to inter-core XT, the proposed model classifies vacant spectrum slots into available vacant slots and unavailable vacant slots when calculating a metric. To suppress the fragmentation, an optimization problem is presented based on the proposed model. The optimization problem is formulated as an ILP problem. A heuristic algorithm for lightpath provisioning is presented in the case that the ILP problem is not tractable. The performances of the proposed model are evaluated in terms of the blocking probability, compared

to a benchmark model. Numerical results observed that the proposed model suppresses the blocking probability better than the benchmark model.

This thesis is organized as follows. Chapter 1 introduces the background of lightpath provisioning in EONs. Chapter 2 investigates the related works in literature. Chapter 3 presents an MPP scheme for EONs. Chapter 4 introduces a lightpath provisioning model considering inter-core XT and intra-core PLIs in SS-EONs. Chapter 5 presents a fragmentation-aware lightpath provisioning model in SS-EONs. Finally, Chapter 6 concludes this thesis.

Acknowledgements

This thesis is the summary of my doctoral study at Kyoto University, Kyoto, Japan. I am grateful to a large number of people who have helped me to accomplish this work.

First of all, I would like to express my sincere gratitude to my supervisor, Professor Eiji Oki, for his continuous support, guidance, and encouragement. I would have never completed this work without his proper assistance and essential advice. By studying under the supervision of Professor Oki, I received an invaluable experience that helped me to shape my academic and professional skills.

I owe a debt of gratitude to Associate Professor Takehiro Sato of the Graduate School of Informatics, Kyoto University, for his close comments and enthusiastic help with my studies. His kind guidance has deeply encouraged me to accomplish this work.

I would like to express my appreciation to Assistant Professor Bijoy Chand Chatterjee of the Department of Computer Science, South Asian University, for his comments and help with my papers.

I would like to thank Assistant Professor Ryuta Shiraki of the Graduate School of Informatics, Kyoto University, for his help and encouragement in my studies.

I would like to express my deep appreciation to Professor Hiroshi Harada and Professor Yasuo Okabe of the Graduate School of Informatics, Kyoto University, for their valuable advice and incisive comments. Their advice and comments have been a great help in improving this thesis.

I would like to thank Professor Ryoichi Shinkuma of the Faculty of Engineering, Shibaura Institute of Technology, for his valuable advice throughout my studies.

I am extremely grateful to Ms. Mariko Tatsumi and all members of the Oki Laboratory of the Graduate School of Informatics, Kyoto University, for their kind help in my research and life.

Finally, I would like to thank my parents, family, and Ms. Seira Matsuda. Without their understanding, constant support, and encouragement, I would have never accomplished this work.

Contents

List of Figures

List of Tables

Notations commonly used in this thesis

Notation	Description
C	Set of cores in each fiber link.
E	Set of links.
Q	Set of modulations.
T	Set of traffic demands.
V	Set of nodes.
W	Set of spectrum slot indices.
b	Required transmission capacity.
d_{ij}	Length of link (i, j).
η	Capacity of single spectrum slot [Gbps/slot].
e_{ij}	Binary variable that equals one if link (i, j) is used, and zero otherwise.
y_w	Binary variable that equals one if wth spectrum slot ($w \in W$) is used, and zero otherwise.

Abbreviations

Abbreviation	Description
ASE	Amplified spontaneous emission
BER	Bit error rate
BPSK	Binary phase-shift keying
DPP	Dedicated path protection
EDFA	Erbium-doped fiber amplifier
EON	Elastic optical network
FSA	Flexible spectrum slots allocation
LQA	Link quality assessment
MCF	Multi-core fiber
MSCA	Modulation, spectrum, and core allocation
MPP	Multipath provisioning
NPLIs	Nonlinear physical layer impairments
NPS	Number of paths selection
OSNR	Optical signal to noise ratio
PLIs	Physical layer impairments
P-XT	Precise inter-core crosstalk
QAM	Quadrature amplitude modulation
QPSK	Quadrature phase-shift keying
RFSA	Routing and flexible spectrum slots allocation
RMSCA	Routing, modulation, spectrum, and core allocation
RMSF	Root mean square factor
RSA	Routing and spectrum allocation
RSCA	Routing, spectrum, and core allocation

Abbreviation	Description
SACA	Same amount of transmission capacity allocation
SBPP	Shared backup path protection
Sch	Super channel
SDM	Space-division multiplexing
SNR	Signal to noise ratio
SNSA	Same number of spectrum slots allocation
SOFM	Self-organizing feature mapping
SPP	Single-path provisioning
SS-EON	Spectrally-spatially EON
XT	Crosstalk
WC-XT	Worst case inter-core crosstalk

Chapter 1

Introduction

1.1 Elastic optical networks (EONs)

The rapid growth in worldwide communications and the rapid adoption of the Internet have led to a growth in the amount of communication traffic every year. An optical network has the potential to support the continuously increasing demands for communications. Therefore, researchers are focusing on new technologies for high-speed, flexible, and scalable optical networks.

Elastic optical networks (EONs) are regarded as promising techniques to achieve flexible utilization of spectrum resources in optical networks. The advances in photonic technologies, such as optical multilevel modulation, optical orthogonal frequency-division multiplexing, and the seamless bandwidth-variable wavelength selective switch make EONs possible to treat spectrum resources as spectrum slots. EONs increase the spectrum efficiency through rate-adaptive super channels (Schs) and distance-adaptive modulation in optical networks [1, 2]. EONs adaptively allocate the minimum necessary number of spectrum slots to a lightpath based on its end-to-end physical conditions. Routing and spectrum allocation (RSA) is one of the challenging issues in EONs, which finds an appropriate route for a lightpath request and allocates suitable spectrum slots to it while satisfying the spectrum contiguity and continuity constraints [3]. The spectrum contiguity constraint imposes that spectrum slots must be allocated to a lightpath spectrally contiguous. The spectrum continuity constraint imposes that the same spectrum slot must be used

along an end-to-end lightpath.

In optical networks, physical layer impairments (PLIs) are the major obstacle, which deteriorate the optical signal, and PLIs increase with the transmission distance [4, 5]. EONs adopt distance-adaptive spectrum allocation that uses an appropriate modulation format considering the path length to enhance spectrum efficiency. Using a more spectrum-efficient modulation format reduces the number of allocated spectrum slots for shorter paths. The transmission reach also differs among modulation formats as the tolerance for signal degradation of each modulation format is different.

1.1.1 Lightpath failure

Since EONs can configure optical paths with flexible transmission capacity, EONs will be used to support various network services. Some types of services, such as bank transactions and securities trading, require high reliability. Therefore, lightpath failures caused by failures of a network component, such as an optical fiber or a network node, can disrupt communications for a lot of users, which can lead to a great loss of revenue. Thus, survivability against failures has become an essential requirement of EONs [3].

Protection is one of the strategies to improve the survivability of EONs. Klinkowski et al. [6] presented 1+1 path protection in EONs. The 1+1 path protection protects one primary path with one backup path which is disjoint from the primary path. If the primary path fails, the backup path transmits the traffic instead of the failed primary path.

The 1+1 path protection is a special case of the single-path provisioning (SPP) scheme. The SPP protects one primary path with one or more backup paths. In the SPP, it is ensured that the traffic tolerates with path failures up to the number of backup paths [7].

Multipath provisioning (MPP) uses multiple disjoint paths for data transmission to tolerate network failures. Ruan et al. [8] presented that the MPP achieves higher spectral efficiency than the SPP. In the SPP, paths are categorized into a primary path and backup paths. In contrast, in the MPP, there is no distinction between a primary path and backup paths. This means that all paths are always used for data transmission. How the MPP scheme

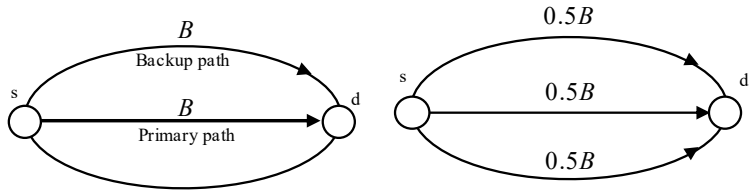

(a) SPP. (b) MPP.

Figure 1.1: Spectrum requirement with SPP and with MPP. (©2021 Elsevier.)

reduces the required spectrum resources compared to the SPP is presented by using Fig. 1.1. Consider a traffic demand between the source and destination nodes which requires spectrum of $\boldsymbol{B}$ and protection against a single failure, i.e., spectrum of $\boldsymbol{B}$ is ensured even if any one path fails. In the SPP, the number of backup paths is set to the number of tolerable failures. Therefore, both number of primary path and backup path are one. Spectrum of $\boldsymbol{B}$ is allocated to each path, as shown in Fig. 1.1a, so the total spectrum requirement is $2\boldsymbol{B}$. On the other hand, in the MPP, multiple paths are used for the transmission. If one of the paths fails, the other paths transmit the traffic that was allocated to the failed path in addition to the traffic that the paths transmit from the beginning. When three paths are used between the source and destination nodes, spectrum of $0.5\boldsymbol{B}$ is allocated for each of the three paths, as shown in Fig. 1.1b, so the total spectrum requirement is $1.5\boldsymbol{B}$. If any one path fails, spectrum $\boldsymbol{B}$ is ensured by the other two paths. Therefore, the MPP scheme reduces the required spectrum resources compared to the SPP. Note that, in this comparison, the probability of a path failure is assumed to be a sufficiently small value, namely p. The probability that two paths fail at the same time is derived by order of p^2, which is a negligible value. Since the probability of multiple failures is negligible, the disadvantage of the MPP by using more paths than the SPP is negligible in this comparison.

The MPP also has been studied in non-optical networks to provide protection. The traffic demand between a source and destination pair is equally divided and sent on each disjoint path to minimize the bandwidth utilization [9, 10].

Yin et al. [11] presented an MPP scheme robust against multiple failures

in an EON. It assumes partial protection, which protects traffic partially under failures. The traffic demands are assumed to be given as the number of spectrum slots. In this assumption, allocating the same number of spectrum slots to each path minimizes the required number of spectrum slots. The work in [11] determines the number of paths and the number of spectrum slots allocated to each path for a traffic demand so as to minimize the total number of spectrum slots required to tolerate a given number of failures.

A modulation-adaptive path selection model for 1+1 protection in EONs was presented in [12]. The model in [12] determines the route of link-disjoint paths so that the total number of required spectrum resources is minimized. Since the model aims to provide 1+1 protection in EONs, the same amount of transmission capacity is allocated to each path. The number of required spectrum slots allocated to each path is determined by the assigned modulation format of each path. Modulation formats applicable to each path depend on the distance of the path.

1.1.2 Spectrum fragmentation

Spectrum fragmentation can cause spectrum utilization inefficiency and increase blocking; it is a major issue in EONs [13]. Vacant spectrum slots that are contiguous in the spectrum are called vacant segments as shown in Fig. 1.2. When the size of vacant segments is less than the required number of slots for a lightpath, the vacant segments cannot satisfy the lightpath request due to the spectrum contiguous constraint; the vacant segments are called the fragmented segments. The fragmented segments may be generated as lightpaths are provisioned and released in a network. Since the fragmented segments lead to inefficient utilization of spectrum resources, they need to be suppressed.

To measure fragmentation, various metrics are introduced [14, 15]. External fragmentation metric [14] can be used to measure fragmentation in each link, which is calculated by the maximum size of the vacant segment and the number of vacant slots in the link. The disadvantage of external fragmentation metric is that it ignores a small vacant segment. Entropy-based fragmentation metric [15] also can be used to measure the fragmentation in each link, which is calculated by the number of slots and the size of each vacant segment.

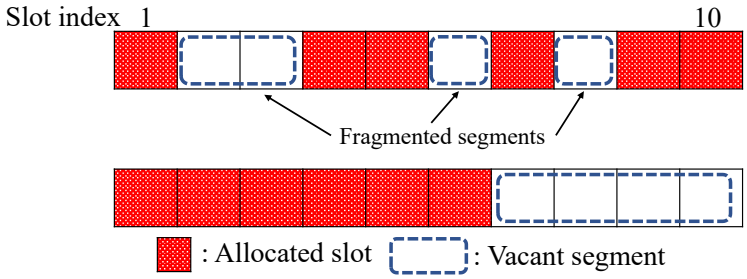

Figure 1.2: Illustration of allocated slots, vacant segments, and fragmented segments in a link.

Entropy-based fragmentation metric can estimate relative fragmentation and allows comparisons of different slot allocations.

Using a fragmentation metric during RSA is one of the approaches to suppress the fragmentation. Wright et al. [16] uses entropy-based fragmentation metric to suppress the fragmentation when RSA is determined. During RSA, the fragmentation metric is minimized.

1.2 Spectrally-spatially EONs (SS-EONs)

To enhance a fiber capacity, multi-core fiber (MCF) is typically used, which is one of the space-division multiplexing (SDM) technologies [17]. In data centers and submarine cables, large-capacity data transmission needs to be achieved in small spaces, and hence the demand for MCF is growing. The incorporation of SDM technologies with EONs is called spectrally-spatially EONs (SS-EONs).

1.2.1 Inter-core crosstalk (XT)

In MCFs, there exist two types of PLIs, which are intra-core PLIs and inter-core crosstalk (XT); intra-core PLIs and inter-core XT are produced within a core and between cores, respectively [18, 19]. Inter-core XT is one of the PLIs that occur in MCFs. When signals are transmitted in the same direction and use the same spectrum slots in two neighboring fiber cores, inter-core XT occurs and degrades the signal quality [20].

In SS-EONs with MCF, the core allocation needs to be considered in addition to RSA; this is called the routing, spectrum, and core allocation (RSCA) problem [21, 22]. RSCA is more complicated than RSA due to the inter-core XT. Moreover, as the different modulation formats have different XT tolerance limits [23], the relationship between inter-core XT and modulation formats needs to be investigated. When modulation formats are considered in RSCA, it is called the routing, modulation, spectrum, and core allocation (RMSCA) problem [24].

In SS-EONs, several researches have been conducted to investigate the impact of XT-aware spectrum allocation [18, 22, 25]. In these works, lightpaths are allocated in such a way that the estimated XT value must be smaller than the given threshold. The approach, which allocates spectrum slots to a lightpath so that the estimated XT value must be smaller than the given threshold, is called the XT-estimated approach. The coupled-power theory is used to estimate the XT value [26]. The XT value is calculated by a simplified linear model:

$$XT \simeq NhL, \tag{1.1}$$

where N denotes the number of adjacent cores that utilize the same spectrum slot, L denotes the MCF length, and h denotes the power-coupling coefficient. The difference between the estimated values of XT calculated by (1.1) and the strict model in [26] is negligible. The inter-core XT value of a lightpath remains consistent irrespective of the modulation format employed.

There are two ways to estimate the XT value of a lightpath. One assumes that, even if a pair of lightpaths uses the same spectrum in an adjacent core pair in only a part of the path, the XT occurs along the end-to-end path. The XT estimated in this way is called worst-case XT (WC-XT). The WC-XT value of a lightpath in a specific spectrum slot depends on the number of adjacent cores in which the spectrum slot is used by other lightpaths sharing a link. The number of such adjacent cores is called the *lightpath-adjacent number* in this thesis. The WC-XT value of lightpath p in the wth spectrum slot is calculated by:

$$WC\text{-}XT(p, w) \simeq N_w hL'(p), \tag{1.2}$$

where N_w denotes the lightpath-adjacent number in the wth spectrum slot, and $L'(p)$ denotes the end-to-end transmission distance of lightpath p. The other way to estimate the XT value takes into account links and their distances where the lightpath is adjacent to the other lightpaths. The XT estimated in this way is called precise XT (P-XT). According to [27], the end-to-end path XT is the sum of the XT on consecutive links of the path. $P\text{-}XT(p,w)$, which is the P-XT value of lightpath p on spectrum slot w, can be estimated by:

$$P\text{-}XT(p,w) = \sum_{e \in \pi(p)} N(p,e,w) h L_e, \tag{1.3}$$

where $\pi(p)$ is the set of links of p, $N(p,e,w)$ is the number of active cores adjacent to the core used by p on e and w, h is the power-coupling coefficient of the MCF, and L_e is the length of e. Different from the WC-XT value, the P-XT value is not proportional to the end-to-end transmission distance of a lightpath. When the estimated XT value does not exceed the XT threshold of a modulation format, the modulation format can be used in the lightpath. In the XT-estimated approach, a vacant spectrum slot is considered unavailable if allocating it to a new lightpath violates the XT threshold of at least one existing lightpath. In other words, some vacant spectrum slots cannot be allocated to a lightpath due to inter-core XT; these slots are named *unavailable vacant slots* in this thesis. The vacant slots that are used for lightpath allocation are named *available vacant slots*.

The work in [18] introduced a model that considers P-XT and PLIs jointly in SS-EONs. It calculates the signal to noise ratio (SNR) of a lightpath by adding P-XT to intra-core PLIs and assigns lightpaths in such a way that the estimated SNR must be greater than the required SNR. For the sake of simplicity, the work in [18] avoids spectrum contiguity constraints, and hence the model introduced in this work is not suitable for RSCA.

Considering P-XT and intra-core PLIs effects for a lightpath, Klinkowski et al. [25] presented an RMSCA model, where intra-core PLIs are considered by configuring the transmission reach. Without accounting for the XT effect, they calculated the transmission reach. The model assigns spectrum slots such that the P-XT value does not cross the threshold, and the length of the path must be smaller than the transmission reach, which means that the work in [25] does not jointly consider inter-core XT and intra-core PLIs.

1.2.2 Spectrum fragmentation

Spectrum fragmentation needs to be suppressed in SS-EONs. Some works [28–35] use a fragmentation metric to suppress the fragmentation. Lechowicz et al. [28] presented a fragmentation-aware lightpath provisioning model. This model introduces a fragmentation metric, which indicates the degree of fragmentation occurring in the network, and allocates spectrum slots to a lightpath to reduce the fragmentation metric. In work [28], inter-core XT is not considered for the sake of simplicity, but the model can be extended to include a XT estimated approach. When a XT estimated approach is included, the XT threshold is set to guarantee signal quality; lightpaths are provisioned by satisfying the XT threshold. When a lightpath is provisioned, the fragmentation metric is calculated for each candidate path, and the path is selected whose fragmentation metric is the lowest.

1.3 Problem statements

This thesis studies three specific problems with lightpath provisioning in EONs. Each problem corresponds to lightpath failure, inter-core XT and intra-core PLIs, and spectrum fragmentation due to inter-core XT, respectively.

1.3.1 Lightpath failure in EONs

There are two issues to address when applying the MPP to tolerate network failures in an EON. The first issue is that, if spectrum slots are allocated equally to each path as is the case with [11], the transmission capacity of each path can be different due to the difference in modulation format; a short-distance path has large transmission capacity but a long-distance path has small transmission capacity. The transmission capacity becomes small when the shorter path fails. As a result, more spectrum slots must be allocated to each path to guarantee certain transmission capacity in case of network failure. The second issue is that, if the same amount of transmission capacity is allocated to each path as is the case with [12], the same amount of traffic capacity is ensured when any path fails. However, since the relationship between the number of slots

and the amount of transmission capacity is nonlinear, the required number of spectrum slots is not always minimized[1].

Several works on MPP in EONs [8, 11, 36, 37] have been presented, where every MPP allocates the same number of spectrum slots or the same amount of transmission capacity. Therefore, the existing works on MPP in EONs do not always minimize the required spectrum resources. The waste of spectrum resources restricts the number of traffic demands accommodated in a network since the total amount of spectrum resources in a network is limited. A question arises: how can we allocate the spectrum slots to each path in MPP to minimize the required spectrum resources.

1.3.2 Inter-core crosstalk and intra-core physical layer impairments in SS-EONs

If inter-core XT and intra-core PLIs are independently considered, the following problems emerge. Suppose that the XT effect is not considered during the deliberation of the transmission reach. In this case, an established lightpath in the network cannot achieve the transmission reach due to the XT effect. The spectrum inefficiency occurs when a margin of the transmission reach is generated to realize the lightpath with the XT effect. Therefore, in RMSCA, the degradation due to inter-core XT and intra-core PLIs must be treated jointly.

However, there has been no work, which performs RMSCA considering both P-XT and intra-core PLIs jointly. A question arises: how can we deal with P-XT and intra-core PLIs jointly in RMSCA to improve spectrum efficiency?

1.3.3 Spectrum fragmentation due to inter-core crosstalk in SS-EONs

The conventional fragmentation-aware model introducing the XT-estimated approach calculates the fragmentation metric by distinguishing spectrum slots

[1]In case that the number of disjoint paths is only two, setting the same amount of traffic capacity for each path leads to minimizing the required number of spectrum slots. However, in case that the number of disjoint paths is more than two in MPP, this does not always lead to minimizing it.

as vacant or not [28]. Even though vacant slots are contiguous, the available vacant slots are fragmented if available vacant and unavailable vacant slots are intermingled in the contiguous vacant slots. The fragmented available vacant slots can cause to fail to accept a lightpath request, which requires more slots than the fragmented available vacant slots. In addition to allocating spectrum slots to lightpaths, the occurrence of inter-core XT can cause fragmentation. The conventional fragmentation-aware model only suppresses fragmentation without the separation of available vacant and unavailable vacant slots. If the fragmentation is suppressed without separating available vacant and unavailable vacant slots, the fragmented available vacant slots can be increased in the network. The fragmentation caused by intermingling available and unavailable vacant slots is called *fragmentation due to inter-core XT*. The fragmentation due to inter-core XT also leads to inefficient utilization of spectrum resources; it is required to suppress fragmented available vacant slots.

However, no fragmentation-aware work with fragmentation metric considers fragmentation due to inter-core XT, i.e., no work calculates the metric with considering intermingled available vacant slots and unavailable vacant slots. A question arises; how can we suppress the fragmentation due to inter-core XT to increase spectrum utilization efficiency when provisioning lightpaths?

1.4 Overview and contributions of this thesis

Figures 1.3 shows the overview of this thesis. Chapter 2 surveys the related works in literature.

Chapter 3 proposes an MPP scheme that allows allocating the different numbers of spectrum slots and different amounts of transmission capacity to each path in order to minimize required spectrum resources in EONs. Two optimization problems in the proposed scheme are presented. One problem considers that the route of link-disjoint paths for a traffic demand is given, and the other determines the routes of link-disjoint paths and the number of spectrum slots allocated to each path simultaneously. The amount of transmission capacity allocated to each path is determined by solving each optimization problem. The optimization problems are formulated as an integer linear programming (ILP) problem. Numerical results show that the proposed scheme,

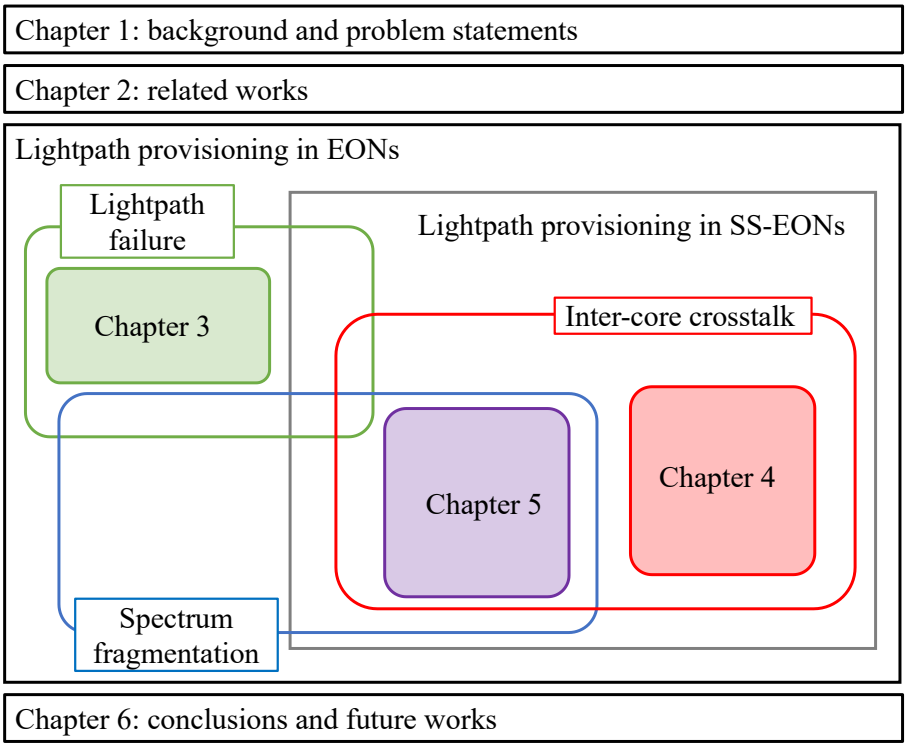

Figure 1.3: Chapter overview of this thesis.

compared to the conventional scheme, reduces the required spectrum resources in several cases. It is also observed that the required spectrum resources can be reduced by considering the routing of link-disjoint paths in the proposed scheme at the expense of more computation time.

Chapter 4 proposes an RMSCA model that jointly considers inter-core XT and intra-core PLIs for SS-EONs by considering the aspect of the optical SNR (OSNR) penalty, which is the value of decreasing amount of OSNR due to inter-core XT. Multiple XT thresholds and their corresponding transmission reaches are set by the proposed model. The transmission reach corresponding to each XT threshold is set in such a way that the optical signal deteriorated by inter-core XT and intra-core PLIs can be delivered to the destination node while maintaining the signal quality. The proposed model relaxes the XT threshold when the transmission reach becomes short as the intra-core PLIs are less due to the shorter transmission reach. On the other hand, the XT threshold becomes severe with the increasing transmission reach. Thus, the

proposed model allows a small XT value for long-distance transmission and a larger XT value for shorter distance transmission, and hence it enhances spectrum efficiency. To minimize the maximum allocated spectrum slot index, an optimization problem, which is based on the proposed model, is presented. The optimization problem is formulated as an ILP problem. A heuristic algorithm for the proposed RMSCA model is presented when the ILP problem is not tractable. The performances of the proposed model are evaluated, in terms of the maximum allocated spectrum slot index and the computation time, and the proposed model is compared with a benchmark model. Numerical results show that the proposed model enhances resource utilization compared to the benchmark model.

Chapter 5 proposes a fragmentation-aware lightpath provisioning model to address the question described in Section 1.3.3 by introducing fragmentation due to inter-core XT. The proposed model suppresses both fragmentation caused by allocating spectrum slots to lightpaths and due to inter-core XT. In order to suppress the fragmentation due to inter-core XT, the proposed model classifies vacant spectrum slots into available vacant slots and unavailable vacant slots when calculating a metric. Based on the proposed model, an optimization problem is presented. The optimization problem is formulated as an ILP problem. The performances of the proposed model are evaluated in terms of the blocking probability, compared to a benchmark model.

Finally, Chapter 6 concludes this thesis and discusses the future works to extend this work.

Chapter 2

Related works

2.1 Protection studies for lightpath failure in EONs

There are two protection schemes in EONs, which are the SPP scheme and the MPP scheme. The difference between them is whether there is a distinction between a primary path and backup paths. The SPP protects one primary path with one or more backup paths. In the MPP, there is no distinction between a primary path and backup paths; all paths are used for data transmission.

The SPP protection is divided into the dedicated path protection (DPP) and the shared backup path protection (SBPP) [38]. The main difference between DPP and SBPP follows from whether spectrum resources are allowed to be shared between backup paths belonging to different demands [39]. Backup paths in DPP have their own dedicated spectrum resources. On the other hand, backup paths in SBPP have spectrum resources that can be shared between backup paths belonging to different demands. Only one demand can use these resources in a specific failure scenario. In the SPP, apart from provisioning a primary path for each traffic demand, backup paths are precalculated.

A number of studies worked on the SPP protection in EONs. Klinkowski [6] studied the routing and spectrum allocation problem in EONs for 1+1 dedicated path protection, which is one of the DPP techniques that tolerate a single failure scenario. Sone et al. [40] presented an architecture and control framework for 1+1 dedicated path protection in EONs. Walkowiak et al. [41] and

Shen et al. [42] presented optimization models for the SBPP in EONs which consider a single link failure. Wang et al. [43] tackles the routing and spectrum allocation problem for the SBPP in EONs in a dynamic scenario. The SBPP techniques [41–43] can share backup capacity among different protection paths as long as their corresponding primary paths do not fail simultaneously.

Compared with the SPP, the MPP achieves higher spectral efficiency to achieve protection. Ruan et al. [8,36] presented MPP schemes in EONs for both static and dynamic traffic demand scenarios. Chen et al. [37] presented protection schemes for dynamic MPP to ensure 100% restoration against single-link failures. Yin et al. [11] adopted an idea of SBPP in the MPP and presented a robust MPP scheme against multiple failures in an EON. These works assume traffic demand as a number of spectrum slots, so spectrum slot allocations of these works do not minimize the required spectrum slots for the traffic demand given by transmission capacity.

Additionally, a bandwidth squeezing technique, first presented by Jinno et al. [44], can be applied to both the SPP scheme and the MPP scheme. The bandwidth squeezing technique is one of the unique features of an EON. If the available bandwidth to recover the paths is not sufficient for the original bandwidth under failures, the bandwidth of the failed working path is squeezed in order to ensure minimum connectivity. The bandwidth squeezing technique has the feature of enhancing network connectivity and availability by partially but maximally recovering the bandwidth [38]. The idea of the bandwidth squeezing technique is adopted in [8, 11, 36, 40]. The work in Chapter 3 also adopts the bandwidth squeezing technique as the partial protection.

The MPP is studied not only for EONs but also for other communication networks. Singh et al. [45] presented multipath provisioning techniques operating at different layers of the Internet in their survey paper. The survivable MPP problem with a differential delay constraint is studied in [46, 47]. The optimization model presented in Chapter 3 can be extended to deal with a differential delay constraint by adding constraints of the distance difference of each link-disjoint path.

2.2 Inter-core XT aware studies in SS-EONs

There exist several studies to deal with inter-core XT in SDM-EONs. In order to deal with inter-core XT, the structure of MCFs has been studied. The core arrangement that suppresses inter-core XT and enhances transmission capacity is preferred. The most prominent structure of MCFs is the hexagonal close-packed structure [17]. Examples of the hexagonal structure with 7 cores [26,48] and 19 cores [49] have been demonstrated and used in experiments.

Alternatively, there have been studies that deal with inter-core XT from the networking aspect. The studies can be classified into two approaches.

The first approach [50–52] allocates spectrum slots to prevent occurrence of inter-core XT without estimating a XT value when each lightpath is provisioned. Fujii et al. [50] presented an RSCA model that does not allocate the same spectrum to different demands that traverse through adjacent cores so that inter-core XT can be negligible. When the model in [50] is adopted, some spectrum slots are not utilized, which leads to low spectrum efficiency. Tode et al. [51] presented an RSCA model, which reduces inter-core XT by avoiding the assignment of the same spectrum to lightpaths in adjacent cores as much as possible. The cores in MCF are weighted so that adjacent cores have a low priority in the allocation for lightpath demands. This model may cause unacceptable XT when adjacent cores become inevitably used as the traffic demands increase. Savva et al. [52] presented an algorithm to solve an RSCA problem, which does not allocate the same spectrum to the adjacent cores. In the algorithm [52], in order to account for intra-core PLIs, a quality of transmission (QoT) estimator tool is used to evaluate all paths. The algorithm initially allocates resources to lightpaths by using a heuristic approach. If there are lightpaths that do not satisfy the required QoT, they are considered blocked. The algorithm repeatedly tries to reallocate the blocked lightpaths until all lightpaths satisfy the QoT.

The second approach estimates the XT value when a lightpath is provisioned. The second approach estimates the XT value, from which a lightpath suffers, and allocates spectrum slots to a lightpath so that the estimated XT value does not exceed a given threshold [18,21,22,24,25,53]. The work in Chapter 4 is classified in this approach. The XT estimation can be categorized into

two ways: worst-case inter-core XT (WC-XT) and P-XT.

The works in [21, 24, 53] consider WC-XT in RSCA. Muhammad et al. [21] presented an RSCA model, which calculates the WC-XT value by using an analytical model based on the coupled-power theory presented in [26]. According to [26], the XT value depends on the number of adjacent cores and the adjacent length of lightpaths. The model in [21] calculates the XT value by assuming that, even if the core used by a lightpath is adjacent to other active cores in only a part of the path, the core is adjacent to the active cores along the end-to-end path. In [21], the RSCA problem is formulated as an ILP problem. Oliveria et al. [24] presented an RMSCA model which estimates the WC-XT value by employing simulation experiments. The model in [24] sets a XT threshold for each modulation format. The transmission reach for each modulation format in [24] is set without considering inter-core XT. Walkowiak et al. [53] presented a transmission reach model that accounts for both WC-XT, which is calculated for the most impacted fiber core, and linear and non-linear intra-core PLIs. One of the causes of signal degradation is the amplified spontaneous emission (ASE) noise, which is generated by optical amplifiers, such as erbium-doped fiber amplifiers (EDFAs). The ASE noise is considered as a linear impairment for the following reason. The value of the ASE noise depends on the number of amplifiers in a lightpath. Since one amplifier is required per span in a fiber, i.e., the number of amplifiers is in proportion to the fiber length, the value of the ASE noise of a lightpath is in proportion to the transmission distance of the lightpath. In addition to the ASE noise, nonlinear physical layer impairments (NPLIs), such as interference among different signals transmitted in the same core, degrade the signals. The transmission reach without XT is set considering the ASE noise and NPLIs. Since the value of WC-XT depends on the transmission distance, a XT threshold can be translated to XT-related transmission reach. The transmission reach in [53] is set by taking the lower of the XT-related transmission reach and transmission reach without XT. Using WC-XT leads to an overestimation of inter-core XT. The work in Chapter 4 estimates P-XT.

The works in [22,25] consider P-XT. The P-XT value is estimated by taking into account links and their distances where the core used by the lightpath is adjacent to the other active cores. The P-XT value is more accurate than

the WC-XT value. Different from the WC-XT value, the P-XT value is not proportional to the end-to-end transmission distance of a lightpath. The RSCA model in [22] does not take account of intra-core PLIs. The RMSCA model in [25] takes account of intra-core PLIs, but inter-core XT and intra-core PLIs are dealt with separately. The work in Chapter 4 jointly considers P-XT and intra-core PLIs in the RMSCA problem.

P-XT and intra-core PLIs can be jointly considered from the viewpoint of SNR in SS-EONs. The model in [18] calculates the SNR of a lightpath by adding P-XT to intra-core PLIs, and provisions lightpaths to ensure the required SNR value. The intra-core PLI values are estimated by using the model in [54]. As mentioned in Section 1.2.1, the model in [18] is not directly applicable to solving the RSCA problem. This is because, in order to reduce the complexity of the formulation, the model in [18] allocates each spectrum slot independently but does not consider each lightpath request. In short, the spectrum contiguity constraint is not considered because of the complexity of the SNR calculation. The contiguity constraint needs to be considered in the RSA problem. SNR can be translated to OSNR [55]; when SNR decreases by a dB, OSNR also decreases by a dB. P-XT and intra-core PLIs can be jointly considered from the viewpoint of OSNR. In Chapter 4, P-XT and intra-core PLIs are jointly considered by transforming P-XT to the OSNR penalty and setting transmission reach corresponding to the OSNR penalty.

2.3 Inter-core XT and fragmentation aware studies in SS-EONs

To suppress the fragmentation in SS-EONs, several studies are presented [28–35, 56–59]. As described in Section 2.2, there are two approaches to deal with inter-core XT: XT-avoided approach [29, 30, 56, 57] and XT-estimated approach [28, 31–34, 58, 59].

There exist several studies to suppress the fragmentation with the XT-avoided approach [29, 30, 56, 57]. Trindade et al. [29, 57] introduced proactive algorithms to handle fragmentation. In [29], cores are prioritized to suppress XT in a way that non-adjacent cores are allocated whenever possible. A metric

combining the path fragmentation ratio and the closeness centrality is defined for lightpath provisioning. In [57], the spectrum resources are divided into sections, called quadrants, and each quadrant comprises non-adjacent cores and a set of their slots. The cores of a quadrant follow a prioritization criterion which defines an order for allocation that generates the least possible XT. By introducing the quadrants, the process of allocating and de-allocating slots can be localized in a quadrant, and it leads to suppression of fragmentation in other quadrants. Beyragh et al. [56] classify cores in MCF into enabled and disabled cores. Only the spectrum slots in the enabled cores are available for a lightpath. The cores adjacent to the enabled cores are regarded as disabled cores to avoid occurring inter-core XT. After the classification, inter-core XT does not need to be considered. Spectrum slots are allocated to a lightpath so as to reduce the fragmentation metric. Yousefi et al. [30] introduced a XT metric and a fragmentation metric to suppress inter-core XT and fragmentation. Using the two metrics, three algorithms are presented. One chooses the core whose XT metric is minimum and allocates slots to minimize the fragmentation metric. The second one chooses the core whose fragmentation metric is minimum and allocates slots to minimize the XT metric. The last one combines the former two algorithms, and it is observed that the last one achieves lower blocking probability than the other ones in their simulation.

There exist several studies to suppress the fragmentation with the XT-estimated approach [28, 31–34, 58, 59]. Lechowicz et al. [28] introduced a fragmentation-aware RSCA algorithm with introducing the concept of bordering SChs. The bordering SChs are the SChs whose spectrum is at the border of already-allocated spectrum slots. In [28], several fragmentation metrics were introduced. The fragmentation metrics are designed so that various indicators are taken into account, such as the number and size of free segments, the highest slot index, and the number of SChs. Lightpaths are provisioned to minimize a selected fragmentation metric. In the work [28], inter-core XT is not considered for the sake of simplicity, but the models can be extended to include the XT estimation. Comellas et al. [58] introduced spectral partitioning that isolates the different traffic types by allocating different spectral resource partitions. The traffic requests are categorized by the amount of their transmission capacity. Although the work [58] does not consider inter-core XT,

the model can be expanded so that it can consider the inter-core XT by using a XT-aware transmission reach estimation model presented in [60]. The works [31,32] introduced metrics incorporating three domains, i.e., the spatial, frequency, and time domains. Zhang et al. [31] presented a model that determines RSCA to minimize the metric, in which the XT threshold is satisfied. Chen et al. [32] introduced a metric based on three domains whose object is suppressing inter-core XT and fragmentation. The metric combines a XT metric and a fragmentation metric. Lightpaths are provisioned by satisfying the XT threshold and minimizing the metric. Jafari-Beyrami et al. [33] presented an RSCA algorithm that uses a fragmentation metric, multi-path routing, and XT estimation in combination. Multi-path routing divides a traffic demand into several sub-demands and assigns the sub-demands to several paths. When a traffic demand is not accommodated by a single path, a multi-path strategy is applied. The works [34, 59] used machine learning in RSCA. Yao et al. [59] introduced an unsupervised association rule mining algorithm to grab the correlation between the inter-core XT and fragmentation. Association rule mining is a rule-based machine learning algorithm that can find a relationship in large database to distinguish strong rules. In the RSCA, the association rule mining algorithm is used. The model in [59] considers different service levels and selects vacant slots classified into different association rules. Yang et al. [34] presented a link quality assessment (LQA) method based on self-organizing feature mapping (SOFM) model. SOFM can learn the distribution of input samples and also recognize the topology of input vectors. Based on LQA, RSCA of lightpaths is determined. In LQA, multiple dimensions are considered, which includes a fragmentation metric.

Using a fragmentation metric when the RSCA of a lightpath is determined is a way to suppress the fragmentation. Several works use a fragmentation metric to suppress the fragmentation [28–35]. The metrics used in [29–35] are path fragmentation metrics, which evaluates the fragmentation in links along a path. The metrics in [28] are network fragmentation metrics, which evaluate the fragmentation in the whole network. To calculate the metrics in [29–32, 34, 35], vacant segments are classified into fragmented segments and non-fragmented segments; they are classified by whether they can accommodate a lightpath request. To classify the vacant segments, it is needed to know

the number of required slots for a lightpath request. When a new lightpath is provisioned adjacent to an existing lightpath, vacant slots adjacent to the slots allocated to the existing lightpath may become unavailable. In that case, unavailable vacant slots are generated in both links along the new lightpath and the existing lightpath. Since these unavailable slots need to be considered, a network fragmentation metric presented in [28] is used in Chapter 4.

The model proposed in Chapter 5 suppresses the fragmentation with the XT-estimated approach. A fragmentation metric is introduced and lightpath is provisioned to minimize the metric. The difference between the proposed model and existing works is whether fragmentation due to inter-core XT is considered. The proposed model classifies vacant slots into available ones and unavailable ones when calculating the metric, which is different from existing works that use a fragmentation metric that does not reflect fragmentation due to inter-core XT.

Chapter 3

Multipath provisioning scheme tolerant to lightpath failure to minimize required spectrum resources in EONs

3.1 Proposed scheme

The proposed MPP scheme allows allocating the different numbers of spectrum slots and different amounts of transmission capacity to each path in order to minimize required spectrum resources in EONs. How to allocate the spectrum slots to each path in the proposed scheme is described as follows. Assume a single traffic demand between a source node and a destination node. An EON in which network nodes switch optical paths in an all-optical manner is considered. The traffic demand is composed of transmission capacity requirement b [Gbps], tolerable number of failures M, and the partial protection requirement ρ. $\rho = 0$ indicates no protection and $\rho = 1$ indicates full protection. When $0 < \rho < 1$, ρ is the rate of traffic to be protected. The situation of no protection is not considered, so the range of ρ is $0 < \rho \leq 1$. The source and destination pair has $|K|$ link-disjoint paths. Since node failure has a high impact on the network, network nodes are designed to have high reliability. Therefore, this thesis focuses on lightpath failure due to link failure. To sur-

Table 3.1: Capacity of single spectrum slot and maximum transmission reach of each modulation format assumed in Chapter 3. (©2021 Elsevier.)

Modulation format	Reach [km]	Capacity of single slot [Gbps]
BPSK	4000	12.5
QPSK	2000	25
8QAM	1000	37.5
16QAM	500	50
32QAM	250	62.5

vive against link failure, link-disjoint paths are used. If we also consider node failure, node-disjoint paths should be used.

The following notations are used. B_k is the number of spectrum slots allocated to path $k \in K$ for the traffic demand. b_k is the amount of the transmission capacity allocated to path k. h_k is the number of hops of path k. η_k represents the capacity of a single spectrum slot in path k. The modulation format that can be applied to each path is limited according to the distance of each path. η_k is decided by choosing the modulation format which is available for path k and provides the largest capacity per spectrum slot. In this chapter, the available modulation formats are assumed to be binary phase-shift keying (BPSK), quadrature PSK (QPSK), 8 quadrature amplitude modulation (8QAM), and 16QAM. Table 3.1 shows the relation between the capacity of a single spectrum slot and the maximum transmission reach of each modulation format assumed in this chapter. The assumption is based on the half-distance law [61]. The bandwidth of one spectrum slot is assumed to be 12.5 GHz. g represents the number of spectrum slots for guard bands required on each path.

In the following, an intuitive example of spectrum slot allocation using Fig. 3.1 is presented to show how the proposed scheme reduces the required spectrum resources compared to the conventional scheme. In this example, the traffic demand between a source and destination pair is set to $b = 400$ [Gbps], $\rho = 0.9$, and $M = 1$. Guard bands are not considered in this example, i.e., $g = 0$. Three disjoint paths, namely $k = 1$, 2, and 3, are configured between the source node and the destination node. The number of hops of each path is set to one, i.e., $h_1 = h_2 = h_3 = 1$. The capacity of a single spectrum slot

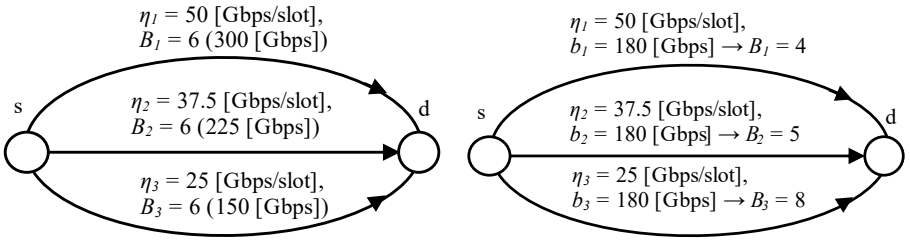

(a) Case 1 (allocating same number of spectrum slots to each path).

(b) Case 2 (allocating same amount of transmission capacity to each path).

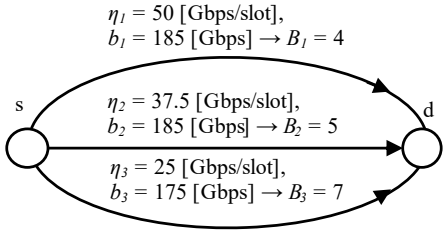

(c) Case 3 (allocating spectrum slots and transmission capacity flexibly).

Figure 3.1: Intuitive example of spectrum slot allocation of proposed and benchmark models. (©2021 Elsevier.)

of each path is set to $\eta_1 = 50$ [Gbps/slot], $\eta_2 = 37.5$ [Gbps/slot], and $\eta_3 = 25$ [Gbps/slot].

At first, the case where the conventional scheme is considered. The conventional scheme allocates the same number of spectrum slots to each path. In order to allocate the same number of spectrum slots, the number of allocated spectrum slots is set to each path to one at first and increase the number one by one until satisfying the traffic demand. Fig. 3.1(a) shows the configuration where the same number of spectrum slots is allocated to each path. This configuration is referred to as Case 1 hereafter. In Case 1, path $k = 1$ has the largest transmission capacity. $\rho b = 360$ [Gbps] must be provided by using paths $k = 2$ and 3 when path $k = 1$ fails. Thus, the number of spectrum slots allocated to each path is determined as $B_1 = B_2 = B_3 = 6$. The transmission capacity of this allocation is more than 400 [Gbps], so this allocation satisfies the traffic demand. The required spectrum resources of Case 1 is 18.

Allocating the same number of spectrum slots to each path can make a

difference in the transmission capacity of each path because of the different distances and modulation formats of each path. Such a difference in transmission capacity among paths leads to excessive allocation of spectrum slots to guarantee certain transmission capacity in case of network failure.

Next, in order to avoid the disadvantage of the conventional scheme, the case that the same amount of transmission capacity is allocated to each path is considered. The transmission capacity allocated to each path, b_k, is derived by (3.1) to satisfy the traffic demand.

$$b_k = \max\left\{\frac{b}{|K|}, \frac{\rho b}{|K| - M}\right\} \tag{3.1}$$

Figure 3.1(b) shows the configuration where the same amount of transmission capacity is allocated to each path. This configuration is referred to as Case 2 hereafter. In Case 2, the allocated transmission capacity to each path, $b_k = \max\{400/3, 360/2\} = 180$ [Gbps], is derived by (3.1). Then, the number of spectrum slots allocated to each path is determined as $B_1 = 4, B_2 = 5$, and $B_3 = 8$. The required spectrum resources of Case 2 is 17.

Allocating the same amount of transmission capacity to each path ensures the same amount of traffic capacity when a certain number of paths fail, no matter which paths fail. However, since the relationship between the number of slots and the amount of transmission capacity is nonlinear, allocating the same amount of transmission capacity does not always minimize the required spectrum resources. The flexible allocation of the number of spectrum slots to each path is demonstrated below.

Figure 3.1(c) shows the configuration where the number of spectrum slots and the amount of transmission capacity of each path are flexibly determined. This configuration is referred to as Case 3 hereafter. In Case 3, the transmission capacity of each path is set to $b_1 = 185$ [Gbps], $b_2 = 185$ [Gbps], and $b_3 = 175$ [Gbps]. Then, the number of spectrum slots allocated to each path is determined as $B_1 = 4, B_2 = 5$, and $B_3 = 7$. The required spectrum resources of Case 3 is 16.

From this example, it can be said that allowing to allocation of the different numbers of spectrum slots and the different amounts of transmission capacity to each path is needed to minimize the required spectrum resources.

3.2 Optimization problem

3.2.1 Overview

The two optimization problems based on the proposed scheme are presented in this section. The two optimization problems minimize the required spectrum resources of a single traffic demand. The first optimization problem determines the number of spectrum slots allocated to each path, where the route of link-disjoint paths for a traffic demand is given. The second determines the routes of link-disjoint paths and the number of spectrum slots allocated to each path, at the same time.

The first optimization problem is referred to as the flexible spectrum slots allocation and the number of paths selection (FSA-NPS) problem, which consists of two subproblems: the FSA problem and the NPS problem. The FSA problem determines the number of allocated spectrum slots to each path to minimize the required spectrum resources under the condition that a set of link-disjoint paths is given. The route of the link-disjoint paths between the source and destination nodes is computed by Bhandari algorithm [62], for example. By using Bhandari algorithm, a set of link-disjoint paths which has the minimum total distance or the minimum total number of hops can be computed. The NPS problem determines the number of link-disjoint paths to minimize the required spectrum resources.

The second optimization problem is referred to as routing and flexible spectrum slots allocation and NPS (RFSA-NPS) problem. Note that the disjoint path selection scheme which minimizes the total distance does not minimize the required spectrum resources [12]. In [12], one of the routing-modulation-spectrum allocation problems is introduced as the optimum model which minimizes the required spectrum resources in $1 + 1$ protected EONs. This optimum model is adopted in the FSA problem, in short; the routing of link-disjoint paths is additionally considered in the FSA problem. The RFSA problem determines the routes of a number of link-disjoint paths and the number of spectrum slots allocated to each path to minimize required spectrum resources.

3.2.2 FSA-NPS Problem

Formulation

The FSA-NPS problem described in Section 3.2.1 is formulated in this section. The FSA problem is solved for each case of all the available number of link-disjoint paths between the source and destination pair. Based on the solutions obtained for the FSA problem, the NPS problem chooses the number of link-disjoint paths that requires the least spectrum resources.

The FSA problem is formulated as an ILP problem. The sets, parameters, and variables of the formulation of the FSA problem are defined as shown in Table 3.2.

Table 3.2: Summary of sets, parameters and variables. (©2021 Elsevier.)

Sets	
K	Set of $\|K\|$ disjoint paths.
F	Set of M paths affected by failures. All the combinations of M paths are considered.
Parameters	
b	Transmission capacity requirement [Gbps].
M	Number of failures that traffic tolerates.
ρ	Partial protection requirement.
g	Slot requirement of guard bands.
η_k	Capacity of single spectrum slot in path k [Gbps/slot].
h_k	Number of hops of path k.
Variables	
B_k	Number of spectrum slots allocated to path k.

The objective function is set to minimize the total number of spectrum slots required on each link. When the number of spectrum slots allocated to each path is determined, it has to be ensured that there are enough resources for traffic transmission in both the non-failure case and the case of M path

failures. The FSA problem is formulated as an ILP problem as follows.

$$\min \quad \sum_{k \in K} h_k \cdot B_k \tag{3.2}$$

$$B_k \geq 1, \forall k \in K \tag{3.3}$$

$$b \leq \sum_{k \in K} \eta_k \cdot B_k \tag{3.4}$$

$$\rho \cdot b \leq \sum_{k \in K \setminus F} \eta_k \cdot B_k, \forall F \subset K, |F| = M \tag{3.5}$$

Equation (3.2) is the objective function that minimizes the required spectrum resources. Equation (3.3) means that every path is used for transmitting traffic. Equation (3.4) ensures that the total transmission capacity provided by $|K|$ paths is equal to or more than the transmission capacity requirement. Equation (3.5) ensures that even if any combination of M paths fails simultaneously, the traffic transmission satisfies the partial protection requirement.

The amount of transmission capacity allocated to path $k \in K$, b_k, is determined based on B_k. b_k is determined so as to satisfy the following equations.

$$b \leq \sum_{k \in K} b_k \tag{3.6}$$

$$b_k \leq B_k \eta_k, \forall k \in K \tag{3.7}$$

The ILP formulation of the FSA problem has $|K|$ variables and $1+|K|+\binom{|K|}{M}$ constraints.

The FSA-NPS problem is formulated as follows.

Objective :

$$\min_{|K| \geq 2} f(K) + \sum_{k \in K} h_k \cdot g \tag{3.8}$$

where

$$f(K) = \min \sum_{k \in K} h_k \cdot B_k \tag{3.9}$$

Subject to :

$$(3.3) - (3.5) \tag{3.10}$$

Equation (3.8) is the objective function that minimizes the required spectrum resources. $f(K)$ is the solution of the FSA problem for $|K|$ paths. The second

term of (3.8) means the sum of the required spectrum resources for guard bands on each path. Equation (3.9) is to get $f(K)$ for each K. Therefore, (3.8) and (3.9) take the suitable $|K|$ among all possible values of $|K|$ ($M+1 \leq |K|$) and minimize the required spectrum resources. The formulation in (3.8)–(3.10) is called as the FSA-NPS model in the rest of this thesis.

Computational time complexity of FSA-NPS problem

The analysis of the computation time complexity of the FSA-NPS problem is described below. First, the analysis of the FSA problem is as follows. When the number of available spectrum slots of each link is assumed as B_{up}, the number of all patterns of spectrum slot allocation is $B_{\mathrm{up}}^{|K|}$. An optimal solution can be obtained, by sorting this $B_{\mathrm{up}}^{|K|}$ patterns of allocations in the non-decreasing order of required spectrum resources in $O(B_{\mathrm{up}}^{|K|} \log B_{\mathrm{up}}^{|K|})$ and picking up the first pattern of allocation which satisfies the transmission capacity requirement in non-failure case and that in the case of M path failures. The total transmission capacity in the non-failure case can be computed in $O(|K|)$. In the M path failures case, the guaranteed transmission capacity can be computed by sorting $|K|$ paths by transmission capacity and calculating total transmission capacity excepting M paths which provide higher transmission capacity. This is computed in $O(|K| \log |K|)$. Therefore, the picking up step can be computed in $O(|K| B_{\mathrm{up}}^{|K|} \log |K|)$. Thus, the computational time complexity of the FSA problem is $O(|K| B_{\mathrm{up}}^{|K|} (\log B_{\mathrm{up}} + \log |K|))$.

The NPS problem can be solved by comparing the solution of the FSA problem for each $|K|$. When the maximum number of link-disjoint paths is $K_{\max}$, the computational time complexity of the FSA-NPS problem is $O(K_{\max} B_{\mathrm{up}}^{K_{\max}} (\log B_{\mathrm{up}} + \log K_{\max}))$.

3.2.3 RFSA-NPS Problem

Formulation

The RFSA-NPS problem described in Section 3.2.1 is formulated in this section. The RFSA problem is solved for each number of all the available number of link-disjoint paths between the source and destination pair. Based on the so-

lutions obtained for the RFSA problem, the NPS problem chooses the number of link-disjoint paths that requires the least spectrum resources.

In order to formulate the RFSA problem, some sets, parameters, and variables of the formulation are newly defined. The network is represented as a directed graph $G = (V, E)$, where V is a set of nodes and E is a set of links. d_{ij} is the length of link $(i, j) \in E$. e_{ij}^k is the binary decision variable that equals one if path $k \in K$ uses link (i, j), and zero otherwise. Since the links used for path k are determined by decision variable e_{ij}^k, the route of path $k \in K$ can be obtained by picking up link $(i, j) \in E$ with $e_{ij}^k = 1$.

The RFSA problem is formulated as follows.

$$\min \sum_{k \in K} \sum_{(i,j) \in E} (B_k + g) \cdot e_{ij}^k \tag{3.11}$$

$$B_k \geq 1, \forall k \in K \tag{3.12}$$

$$b \leq \sum_{k \in K} B_k \cdot \eta \left(\sum_{(i,j) \in E} d_{ij} \cdot e_{ij}^k \right) \tag{3.13}$$

$$\rho \cdot b \leq \sum_{k \in K \setminus F} B_k \cdot \eta \left(\sum_{(i,j) \in E} d_{ij} \cdot e_{ij}^k \right), \forall F \subset K, |F| = M \tag{3.14}$$

$$\sum_{j:(i,j) \in E} e_{ij}^k - \sum_{j:(j,i) \in E} x_{ji}^k = 1, \text{ if } i = s, \forall k \in K \tag{3.15}$$

$$\sum_{j:(i,j) \in E} e_{ij}^k - \sum_{j:(j,i) \in E} x_{ji}^k = 0, \forall i \in V \setminus \{s, d\}, \forall k \in K \tag{3.16}$$

$$\sum_{k \in K} (e_{ij}^k + x_{ji}^k) \leq 1, \forall (i, j) \in E \tag{3.17}$$

$$e_{ij}^k \in \{0, 1\}, \forall (i, j) \in E, \forall k \in K \tag{3.18}$$

Equation (3.11) is the objective function that minimizes required spectrum resources. Since spectrum slots are used in each link composing a path, required spectrum resources in path k are represented by $\sum_{(i,j) \in E} (B_k + g) e_{ij}^k$. Equations (3.13) and (3.14) correspond to (3.3) and (3.4), respectively. $\eta(\theta_k)$ is a function, which gives the capacity of a single spectrum slot in path k whose length is θ_k. Length θ_k is represented by $\theta_k = \sum_{(i,j) \in E} d_{ij} e_{ij}^k$. Equations (3.15) and (3.16) represent the traffic flow constraints, which ensure that each path leaving source node $s \in V$ is routed to destination node $d \in V$.

Equation (3.17) represents the condition of link-disjoint paths, and link (i, j) is used in $|K|$ paths at most one time.

$B_k \cdot e_{ij}^k$ is nonlinear, which cannot be directly handled by ILP. In order to reformulate (3.11) in a linear expression, decision variable a_{ij}^k that satisfies (3.19)–(3.21) is introduced.

$$a_{ij}^k \geq B_k + \alpha \cdot (e_{ij}^k - 1), \forall (i,j) \in E, \forall k \in K \tag{3.19}$$

$$a_{ij}^k \leq \alpha \cdot e_{ij}^k, \forall (i,j) \in E, \forall k \in K \tag{3.20}$$

$$a_{ij}^k \geq 0, \forall (i,j) \in E, \forall k \in K \tag{3.21}$$

In the above equations, α is at least the maximum number of slots that can be allocated to a link. Equation (3.11) is represented as follow by using a_{ij}^k.

$$\min \sum_{k \in K} \sum_{(i,j) \in E} (a_{ij}^k + g \cdot e_{ij}^k) \tag{3.22}$$

$\eta \left(\sum_{(i,j) \in E} d_{ij} \cdot e_{ij}^k \right)$ is a nonlinear function, which cannot be directly handled by ILP. Therefore, it is devised in a linear expression as follows.

$$\sum_{k \in K} \sum_{(i,j) \in E} d_{ij} \cdot e_{ij}^k \leq \sum_{l \in L} D_c \cdot \phi_l^k, \forall k \in K \tag{3.23}$$

$$\sum_{l \in L} \phi_l^k = 1, \forall k \in K \tag{3.24}$$

$$\phi_l^k \in \{0, 1\}, \forall k \in K, \forall l \in L \tag{3.25}$$

In EONs, the relationship between the maximum transmission reach and available modulation format is given as shown in Table 3.1. $L = \{1, \cdots, |L|\}$ is a set of path length classes, and an available modulation format is defined for each path length class. ϕ_l^k is a binary decision variable; it is set to one if path k belongs to path length class $l \in L$, and zero otherwise. Equation (3.24) indicates that path k belongs to the only path length class with $\phi_l^k = 1$. Let D_c be the upper limit of the path length of $l \in L$. Equation (3.23) indicates that the length of path k is less than or equal to the maximum transmission reach of the path length class to which path k belongs. $\eta \left(\sum_{(i,j) \in E} d_{ij} \cdot e_{ij}^k \right)$ is expressed by (3.26).

$$\sum_{l \in L} \Lambda_l \cdot \phi_l^k \tag{3.26}$$

Λ_l is a given parameter that represents the capacity of a single spectrum slot in the path whose length belongs to the path length class c. Equations (3.13) and (3.14) are expressed by (3.27) and (3.28), respectively.

$$b \leq \sum_{k \in K} \sum_{l \in L} \Lambda_l \cdot B_k \cdot \phi_l^k \tag{3.27}$$

$$\rho \cdot b \leq \sum_{k \in K \setminus F} \sum_{l \in L} \Lambda_l \cdot B_k \cdot \phi_l^k \tag{3.28}$$

$B_k \cdot \phi_l^k$ is nonlinear, so decision variable z_c^k that satisfies (3.29)–(3.32) is introduced to reformulate (3.27) and (3.28) in a linear expression.

$$z_c^k \leq B_k, \forall k \in K, \forall l \in L \tag{3.29}$$

$$z_c^k \geq B_k + \alpha \cdot (\phi_l^k - 1), \forall k \in K, \forall l \in L \tag{3.30}$$

$$z_c^k \leq \alpha \cdot \phi_l^k, \forall k \in K, \forall l \in L \tag{3.31}$$

$$z_c^k \geq 0, \forall k \in K, \forall l \in L \tag{3.32}$$

Equations (3.27) and (3.28) are represented as follow by using z_{ij}^k.

$$b \leq \sum_{k \in K} \sum_{l \in L} \Lambda_l \cdot z_c^k \tag{3.33}$$

$$\rho \cdot b \leq \sum_{k \in K \setminus F} \sum_{l \in L} \Lambda_l \cdot z_c^k \tag{3.34}$$

The linear form of the RFSA problem is summarized in the following. The decision variables are B_k, e_{ij}^k, a_{ij}^k, ϕ_l^k and z_c^k.

$$f(K) = \min \sum_{k \in K} \sum_{(i,j) \in E} (a_{ij}^k + g \cdot e_{ij}^k) \tag{3.35}$$

$$B_k \geq 1, \forall k \in K \tag{3.36}$$

$$b \leq \sum_{k \in K} \sum_{l \in L} \Lambda_l \cdot z_c^k \tag{3.37}$$

$$\rho \cdot b \leq \sum_{k \in K \setminus F} \sum_{l \in L} \Lambda_l \cdot z_c^k, \forall F \subset K, |F| = M \tag{3.38}$$

$$\sum_{j:(i,j) \in E} e_{ij}^k - \sum_{j:(i,j) \in E} x_{ji}^k = 1, \text{ if } i = s, \forall k \in K \tag{3.39}$$

$$\sum_{j:(i,j) \in E} e_{ij}^k - \sum_{j:(i,j) \in E} x_{ji}^k = 0, \forall i \in V \setminus \{s, d\}, \forall k \in K \tag{3.40}$$

$$\sum_{k\in K}(e_{ij}^k + x_{ji}^k) \leq 1, \forall (i,j) \in E \tag{3.41}$$

$$e_{ij}^k \in \{0,1\}, \forall (i,j) \in E, \forall k \in K \tag{3.42}$$

$$a_{ij}^k \geq B_k + \alpha \cdot (e_{ij}^k - 1), \forall (i,j) \in E, \forall k \in K \tag{3.43}$$

$$a_{ij}^k \leq \alpha \cdot e_{ij}^k, \forall (i,j) \in E, \forall k \in K \tag{3.44}$$

$$a_{ij}^k \geq 0, \forall (i,j) \in E, \forall k \in K \tag{3.45}$$

$$\sum_{k\in K}\sum_{(i,j)\in E} d_{ij} \cdot e_{ij}^k \leq \sum_{l\in L} L_c \cdot \phi_l^k, \forall k \in K \tag{3.46}$$

$$\sum_{l\in L} \phi_l^k = 1, \forall k \in K \tag{3.47}$$

$$\phi_l^k \in \{0,1\}, \forall k \in K, \forall l \in L \tag{3.48}$$

$$z_c^k \leq B_k, \forall k \in K, \forall l \in L \tag{3.49}$$

$$z_c^k \geq B_k + \alpha \cdot (\phi_l^k - 1), \forall k \in K, \forall l \in L \tag{3.50}$$

$$z_c^k \leq \alpha \cdot \phi_l^k, \forall k \in K, \forall l \in L \tag{3.51}$$

$$z_c^k \geq 0, \forall k \in K, \forall l \in L \tag{3.52}$$

The ILP formulation of the RFSA problem has $|K| + 2|K||E| + 2|K||C|$ variables and $1 + 4|K| + |E| + \binom{|K|}{M}(|V| - 2)|K| + 2|K||E| + 3|K||E|$ constraints.

The RFSA-NPS problem is formulated as follows.

Objective :

$$\min_{|K|\geq 2} f(K) \tag{3.53}$$

where

$$f(K) = \min \sum_{k\in K}\sum_{(i,j)\in E} (a_{ij}^k + g \cdot e_{ij}^k) \tag{3.54}$$

Subject to :

$$(3.36) - (3.52) \tag{3.55}$$

Equation (3.53) is the objective function, which minimizes required spectrum resources. Equation (3.54) is to get the required spectrum resources for each number of link-disjoint paths. Equations (3.53) and (3.54) correspond to (3.8) and (3.9), respectively. The formulation in (3.53)–(3.55) is called as the RFSA-NPS model in the rest of this thesis.

Proof of NP-completeness

The proof that the RFSA-NPS decision problem is NP-complete is described as follows. The RFSA decision problem is defined as Q.

Definition Q: Graph $G = (V, E)$, non-negative length $l(e)$ for link $e \in E$, source and destination nodes $s, t \in V$, the transmission capacity requirement b, the tolerable number of failures M, the partial protection requirement ρ, the spectrum slot requirement of guard band g, positive integer S, and the maximum transmission reach of the modulation $r(\eta_c)$ with the capacity of a single spectrum slot η_c are given. Is there any set of routing and spectrum slots allocation of $|K|$ link-disjoint paths from s to t that provides total transmission capacity b in the non-failure case and ρb when M path failures happen, in which the required spectrum resources is at most S?

Theorem: Q is NP-complete.

Proof. First, it is shown that Q is in NP. If a certificate of any instance of Q is given, the verification of total transmission capacity b in the non-failure case and ρb in any M path failure case is needed. In addition, the verification that the required spectrum resources are at most S is needed. The total transmission capacity in the non-failure case can be computed in $O(|K|)$. In the M path failures case, the guaranteed transmission capacity can be computed by sorting $|K|$ paths by transmission capacity and calculating total transmission capacity excepting M paths which provide higher transmission capacity. This is computed in $O(|K| \log |K|)$. The required spectrum resources can be computed in $O(|E|)$. As a result, whether a certificate of any instance of Q provides total transmission capacity b in the non-failure case and ρb in any M path failure case and requires spectrum resources at most S can be verified in polynomial time of $O(|E| + |K| \log |K|)$. Therefore, Q is in NP.

The modulation-adaptive link-disjoint path selection problem, which is introduced as P_0 and proved to be NP-complete in [12], is shown to be a subset of Q. Set $|K| = 2$, $g = 0$ and a traffic demand as b, $\rho = 1$, $M = 1$ in Q. Since $M = 1, \rho = 1$ and $|K| = 2$, each link-disjoint path must transmit at least b. This means that the same amount of transmission capacity must be allocated to the two link-disjoint paths. Therefore, Q in this setting is the same problem

as P_0, in other words, P_0 is a subproblem of Q.

Since Q is in NP and P_0, which is a known NP-complete problem, is a subproblem of Q, Q is NP-complete. □

3.2.4 Application of proposed scheme for multiple traffic demands

The proposed scheme determines the spectrum allocation for a single traffic demand, which occurs between a pair of source and destination nodes. When the proposed scheme is adopted for multiple traffic demands, a strategy is needed to allocate spectrum slots to them. A basic strategy for allocating spectrum slots to multiple traffic demands is described as follows. In a basic strategy, spectrum slots are greedily allocated to each traffic demand based on the FSA-NPS model with some modifications. In the modified FSA-NPS model, in addition to a set of link-disjoint paths and the modulation format for each path, the maximum number of available spectrum slots on each path is imposed as a constraint. Let Γ_k denote the maximum number of available spectrum slots on path $k \in K$. Γ_k is calculated by considering the condition of allocated spectrum slots for the existing traffic demands in the network. The constraint below is added for the FSA problem, which is formulated in (3.2)–(3.5).

$$B_k \leq \Gamma_k, \forall k \in K \tag{3.56}$$

A greedy algorithm based on the FSA-NPS model for multiple traffic demands is described as follows. For each traffic demand, Steps 1 to 6 are executed, as described below.

Step 1: The number of paths, n, is set to $M + 1$. The required spectrum resources, Λ, is set to ∞. The candidate set of paths is initialized by an empty set. The list of the number of spectrum slots allocated to each path, which belongs to the candidate set of paths, is set to empty.

Step 2: Get a set of n link-disjoint paths, K, and determine the modulation format for each path. If n link-disjoint paths cannot be set in the network, go to Step 6.

Step 3: Compute the maximum number of available spectrum slots of path $k \in K$, Γ_k.

Step 4: Determine the number of spectrum slots allocated to path $k \in K$, B_k, and obtain the required spectrum resources in the case of n paths, Λ_n, by solving the modified FSA problem. If there is no solution, increment n and return to Step 2.

Step 5: If $\Lambda_n \leq \Lambda$, set $\Lambda = \Lambda_n$, set the candidate set of paths to K, and update the list of the number of spectrum slots allocated to each path. Increment n and return to Step 2.

Step 6: If $\Lambda = \infty$, the traffic demand is blocked. Otherwise, allocate the spectrum slots for each path based on the list of the number of spectrum slots so that the indices of allocated spectrum slots become as low as possible, where the spectrum slots satisfy the spectrum continuity and contiguity.

In Step 2, n link-disjoint paths are selected; for example, they are obtained so as to minimize the total distance of paths.

The basic strategy described above does not always minimize the total amount of required spectrum resources for multiple traffic demands due to the nature of the greedy algorithm. In order to reduce the amount of required spectrum resources for multiple traffic demands, another strategy is devised; it develops an optimization model that determines the spectrum allocation for a set of multiple traffic demands. The optimization model considers spectrum contiguity and continuity constraints and ensures that different traffic demands do not use the same spectrum slots in the same link. As the number of traffic demands that are considered in the optimization model increases, the number of decision variables increases; this leads to the computation time. A network operator needs to choose an appropriate set of traffic demands that the optimization model handles, considering both resource utilization and computation time. A network operator may combine both strategies appropriately, where the objective function in each strategy can be modified accordingly.

3.3 Evaluation

3.3.1 Comparison of proposed scheme and conventional scheme

In order to observe the effect of the proposed scheme, the proposed scheme is compared with the conventional scheme in terms of the required spectrum resources and the computation time. In the evaluation, the proposed scheme and conventional scheme are adopted for the spectrum allocation for various single traffic demand. The proposed and conventional schemes are evaluated by examining every case of all the available numbers of paths and choosing the number of paths that provides the least amount of utilized spectrum resources. In order to evaluate the proposed scheme, the FSA-NPS model is used to determine the number of link-disjoint paths and the number of allocated spectrum slots to each path. For each number of paths, the route of that number of link-disjoint paths between the source and destination nodes is given. The link-disjoint paths have the minimum total distance and they can be computed by Bhandari algorithm [62]. It is confirmed that the FSA problem can be solved by using an ILP solver in a shorter computational time than the algorithm described in Section 3.2.2 in the simulation of this section. The ILP model for the FSA problem is employed in the simulation since it is preferable to suppress the computational time from the network operation aspect. For each number of paths, the number of allocated spectrum slots to each path is obtained by solving the ILP formulation of the FSA problem in (3.2)–(3.5).

Two approaches to allocating spectrum slots to each path in the conventional scheme are considered. One allocates the same number of spectrum slots to each path, and the other allocates the same amount of transmission capacity to each path. The former is defined as the conventional scheme with the same number of spectrum slots allocation (SNSA) and the latter is defined as the conventional scheme with the same amount of transmission capacity allocation (SACA).

In this evaluation, the number of slots required for each guard band is set to one ($g = 1$). The capacity of a single spectrum slot of each path is predeter-

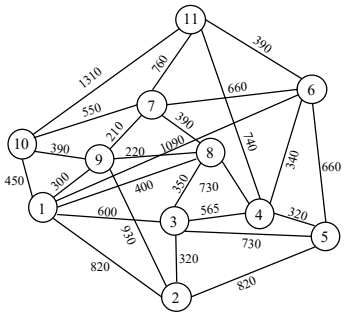

Figure 3.2: COST239 network.

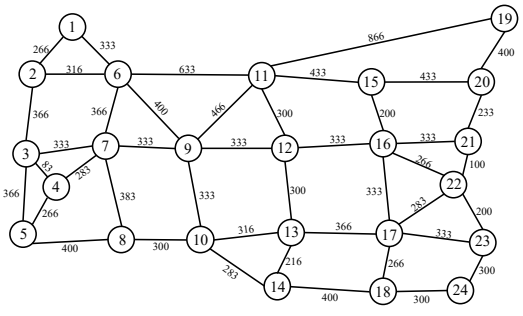

Figure 3.3: US backbone network.

mined by choosing the most efficient modulation format that is available to the path. It is assumed that $\eta_k = 62.5, 50, 37.5, 25, 12.5$, when 32QAM, 16QAM, 8QAM, QPSK, and BPSK are used, respectively. The COST239 network [63] and the US backbone network [64] are used, which are shown in Figs. 3.2 and 3.3, respectively. Note that the link distance of US backbone network is set to one third of that introduced in [64]. The link distance is shown in units of km next to each link. The COST239 network has 11 nodes and 52 directional links with average node degrees of 4.73. The US backbone network has 24 nodes and 84 directional links with average node degrees of 3.50.

Both proposed scheme and conventional scheme calculate the required spectrum resources to transmit traffic to each destination node. Various single traffic demand is assumed as follows. A traffic demand occurs between a pair of source and destination nodes. The transmission capacity requirement is set to $b = 10, 20, 50, 100, 200, 500, 1000$, and 2000 [Gbps]. Three kinds of partial protection requirement, ρ, which are $1.0, 0.8$, and 0.5, are assumed. Both single failure scenario and multiple failure scenario are examined, in which the number of failures that a traffic tolerates is set to $M = 1$ and 2, respectively.

All possible pairs of source and destination nodes in which more than M link-disjoint paths can be set are examined.

Intel Xeon e3-1270 3.80 GHz 4-core CPU with 64 GB memory is used through the evaluations in this chapter. The ILP problems are solved by CPLEX Optimization Studio 12.8 [65].

Fig. 3.4 shows the average amount of the required spectrum resources for the transmission between each source and destination node pair with respect

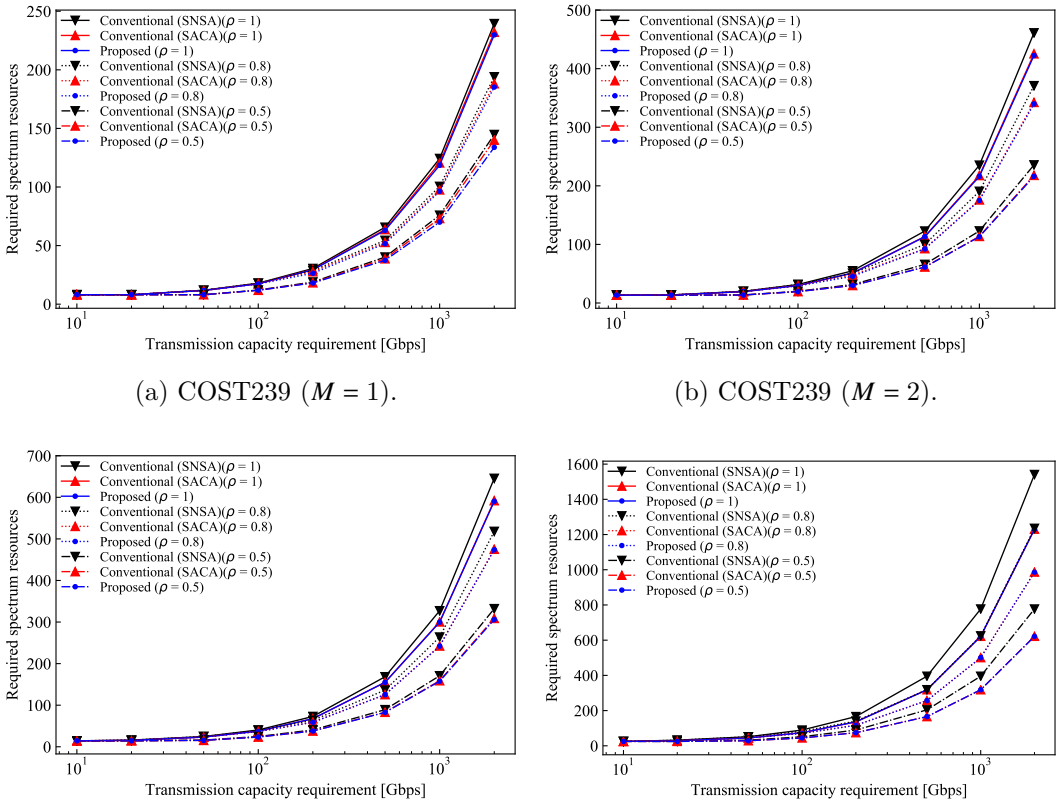

(a) COST239 ($M = 1$).

(b) COST239 ($M = 2$).

(c) US backbone ($M = 1$).

(d) US backbone ($M = 2$).

Figure 3.4: Average required spectrum resources in conventional and proposed schemes. (©2021 Elsevier.)

to traffic demands. Figs. 3.4(a) and (b) show the result in the COST239 network, in the single failure scenario ($M = 1$) and in the multiple failure scenario ($M = 2$), respectively.

Fig. 3.4(a) shows that, compared to the conventional scheme with SNSA, the proposed scheme reduces the average amount of the required spectrum resources by at most 7.5%, which can be observed when $b = 2000$ and $\rho = 0.5$. Compared to the conventional scheme with SACA, the proposed scheme reduces the average amount of the required spectrum resources by at most 4.4%, which can be observed when $b = 2000$ and $\rho = 0.5$.

When b =10 and 20 [Gbps], the proposed scheme and the two approaches of the conventional scheme require the same amount of spectrum resources.

When b is sufficiently large compared to the bit rate of a single slot, the reduction ratio of the required spectrum resources in the proposed scheme to that in the conventional scheme does not increase in proportion to b.

In another point of view, ρ influences the effectiveness of the proposed scheme. When ρ becomes smaller, the proposed scheme has more chances to make the transmission capacity allocated to each path unbalanced. Therefore, the proposed scheme can reduce the required spectrum resources efficiently in the smaller ρ case, compared to the conventional scheme.

By comparing Fig. 3.4(b) with Fig. 3.4(a), the influence of M is discussed. When M becomes large, the proposed scheme reduces more required spectrum resources compared to the conventional scheme with SNSA. In SNSA, the number of spectrum slots allocated to each path is determined so that $|K| - M$ paths that use the lower modulation format provide the transmission capacity of ρb. This means that spectrum slots are excessively allocated to paths with a better modulation format. Therefore, the conventional scheme with SNSA cannot use spectrum resources effectively under multiple failures. On the other hand, the reduction ratio of the required spectrum resources in the proposed scheme to that in the conventional scheme with SACA becomes smaller in the case of $M = 2$ than in the case of $M = 1$. This is because it becomes difficult for the proposed scheme to make the transmission capacity allocation unbalanced as M becomes large. Therefore, the proposed scheme hardly reduces the required spectrum resources as is the case of $M = 1$.

Figs. 3.4(c) and (d) show the result in the US backbone network, in the single failure scenario ($M = 1$) and in the multiple failure scenario ($M = 2$), respectively. Compared to the conventional scheme with SNSA, the proposed scheme reduces the required spectrum resources. Compared to the conventional scheme with SACA, the proposed scheme reduces a little required spectrum resources. The reduction ratio of the required spectrum resources in the proposed scheme to that in the conventional scheme with SACA is smaller than when evaluated in the COST239 network. This is because the US backbone network has smaller average node degrees than the COST239 network; in other words, a smaller number of link-disjoint paths between source and destination can get in the US backbone network than in the COST239 network. Comparing Fig. 3.4(d) with Fig. 3.4(c), the influence of M as observed

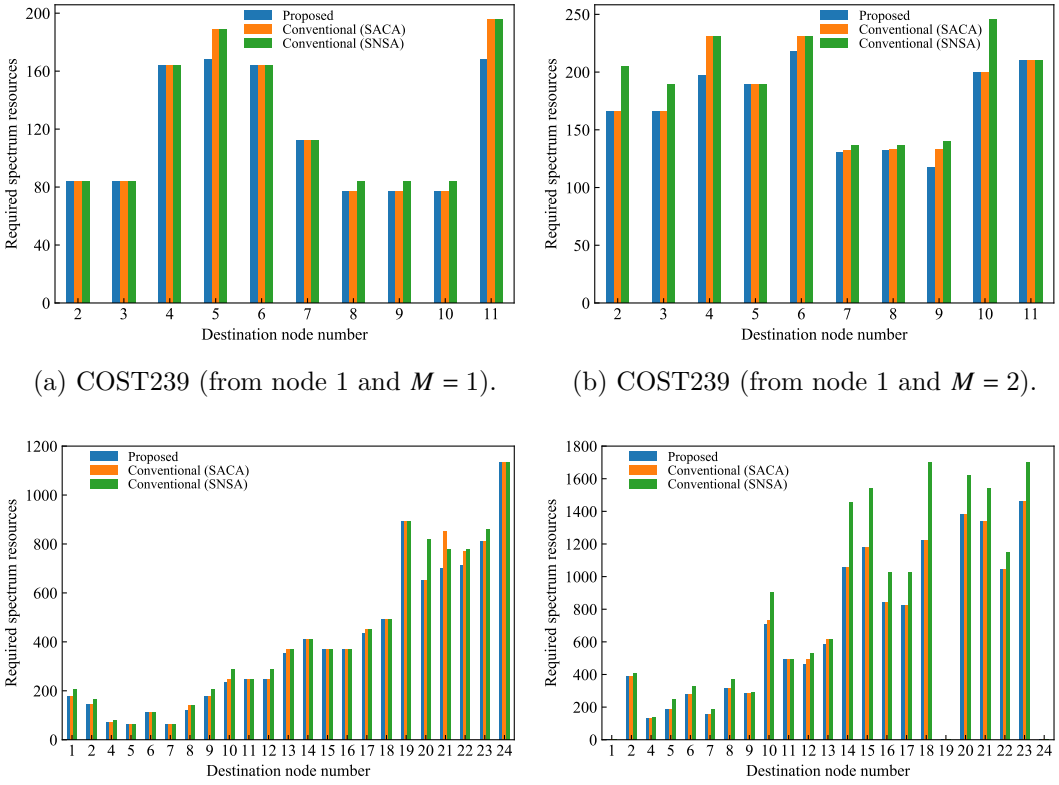

(a) COST239 (from node 1 and $M = 1$).

(b) COST239 (from node 1 and $M = 2$).

(c) US backbone (from node 3 and $M = 1$).

(d) US backbone (from node 3 and $M = 2$).

Figure 3.5: Required spectrum resources from specific node to each node in conventional and proposed schemes ($b = 2000$ [Gbps] and $\rho = 0.5$). (©2021 Elsevier.)

in the evaluation in the COST239 network also can be seen in the US backbone network.

Fig. 3.5 shows the required spectrum resources for the transmission from a specific node to each destination when $b = 2000$ [Gbps] and $\rho = 0.5$. The source node is set to node 1 and node 3 in the evaluations in the COST239 network and in the US backbone network, respectively.

Fig. 3.5(a) shows the result in the COST239 network in the single failure scenario; $M = 1$. The proposed scheme, compared to the conventional scheme, reduces the required spectrum resources in several cases. The proposed scheme requires less amount of spectrum resources than the conventional scheme with

SACA when the destination is set to node 5 and node 11. Especially, when the destination node is node 11, the reduction rate is 14.3%.

Fig. 3.5(b) shows the result in the multiple failure scenario; $M = 2$. The proposed scheme requires less amount of spectrum resources than the conventional scheme with SACA when the destination is set to node 4, 7, 8, and 9. As well as the result of the single failure scenario, the proposed scheme reduces the required spectrum resources in several cases in the multiple failures scenario.

Figs. 3.5(c) and (d) show the results in $M = 1$ and $M = 2$ in the US backbone network. The proposed scheme reduces the required spectrum resources in several cases in the same way as the COST239 network. In the single failure scenario ($M = 1$), the proposed scheme reduces the required spectrum resources compared to the conventional scheme with SACA in six cases, where the destination is set to node 8, 10, 13, 17, 21, and 22. In the multiple failure scenario ($M = 2$), the proposed scheme reduces the required spectrum resources compared to the conventional scheme with SACA in three cases, where the destination is set to node 10, 12, and 13.

In this evaluation environment with $M = 1$, the proposed scheme, compared to the conventional scheme with SACA, reduces the required spectrum resources in some cases where the length of the shortest path between the source and destination node pair is more than 700 [km]. When the distance between the source and destination nodes becomes long, disjoint paths tend not to contain circuitous paths that cost more spectrum resources than the other paths. In that case, the region of feasible solutions that can be the optimal solution becomes large since more paths can be candidates for the solution of the NPS problem. This is why the proposed scheme tends to reduce the required spectrum resources than the benchmark scheme when the distance between the source and destination nodes becomes long.

In order to confirm how the proposed scheme reduces the required spectrum resources, the transmission from node 1 to node 7 with $M = 2$ in the COST239 network is analyzed. Table 3.3 shows the spectrum slots allocation when $b = 2000$ [Gbps], $\rho = 0.5$, and $M = 2$. The proposed scheme, the conventional scheme with SACA, and the conventional scheme with SNSA adopt $|K| = 4$. The number of hops of each path is $h_1 = h_2 = h_3 = h_4 = 2$ and the capacity

Table 3.3: Spectrum slots allocation for transmission from node 1 to node 7 in conventional and proposed schemes. (©2021 Elsevier.)

	Proposed	Conventional (SACA)	Conventional (SNSA)
Path $k = 1$ (2 hops)	14	14	16
Path $k = 2$ (2 hops)	14	14	16
Path $k = 3$ (2 hops)	14	14	16
Path $k = 4$ (2 hops)	19	20	16
Guard bands	8	8	8
Required spectrum resources	130	132	136

of a single spectrum slot of each path is $\eta_1 = \eta_2 = \eta_3 = 37.5$ and $\eta_4 = 25$ [Gbps/slot]. The required spectrum resources of the proposed scheme, the conventional scheme with SACA, and the conventional scheme with SNSA are 130, 132, and 136, respectively. This indicates that the proposed scheme minimizes the required spectrum resources by allocating the spectrum slots flexibly as described in Section 3.2.

The computation times when the traffic demand is $b = 2000$ [Gbps], $M = 1$, and $\rho = 0.5$ are evaluated. Table 3.4 shows the computation times for COST239 network, from node 1 to each destination for the proposed scheme and the conventional scheme. Table 3.5 shows the computation times for US backbone network, from node 3 to each destination for the proposed scheme and the conventional scheme. The computation time of the proposed scheme is larger than that of the conventional scheme.

In this thesis, an optical backbone network design is considered. In general, lightpaths are used for several months or several years in an optical backbone network [66]. It is allowed to take the computation time to provision a lightpath; according to the report in [67], the time for a lightpath provisioning of the order of days or weeks is acceptable. It is observed that the FSA-NPS model computes a solution in COST239 network and US backbone network with a practical time, as shown in Tables 3.4 and 3.5. The FSA-NPS model gets an optimal solution under the condition that the route of link-disjoint paths is given. The computational time complexity of the FSA-NPS problem depends on the maximum number of link-disjoint paths, $K_{\max}$, and the scale of the network does not matter. In optical networks, it is considered that the

Table 3.4: Comparison of computation times between conventional and proposed schemes in [sec] for COST239 network.

Destination node	Computation time [sec] Proposed	Conventional (SACA)	Conventional (SNSA)
1	-	-	-
2	0.0209	0.0037	0.0034
3	0.0209	0.0048	0.0049
4	0.0192	0.0052	0.0017
5	0.0132	0.0011	0.0011
6	0.0185	0.0015	0.0015
7	0.0196	0.0013	0.0014
8	0.0188	0.0012	0.0013
9	0.0207	0.0012	0.0013
10	0.0134	0.0010	0.0033
11	0.0122	0.0011	0.0037

maximum number of link-disjoint paths is limited, according to the analysis in [68] of the 29 transport networks. The computational time complexity of the FSA-NPS problem is bounded by $O(K_{\max} B_{\mathrm{up}}^{K_{\max}} (\log B_{\mathrm{up}} + \log K_{\max}))$ with the limited value of $K_{\max}$.

Since the proposed scheme gets an optimal spectrum allocation, the amount of required spectrum resources of the proposed scheme is equal to or less than that of the conventional scheme. The proposed scheme can accommodate more traffic demands by improving spectrum efficiency than the conventional scheme. The proposed scheme gives a benefit for a network operator, compared to the conventional scheme.

3.3.2 Comparison of RFSA-NPS and FSA-NPS

In order to observe the effect of the routing optimization with the proposed scheme, the RFSA-NPS model is compared with the FSA-NPS model. The ILP model for the RFSA-NPS problem is employed in order to get an optimal solution. Two approaches for choosing a set of link-disjoint paths are considered in the FSA-NPS model. One uses link-disjoint paths that have the minimum total distance and the other uses those that have the minimum total number of hops. By using Bhandari algorithm with the network where the

Table 3.5: Comparison of computation times between conventional and proposed schemes in [sec] for US backbone network.

Destination node	Computation time [sec] Proposed	Conventional (SACA)	Conventional (SNSA)
1	0.008	0.004	0.004
2	0.011	0.002	0.003
3	-	-	-
4	0.011	0.002	0.003
5	0.012	0.003	0.003
6	0.016	0.004	0.004
7	0.016	0.004	0.004
8	0.010	0.003	0.003
9	0.016	0.004	0.004
10	0.018	0.004	0.004
11	0.016	0.012	0.004
12	0.018	0.008	0.004
13	0.017	0.006	0.004
14	0.012	0.004	0.003
15	0.011	0.003	0.003
16	0.017	0.004	0.004
17	0.017	0.004	0.004
18	0.011	0.003	0.003
19	0.005	0.002	0.002
20	0.010	0.003	0.003
21	0.009	0.003	0.003
22	0.014	0.004	0.004
23	0.009	0.003	0.003
24	0.005	0.002	0.002

weight of a link represents the distance, the link-disjoint paths that have the minimum total distance can be computed. By using Bhandari algorithm with the network where the weight of every link is set to one, the link-disjoint paths that have the minimum total number of hops can be computed. The other environment of the evaluation is the same as Section 3.3.1.

Fig. 3.6 shows the average amount of the required spectrum resources for the transmission between each source and destination node pair with respect to traffic demands. Figs. 3.6(a) and (b) show the result in the COST239 network, in the single failure scenario ($M = 1$) and in the multiple failure scenario ($M = 2$), respectively. Figs. 3.6(c) and (d) show the result in the US backbone

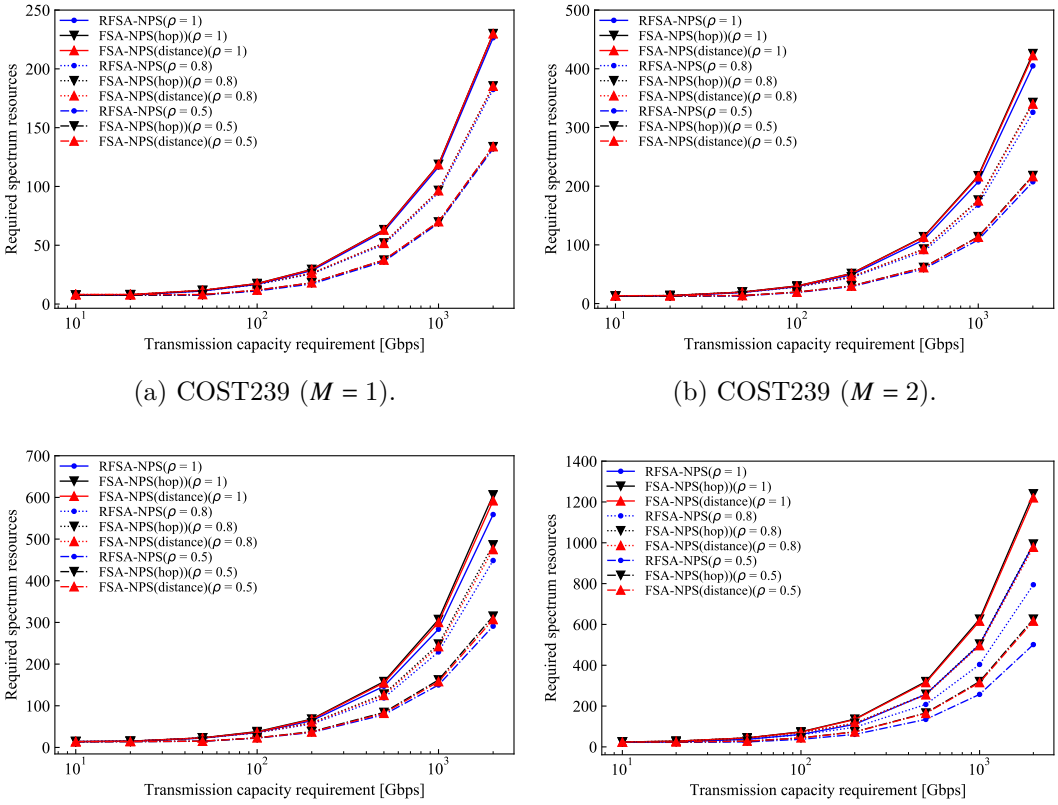

(a) COST239 ($M = 1$). (b) COST239 ($M = 2$).

(c) US backbone ($M = 1$). (d) US backbone ($M = 2$).

Figure 3.6: Average required spectrum resources in FSA-NPS and RFSA-NPS models. (©2021 Elsevier.)

network, in the single failure scenario ($M = 1$) and in the multiple failure scenario ($M = 2$), respectively. Fig. 3.6 shows that the RFSA-NPS model, compared to the FSA-NPS model, reduces the required spectrum resources in both the COST239 network and the US backbone network, and in both $M = 1$ and $M = 2$.

Comparing the result in $M = 1$ with that in $M = 2$, the reduction ratio of the RFSA-NPS model to the FSA-NPS model in $M = 2$ is larger than that in $M = 1$. This is because the difference among link-disjoint paths in terms of modulation format and the number of hops tends to be large when the paths are given in the FSA-NPS model compared to when the paths are computed in the RFSA-NPS model. In the multiple failure scenario, more spectrum slots

Table 3.6: Reduction ratio of required spectrum resources in RFSA-NPS model to that in FSA-NPS model in percentage in US backbone network. (©2021 Elsevier.)

Transmission capacity requirement [Gbps]	$M = 1$						$M = 2$					
	$\rho = 1$		$\rho = 0.8$		$\rho = 0.5$		$\rho = 1$		$\rho = 0.8$		$\rho = 0.5$	
	Distance	Hop	Distance	Hop	Distance	Hop	Distance	Hop	Distance	Hop	Distance	Hop
10	0.00	0.00	0.00	0.00	0.00	0.00	7.25	7.25	7.25	7.25	7.25	7.25
20	1.16	1.16	1.16	1.16	0.00	0.00	13.34	13.34	13.34	13.34	7.25	7.25
50	2.82	2.82	2.82	2.82	1.16	1.16	15.72	15.72	15.72	15.72	13.36	13.36
100	2.97	5.52	2.46	2.46	2.80	2.80	16.22	17.35	15.50	15.50	15.73	15.73
200	4.10	5.51	2.98	4.62	2.78	5.34	17.43	18.65	16.37	17.09	16.22	17.35
500	5.27	7.07	4.90	7.12	4.29	6.57	18.32	19.60	18.46	19.41	17.94	18.93
1000	5.42	7.58	5.27	7.56	5.12	7.46	18.64	19.93	18.56	19.85	18.32	19.60
2000	5.59	7.77	5.57	7.70	5.20	7.60	18.82	20.13	18.76	20.07	18.64	19.93

are allocated to a worse path, i.e., a path that uses a lower modulation format and has a larger number of hops, to ensure the required transmission capacity to tolerate failures of any set of $\boldsymbol{M}$ paths. Therefore, if there is a large difference between a better path and a worse path, it consumes spectrum resources in the multiple failure scenario. The RFSA-NPS problem routes link-disjoint paths to relax this difference, so the reduction ratio of required spectrum resources in the RFSA-NPS model to the FSA-NPS model improves in the multiple failure scenario than in the single failure scenario.

Comparing the results in the US backbone network with those in the COST239 network, the reduction ratio of the required spectrum resources in the RFSA-NPS model to the FSA-NPS model in the US backbone network is larger than that in the COST239 network. This is because, since the link-disjoint paths in the US backbone network tend to have more hops than in the COST239 network, there are more options to route link-disjoint paths in the US backbone network than in the COST239 network.

The results in the US backbone network are focused below. Table 3.6 shows the reduction ratio of required spectrum resources in the RFSA-NPS model to the FSA-NPS model using the paths that have the minimum total distance and the minimum total number of hops. In the US backbone network, as the transmission capacity requirement b becomes large, the reduction ratio of required spectrum resources in the RFSA-NPS model to the FSA-NPS model becomes large. This is because, as b becomes large, the modulation format of

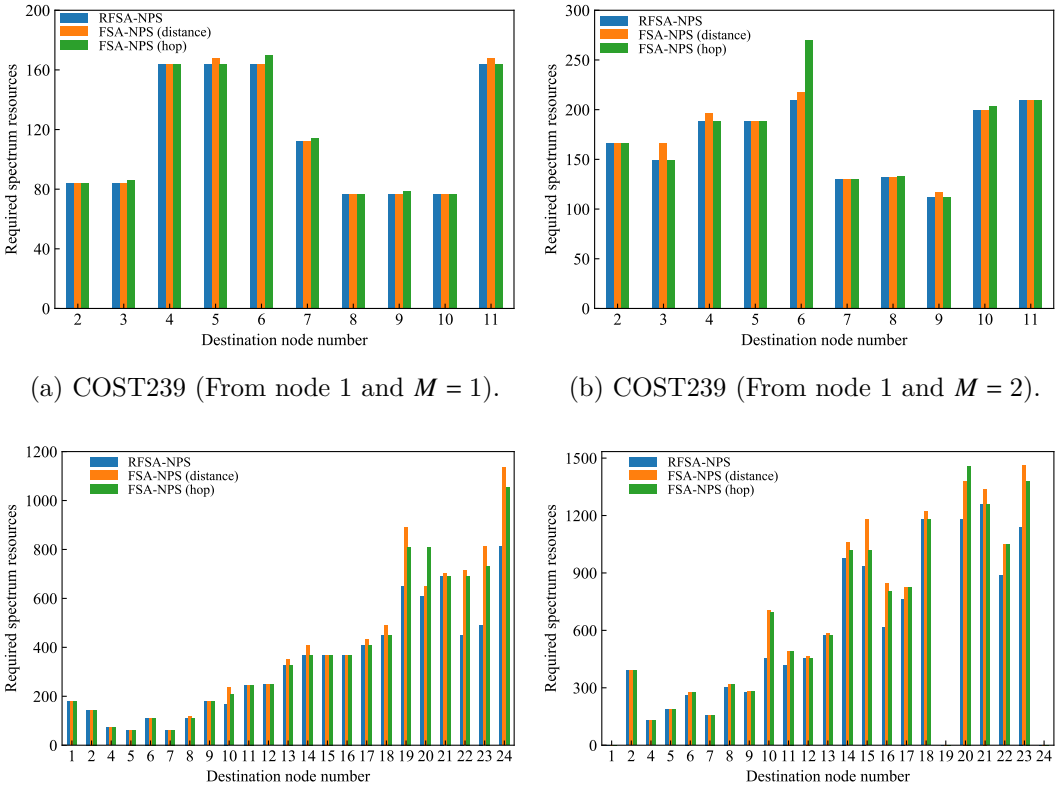

(a) COST239 (From node 1 and $M = 1$).

(b) COST239 (From node 1 and $M = 2$).

(c) US backbone (From node 3 and $M = 1$).

(d) US backbone (From node 3 and $M = 2$).

Figure 3.7: Required spectrum resources from specific node to each node in FSA-NPS and RFSA-NPS models ($b = 2000$ [Gbps] and $\rho = 0.5$). (©2021 Elsevier.)

each path has more impact on the reduction of required spectrum resources, so the routing advantage of the RFSA-NPS model affects well. Table 3.6 shows that, compared with M and b, ρ is not an important factor for the reduction ratio.

Fig. 3.7 shows the required spectrum resources for the transmission from a specific node to each destination when $b = 2000$ [Gbps] and $\rho = 0.5$. The source node is set to node 1 and node 3 in the evaluations in the COST239 network and in the US backbone network, respectively.

Figs. 3.7(a) and (b) show that, in the COST239 network, by choosing the better result of the minimum total distance or the minimum total number

Table 3.7: Comparison of computation times between FSA-NPS and RFSA-NPS models in [sec] for COST239 network. (©2021 Elsevier.)

Destination node	Computation time [sec] RFSA-NPS	FSA-NPS (distance)	FSA-NPS (hop)
1	-	-	-
2	2.358	0.021	0.021
3	123.490	0.021	0.026
4	469.129	0.019	0.023
5	13.081	0.013	0.014
6	342.966	0.018	0.021
7	184.187	0.020	0.021
8	69.142	0.019	0.021
9	55.328	0.021	0.020
10	3.219	0.013	0.016
11	30.312	0.012	0.013

of hops, the FSA-NPS model can get the solution close to the RFSA-NPS model. Figs. 3.7(c) and (d) show that the RFSA-NPS model, compared to the FSA-NPS model, tends to reduce more required spectrum resources to the transmission between the source and destination pairs which have more number of hops. When the number of hops increases, the region of feasible solutions of the RFSA problem becomes large since there are more candidate routes between the source and destination node pair. This is why the effect of the routing optimization tends to appear when the number of hops between the source and destination nodes is large.

The computation times of the RFSA-NPS model and the FSA-NPS model are evaluated in the same way as Section 3.3.1. Table 3.7 shows computation times for COST239 network, from node 1 to each destination for the RFSA-NPS model and the FSA-NPS model. Table 3.8 shows computation times for US backbone network, from node 3 to each destination for the RFSA-NPS model and the FSA-NPS model. It is observed that the computation time of the RFSA-NPS model is larger than that of the FSA-NPS model. Comparing the computation time of the RFSA-NPS model in Tables 3.7 and 3.8, the computation time in the COST239 network is larger than that in the US backbone network. This is because the COST239 network has a larger average of node degree than the US backbone network; more link-disjoint paths per

Table 3.8: Comparison of computation times between FSA-NPS and RFSA-NPS models in [sec] for US backbone network. (©2021 Elsevier.)

Destination node	Computation time [sec] RFSA-NPS	FSA-NPS (distance)	FSA-NPS (hop)
1	0.089	0.008	0.008
2	1.165	0.011	0.011
3	-	-	-
4	0.502	0.011	0.011
5	0.355	0.012	0.013
6	1.300	0.016	0.017
7	0.933	0.016	0.018
8	0.585	0.010	0.011
9	2.189	0.016	0.018
10	3.658	0.018	0.019
11	6.779	0.016	0.018
12	11.523	0.018	0.020
13	19.969	0.017	0.018
14	3.168	0.012	0.012
15	2.665	0.011	0.012
16	7.778	0.017	0.018
17	6.642	0.017	0.018
18	2.346	0.011	0.013
19	0.140	0.005	0.006
20	3.523	0.010	0.011
21	7.247	0.009	0.011
22	37.052	0.014	0.015
23	7.924	0.009	0.010
24	0.245	0.005	0.005

source-destination pair can be taken in the COST239 network than in the US backbone network.

The RFSA-NPS model and the FSA-NPS model are compared to observe the effect of the routing optimization with the proposed scheme. It is observed that the RFSA-NPS model improves spectrum efficiency compared to the FSA-NPS model at the expense of longer computation time. The RFSA-NPS problem is NP-complete as described in Section 3.2.3. By using an ILP solver, the RFSA-NPS model gets optimal solutions in the COST239 network and the US backbone network within a practical time in the simulation environment, as shown in Tables 3.7 and 3.8. In a large-scale network, there is

a possibility that the RFSA-NPS model cannot get an optimal solution in a practical time. A network operator can choose the FSA-NPS model or the RFSA-NPS model for a multipath provisioning according to the operator's requirements.

3.3.3 Multiple traffic demands

The proposed scheme is compared with the conventional scheme when they are adopted to multiple traffic demands. The comparison is examined in terms of the total required spectrum resources, which is the cumulative sum of the required spectrum resources in a set of multiple traffic demands. In the evaluation of the proposed scheme, the basic strategy described in Section 3.2.4 is used for the spectrum allocation for multiple traffic demands. In Step 2 of the strategy, n link-disjoint paths are computed by Bhandari algorithm, which minimizes the total distance. The conventional scheme is evaluated by using the two approaches, SACA and SNSA, described in Section 3.3.1. Both approaches are adopted to the spectrum allocation for multiple traffic demands by changing Step 4 in the strategy in Section 3.2.4; the two approaches are used instead of solving the FSA problem to determine the number of spectrum slots allocated to path $k \in K$, B_k, and obtain the required spectrum resources in the case of n paths, Λ_n.

In this comparison, each traffic demand occurs between a different source and destination node pair randomly. The transmission capacity requirement of each traffic demand is selected from uniform random values between 100 and 1000 [Gbps]. The partial protection requirement, ρ, is selected from uniform random values between 0.5 and 1. The available number of spectrum slots in each link is assumed to be 320. The single failure scenario is assumed in the COST239 network and the US backbone network.

Fig. 3.8 shows the total required spectrum resources for a set of traffic demands. Figs. 3.8(a) and (b) show the results in the COST239 network and the US backbone network, respectively. Compared to the conventional scheme, the proposed scheme reduces the total required spectrum resources.

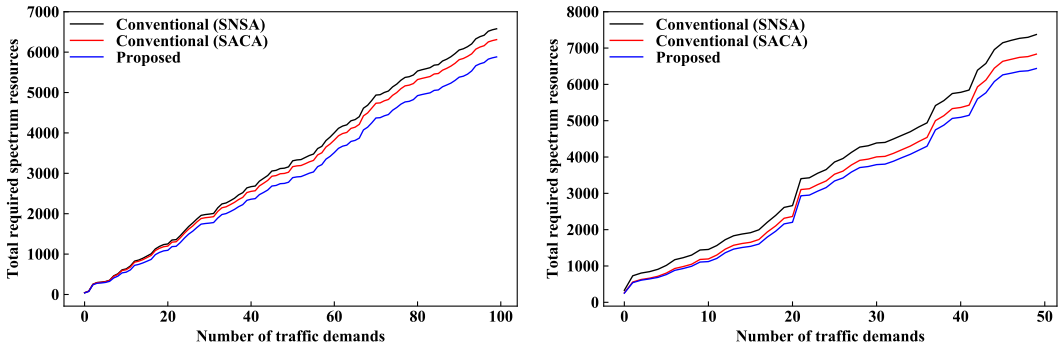

(a) COST239. (b) US backbone.

Figure 3.8: Total required spectrum resources for multiple traffic demands with proposed scheme and conventional scheme. (©2021 Elsevier.)

3.4 Summary

This chapter proposed the MPP scheme for fault tolerance to minimize required spectrum resources in EONs. The proposed scheme allows allocating different numbers of spectrum slots and different amounts of transmission capacity to each path to minimize the required spectrum resources. Two optimization problems in the proposed scheme were presented. One problem considers that the route of link-disjoint paths for a traffic demand is given, and the other determines the routes of link-disjoint paths and the number of spectrum slots allocated to each path simultaneously. The two optimization problems were formulated as the FSA-NPS model and the RFSA-NPS model. Numerical results revealed that the conventional scheme does not always minimize the required spectrum resources and showed that the proposed scheme reduces the required spectrum resources in several cases. It was also observed that the required spectrum resources can be reduced by considering the routing of link-disjoint paths in the proposed scheme at the expense of more computation time; the reduction effect especially becomes large in the case where the network has a large number of nodes and needs to tolerate with multiple failures.

Chapter 4

Joint inter-core crosstalk- and intra-core impairment-aware lightpath provisioning in spectrally-spatially EONs

4.1 Routing, modulation, spectrum, and core allocation model based on precise-XT estimation

In this section, an RMSCA model based on P-XT estimation is described, and a benchmark model considered in this chapter is introduced.

The RMSCA model in [25] sets the XT threshold and the transmission reach of each modulation format. This model calculates inter-core XT and decides the modulation format and the spectrum allocation of a lightpath so that the estimated P-XT value and the path distance do not exceed the XT threshold and the transmission reach, respectively. The P-XT value is estimated by (1.3).

The model presented in [25] sets the transmission reach for each modulation format without considering XT. If there is any deterioration of the lightpath due to XT, the transmission reach, which is set without considering XT, cannot

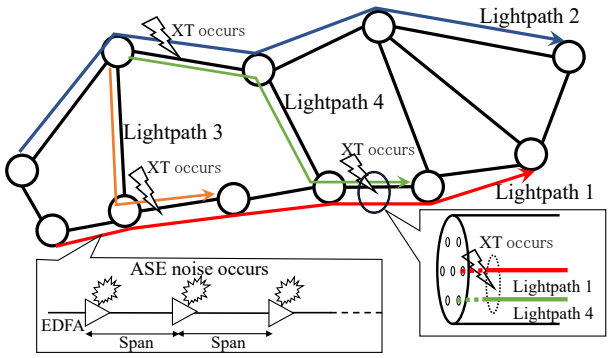

Figure 4.1: Schematic view of inter-core XT and intra-core PLIs during lightpath establishment in SS-EONs. (©2022 IEEE.)

be achieved. We can apply the model in [25] for RMSCA by considering a margin to the transmission reach. The margin is made by setting the transmission reach to a shorter value for tolerating inter-core XT for the lightpath. In this chapter, the applicable model with a margin is considered as the benchmark model, which decides the modulation format and performs core and spectrum slot allocation of a lightpath to satisfy the XT threshold and the transmission reach that has a margin.

4.2 Proposed model

The proposed model considers inter-core XT and intra-core PLIs jointly. Fig. 4.1 shows a schematic view of inter-core XT and intra-core PLIs during lightpath establishment in SS-EONs considered in this paper. We assume that the intra-core PLIs are generated from ASE noise, which is regarded as a linear impairment. In the proposed model, inter-core XT is considered by setting multiple XT thresholds. Intra-core PLIs are considered by setting the transmission reach corresponding to each XT threshold.

The multiple XT thresholds and corresponding transmission reaches are set as follows. We introduce OSNR penalty to consider inter-core XT and intra-core PLIs jointly. OSNR penalty means the OSNR decline caused by inter-core XT. We select some OSNR penalty values such as 0.25, 0.5, 0.75, 1.0, 1.5, and 2.0 dB. We set XT values, each of which corresponds to one of

the OSNR penalty values, as the XT thresholds by using the theoretical Q^2-penalty caused by inter-core XT [69]. The value of OSNR penalty is equivalent to that of Q^2-penalty. Q^2-penalty caused by inter-core XT can be expressed by:

$$\frac{Q_{\mathrm{n}}^2}{Q_{\mathrm{x}}^2} = \left(1 - Q_{\mathrm{x}}^2 \mu_{\mathrm{x,total}} C_s\right), \tag{4.1}$$

where Q_{n}^2 denotes the Q^2-factor without XT noise, Q_{x}^2 denotes the Q^2-factor affected by XT, $\mu_{\mathrm{x,total}}$ denotes total mean XT, and C_s is the value determined by the modulation format. The relationship between Q^2-penalty caused by inter-core XT and $\mu_{\mathrm{x,total}}$ is calculated by (4.1) at Q_{x}^2 = 9.8 dB (bit-error rate = 1.0×10^{-3}), as shown in Table 4.1. The XT thresholds are set for each modulation format by using Table 4.1. In this chapter, the available modulation formats are assumed to be BPSK, QPSK, 8QAM, and 16QAM. Note that the XT value corresponding to 1.0 dB OSNR penalty for BPSK is assumed to be -14 dB in this paper. Since the XT value corresponding to 1.0 dB OSNR penalty for BPSK and QPSK are assumed to be -14 dB and -17 dB, respectively, the XT thresholds for BPSK are assumed to be 3 dB larger than those for QPSK.

The transmission reach is set considering the OSNR penalty due to XT. In this chapter, the transmission reach without XT of BPSK, QPSK, 8QAM, and 16QAM are assumed to be 4000, 2000, 1000, and 500 km, respectively, using the half-distance law [61]. The transmission reach at a certain OSNR penalty value is computed where OSNR and transmission distance are proportional; the PLIs are assumed to be linear. For example, the transmission reach of the XT threshold for 1.0 dB OSNR penalty is calculated by multiplying 0.79, which is equivalent to -1.0 dB, by the transmission reaches without XT. Table 4.2 shows the transmission reaches of each modulation format at a certain OSNR penalty value. Incorporating Tables 4.1 with 4.2, Table 4.3 is obtained. Table 4.3 shows multiple thresholds and corresponding transmission reaches for each modulation format. The proposed model is the lightpath provisioning model which allocates spectrum slots based on Table 4.3. Note that the proposed model is also applicable where NPLIs are assumed by setting the transmission reach based on NPLIs.

Table 4.1: XT values [dB] corresponding to OSNR penalty for each modulation format.

Modulation format	OSNR penalty [dB]					
	0.25	0.5	0.75	1.0	1.5	2.0
BPSK	-19	-17	-15	-14	-12	-11
QPSK	-22	-20	-18	-17	-15	-14
8PSK	-27	-25	-23	-22	-21	-20
16QAM	-29	-27	-25	-24	-22	-21

Table 4.2: Transmission reach [km] of each modulation format at certain OSNR penalty due to XT.

Modulation format	OSNR penalty [dB]						
	No XT	0.25	0.5	0.75	1.0	1.5	2.0
BPSK	4000	3760	3560	3360	3160	2840	2520
QPSK	2000	1880	1780	1680	1580	1420	1260
8QAM	1000	940	890	840	790	710	630
16QAM	500	470	445	420	395	355	315

How the proposed model achieves higher spectrum efficiency than the benchmark model is demonstrated below. The benchmark model is assumed to set the XT threshold for 1 dB SNR penalty and the corresponding transmission reach, as shown in Table 4.4. The proposed model improves spectrum efficiency in two cases. In the first case, the proposed model relaxes the XT threshold by making the transmission reach short since intra-core PLIs depend on the transmission reach. In the second case, the proposed model makes transmission reach long by setting the strict XT threshold. Two examples are shown using Fig. 4.2, which corresponds to the above two cases.

In Fig. 4.2(a), which corresponds to lightpath 1 in Fig. 4.1, the transmission distance between source node s_1 and destination node d_1 is assumed to be 1200 km, and -16 dB inter-core XT is assumed to occur in the lightpath. The benchmark model cannot use QPSK in the lightpath since the XT is more than -17 dB, which is the XT threshold of QPSK. Meanwhile, the proposed model can use QPSK in the lightpath since the XT does not exceed -15 dB

Table 4.3: Transmission reach [km] corresponding to XT threshold [dB] for each modulation format.

Modulation format	XT threshold [dB]								
	No XT	-29	-27	-25	-24	-23	-22	-21	-20
BPSK	4000	3760	3760	3760	3760	3760	3760	3760	3760
QPSK	2000	1880	1880	1880	1880	1880	1880	1780	1780
8QAM	1000	940	940	890	840	840	790	710	630
16QAM	500	470	445	420	395	355	355	315	-

Modulation format	XT threshold [dB]						
	-19	-18	-17	-15	-14	-12	-11
BPSK	3760	3560	3560	3360	3160	2840	2520
QPSK	1680	1680	1580	1420	1260	-	-
8QAM	-	-	-	-	-	-	-
16QAM	-	-	-	-	-	-	-

and the transmission distance is within 1420 km.

In Fig. 4.2(b), which corresponds to lightpath 2 in Fig. 4.1, the transmission distance between s_2 and d_2 is assumed to be 1700 km, and -20 dB inter-core XT is assumed to occur in the lightpath. The benchmark model cannot use QPSK in the lightpath since the transmission distance is more than 1580 km, which is the transmission reach of QPSK. Meanwhile, the proposed model can use QPSK in the lightpath as the XT does not exceed -20 dB and the transmission distance is within 1780 km.

Since the available modulation format in the proposed model has a higher

Table 4.4: Assumption of XT threshold and transmission reach for each modulation format in benchmark model.

	XT threshold [dB]	Transmission reach [km]
BPSK	-14	3160
QPSK	-17	1580
8PSK	-22	790
16QAM	-24	395

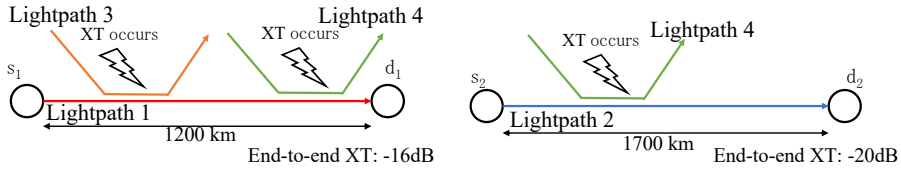

(a) Case 1. (b) Case 2.

Figure 4.2: Demonstration of spectrum efficiency of proposed model. (©2022 IEEE.)

capacity per spectrum slot than that of the benchmark model, the proposed model enhances spectrum efficiency.

4.3 Optimization problem

This section presents an optimization problem based on the proposed model and formulates it as an ILP problem.

4.3.1 Overview

We present an optimization problem based on the proposed model to minimize the maximum index of allocated spectrum slots. The optimization problem considers inter-core XT and intra-core PLIs jointly for lightpath provisioning. A set of traffic demands, each of which consists of a transmission capacity and a source-destination node pair, is given. Lightpaths for the set of traffic demands are provisioned by determining routing, modulation, spectrum, and core allocation in the optimization problem. In the lightpath provisioning, both transmission reach and XT threshold in Table 4.3 need to be satisfied. The optimization problem is formulated as an ILP problem.

4.3.2 Assumption and notations

An optical network is modeled as directed graph $G(V, E)$, where V is a set of nodes and E is a set of MCF links. We consider that a set of traffic demands, T, is given. The distance of each link is denoted by d_{ij} for $(i, j) \in E$. We assume

Table 4.5: Summary of sets in Chapter 4.

Sets	Description
T	Set of traffic demands.
V	Set of nodes.
E	Set of fiber links.
C	Set of cores in each fiber link.
α	Set of adjacent core pairs.
W	Set of spectrum slot indices.
Q	Set of modulation formats.
K	Set of XT levels.

that each MCF link has the same number of cores, and their arrangement is identical. Let C denote a set of cores in each link and α denote a set of adjacent core pairs. The same number of spectrum slots is available in each core. W denotes a set of indices of the spectrum slots. A set of modulation formats is represented by Q. Let K denote a set of XT levels, which are configured based on the XT thresholds.

The given parameters in the problem are described below. Traffic demand $t \in T$ has transmission capacity request b_t, and source and destination node pair (s_t, d_t). The capacity per spectrum slot of modulation format $q \in Q$ is represented by η_q. δ_k represents the acceptable length that a lightpath is adjacent to other lightpaths at XT level $k \in K$. r_{qk} denotes the transmission reach of modulation format $q \in Q$ in XT level $k \in K$, which corresponds to the transmission reach in Table 4.3. Let A denote a value, which is larger than or equal to any required transmission capacity, i.e., $A \geq b_t, \forall t \in T$. Let Γ denote a value, which is larger than or equal to any lightpath length, i.e., $\Gamma \geq r_{qk}, \forall q \in Q, k \in K$.

The spectrum contiguity and continuity constraints are assumed to be imposed in provisioning lightpaths. The core continuity constraint is assumed to be imposed in core allocation, i.e., the same core must be used along a lightpath. The modulation format is unchangeable over a lightpath.

The following decision variables are considered in the optimization problem.

Table 4.6: Summary of parameters in Chapter 4.

Parameters	Description
b_t	Required transmission capacity for traffic demand $t \in T$.
d_{ij}	Length of fiber link $(i, j) \in E$.
η_q	Capacity of single spectrum slot of modulation $q \in Q$.
δ_k	Maximum length that a lightpath can be adjacent to other lightpaths at XT level $k \in K$.
r_{qk}	Transmission reach of modulation $q \in Q$ in XT level $k \in K$.
A	Large value which is larger than or equal to any required transmission capacity, i.e., $A \geq b_t, \forall t \in T$.
Γ	Large value which is larger than or equal to any lightpath length, i.e., $\Gamma \geq r_{qk}, \forall q \in Q, k \in K$.

F is the maximum index of allocated spectrum slots in the network, which is minimized in the optimization problem. e_{ij}^t is a binary variable that is set to one if traffic demand $t \in T$ uses link $(i, j) \in E$, and zero otherwise. x_{cq}^t is a binary variable that is set to one if traffic demand $t \in T$ uses core $c \in C$ and modulation format $q \in Q$, and zero otherwise. y_w^t is a binary variable that is set to one if traffic demand $t \in T$ uses the wth spectrum slot ($w \in W$), and zero otherwise. $z_{wij}^{tt'}$ is a binary variable that is set to one if traffic demands of $t, t' \in T$ use adjacent cores, in the wth spectrum slot ($w \in W$) of link $(i, j) \in E$, and zero otherwise. f_t is an integer variable that represents the starting spectrum slot index for traffic demand $t \in T$. τ_k^t is a binary variable that is set to one if the lightpath for traffic demand $t \in T$ belongs to XT level $k \in K$, and zero otherwise.

The sets, parameters, and variables are summarized, as shown in Tables 4.5–4.7, respectively.

4.3.3 Formulation

The optimization problem for the proposed model is formulated as follows.

$$\min F \tag{4.2a}$$

Table 4.7: Summary of variables in Chapter 4.

Variables	Description
F	Maximum allocated spectrum slot index.
e_{ij}^{t}	Binary variable that equals one if traffic demand $t \in T$ uses link $(i, j) \in E$, and zero otherwise.
x_{cq}^{t}	Binary variable that equals one if traffic demand $t \in T$ uses core $c \in C$ and modulation format $q \in Q$, and zero otherwise.
y_{w}^{t}	Binary variable that equals one if traffic demand $t \in T$ uses the wth spectrum slot ($w \in W$), and zero otherwise.
$z_{wij}^{tt'}$	Binary variable that equals one if traffic demands $t, t' \in T$ use adjacent cores in the wth spectrum slot ($w \in W$) of link $(i, j) \in E$, and zero otherwise.
f_t	Starting spectrum slot index for traffic demand $t \in T$.
τ_{k}^{t}	Binary variable that equals one if traffic demand $t \in T$ belongs to XT level $k \in K$, and zero otherwise.

$$f_t + \sum_{w \in W} y_w^t - 1 \leq F, \forall t \in T \tag{4.2b}$$

$$\sum_{c \in C} \sum_{q \in Q} x_{cq}^t = 1, \forall t \in T \tag{4.2c}$$

$$f_t - w \leq (1 - y_w^t)|W|, \forall t \in T, w \in W \tag{4.2d}$$

$$f_t + \sum_{w' \in W} y_{w'}^t - w \geq (y_w^t - 1)|W| + 1, \forall t \in T, w \in W \tag{4.2e}$$

$$\sum_{j:(i,j) \in E} e_{ij}^t - \sum_{j:(j,i) \in E} e_{ji}^t = 1, \forall t \in T, i = s_t \tag{4.2f}$$

$$\sum_{j:(i,j) \in E} e_{ij}^t - \sum_{j:(j,i) \in E} e_{ji}^t = 0, \forall t \in T, i \in V \backslash \{s_t, d_t\} \tag{4.2g}$$

$$b_t \leq \eta_q \sum_{w \in W} y_w^t + A \left(1 - \sum_{c \in C} x_{cq}^t\right), \forall t \in T, q \in Q \tag{4.2h}$$

$$\sum_{t' \in T \backslash \{t\}} \sum_{(i,j) \in E} d_{ij} z_{wij}^{tt'} \leq \sum_{k \in K} \delta_k \tau_k^t, \forall t \in T, w \in W \tag{4.2i}$$

$$\sum_{(i,j)\in E} d_{ij} e_{ij}^{t} \leq (r_{qk} - \Gamma)\left(\sum_{c\in C} x_{cq}^{t} + \tau_{k}^{t} - 1\right) + \Gamma, \tag{4.2j}$$
$$\forall t \in T, q \in Q, k \in K$$

$$z_{wij}^{tt'} \geq \sum_{q\in Q} x_{cq}^{t} + \sum_{q'\in Q} x_{c'q'}^{t'} + y_{w}^{t} + y_{w}^{t'} + e_{ij}^{t} + e_{ij}^{t'} - 5, \tag{4.2k}$$
$$\forall t \in T, t' \in T\backslash\{t\}, (c, c') \in \alpha, w \in W, (i, j) \in E$$

$$\sum_{q\in Q} x_{cq}^{t} + \sum_{q'\in Q} x_{cq'}^{t'} + y_{w}^{t} + y_{w}^{t'} + e_{ij}^{t} + e_{ij}^{t'} \leq 5, \tag{4.2l}$$
$$\forall t \in T, t' \in T\backslash\{t\}, c \in C, w \in W, (i, j) \in E$$

$$\sum_{k\in K} \tau_{k}^{t} = 1, \forall t \in T \tag{4.2m}$$

Equation (3.9) is the objective function that minimizes the maximum index of allocated spectrum slots, F. F is determined by (4.2b). Equation (4.2b) ensures that the index of any allocated spectrum slot is not larger than F. To minimize F, F needs to be equal to the maximum index of allocated spectrum slots. Equation (4.2c) represents that one core and one modulation are determined for each traffic demand; they are not changed over a lightpath for the traffic demand. Equations (4.2d) and (4.2e) represent the spectrum contiguity constraint. The spectrum continuity constraint is ensured by the existence of y_{w}^{t}; $y_{w}^{t} = 1$ indicates that spectrum slot w is used consistently in a lightpath for traffic demand t. Equations (4.2f)–(4.2g) represent the traffic flow constraint. Equation (4.2h) ensures that spectrum slots allocated to traffic demand t provide at least the required transmission capacity b_t. Equation (4.2i) estimates the XT level of a lightpath. In the left side of (4.2i), the total length, where the lightpath for traffic demand $t \in T$ is adjacent to other lightpaths, is computed; the P-XT value of the lightpath is estimated. Equation (4.2j) ensures that the length of the lightpath for traffic demand $t \in T$ does not exceed the transmission reach corresponding to XT level k and modulation format $q \in Q$ allocated to the lightpath. Equation (4.2k) ensures that $z_{wij}^{tt'}$ is one when traffic demands of $t, t' \in T$ use adjacent cores $(c, c') \in \alpha$, respectively, in the wth spectrum slot $(w \in W)$ of link $(i, j) \in E$. Equation (4.2l) ensures that traffic demands of $t, t' \in T$ do not use the same core, $c \in C$, in the wth spectrum slot $(w \in W)$ of link $(i, j) \in E$. Equation (4.2m) represents that a lightpath

belongs to only one XT level.

4.3.4 NP-completeness

We prove the RMSCA decision problem is NP-complete. We define the RMSCA decision problem as P.

Definition P: Graph $G = (V, E)$, non-negative length d_{ij} for link $(i, j) \in E$, set of cores in each fiber link C, set of spectrum slot indices W, set of modulation formats Q, set of XT levels K, and set of traffic demands T are given. Modulation format $q \in Q$ has the capacity of a single spectrum slot and transmission reach in XT level $k \in K$. XT level $k \in K$ has acceptable adjacent length δ_k. Traffic demand $t \in T$ consists of source and destination nodes $s_t, d_t \in V$ and transmission capacity requirement b_t. Is it possible to provision all lightpaths for all traffic demands, where the maximum index of allocated spectrum slots is at most F?

Theorem: P is NP-complete.

Proof. First, P is in NP is shown. If a certificate of any instance of P is given, we need to verify that all the spectrum slots are allocated correctly, and each lightpath satisfies its traffic demand, transmission reach, and XT threshold. In addition, we need to verify that only one modulation format is used by each lightpath and only one XT level is allocated to the lightpath. The correctness of allocated spectrum slots needs to be verified that the spectrum slots satisfy spectrum contiguity, continuity, and core continuity, and different lightpaths do not use the same spectrum slots of the same core in the same link. The verification of the allocated spectrum slots is computed by $O(|T||E||C||W|)$. We can verify whether the transmission capacity provided by a lightpath satisfies the capacity requirement of corresponding traffic demand in $O(|W|)$. We can verify whether a lightpath transfers traffic flow from the source node of corresponding traffic demand to the destination node in $O(|V||E|)$. Therefore, the verification of traffic demands is computed by $O(|T|(|V||E| + |W|))$. The verification of the transmission reach of lightpaths is computed by $O(|T||E|)$. We can verify whether XT does not exceed XT threshold by computing the adjacent length of each lightpath and this is computed by $O(|T||E||C|^2|W|)$.

The verification that each lightpath uses one modulation format is computed by $O(|T||Q|)$. The verification that one XT level is allocated to each lightpath is computed by $O(|T||K|)$. As a result, we can verify a certificate of any instance of P in polynomial time of $O(|T|(|E|(|C|^2|W| + |V|) + |Q| + |K|))$.

The static lightpath establishment (SLE) problem, which is proved to be NP-complete in [70], is shown to be a subset of P as follows. Set $|C| = 1$ and $|Q| = 1$. All traffic demands are given their routes and their transmission capacity requirement is set to b. Since $|C| = 1$, the fiber is considered as single core fiber and no inter-core XT occurs, so the XT level does not need to be considered. The single slot capacity of the modulation format is set to b. The modulation format is assumed to have no transmission reach restriction, so all traffic demands require one spectrum slot. Therefore, P in this setting is the same problem as the SLE problem, in other words, the SLE problem is a subset of P.

Since P is in NP and the SLE problem, which is a known NP-complete problem, is a subset of P, P is NP-complete. □

4.4 Heuristic algorithm

This section introduces a heuristic algorithm when the ILP problem in Section 4.3.3 is not tractable. In the ILP problem presented in Section4.3.3, lightpaths for all traffic demands are provisioned at once. On the other hand, the heuristic algorithm presented here picks a set of traffic demands and provisions lightpaths for them greedily, and the lightpaths provisioned once are not changed. Let T' denote a set of traffic demands picked for provisioning lightpaths, where $T' \subset T$. When lightpaths for $|T'|$ traffic demands are provisioned, information on existing lightpaths already provisioned is given as parameters. The information includes the status of links, spectrum slots, and cores used for the existing lightpaths and the acceptable XT level and the adjacent length of each lightpath. When the lightpaths for $|T'|$ traffic demands are provisioned, the XT value of each existing lightpath, which includes the XT from additional lightpaths, is ensured not to exceed the acceptable XT level of each existing lightpath.

Another ILP problem based on the ILP problem presented in Section 4.3.3

is utilized in the heuristic algorithm. The ILP problem utilized in the heuristic algorithm determines routing, modulation, spectrum, and core allocation to the lightpaths for a set of traffic demands T' to minimize the maximum index of spectrum slots allocated to the lightpaths for T'. In this ILP problem, in addition to the input parameters of the ILP problem in Section 4.3.3, the information on lightpaths, which have been already provisioned, are given as parameters. XT levels in K are indexed so that if $k < k'$ and $k, k' \in K$, $\delta_k \leq \delta_{k'}$. Cores in C are indexed so that if $c < c'$ and $c, c' \in C$, c' has equal to or more number of neighboring cores than c. Modulation formats in Q are indexed so that, if $q < q'$ and $q, q' \in Q$, q has more capacity per slot than q'. A new decision variable, ζ^t_{cwij}, is introduced, which is a binary variable that equals one if traffic demand $t \in T'$ is adjacent to an existing lightpath, which uses core $c \in C$ of link $(i, j) \in E$ in the wth spectrum slot ($w \in W$), and zero otherwise. The number of decision variables in the ILP problem in the heuristic algorithm is $|T'|((|T'|-1)|W||E|+|C||W||E|+|E|+|W|+|C||Q|+|K|+1)+1$. The number of decision variables in the ILP problem in Section 4.3.3 is $|T|(|T||W||E|+|E|+|W|+|C||Q|+|K|+1)+1$. The ILP problem in the heuristic algorithm becomes tractable as $|T'|$ becomes small. When the heuristic algorithm is adopted, we set a suitable value to $|T'|$ for the size of a problem.

The procedure of the heuristic algorithm is described as Algorithm 1. The number of iterations in the while loop depends on $|T'|$; as $|T'|$ becomes large, the number of iterations becomes small. In contrast, the number of decision variables of the ILP problem in the heuristic algorithm becomes large as $|T'|$ becomes large.

The following set and parameters are additionally considered in the ILP problem in the heuristic algorithm. Let T_d denote a set of traffic demands whose lightpaths have been provisioned. $L^{t_d}_w$ is the adjacent length of existing lightpath for traffic demand $t_d \in T_d$ in the wth spectrum slot ($w \in W$) before provisioning lightpaths for T'. ϵ is equal to or smaller than $\frac{1}{5|T'|+1}$. Δ^{t_d} denotes the maximum length with which existing lightpath t_d can be adjacent to other active cores. $X^{t_d}_c$ is a binary parameter that equals one if traffic demand $t_d \in T_d$ uses core $c \in C$, and zero otherwise. $Y^{t_d}_w$ is a binary parameter that equals one if traffic demand $t_d \in T_d$ uses the wth spectrum slot ($w \in W$), and zero otherwise. $E^{t_d}_{ij}$ is a binary parameter that equals one if traffic demand $t_d \in T_d$ uses link

Algorithm 1 Heuristic algorithm

Input: Same as ILP problem in Section 4.3.3

Output: Same as ILP problem in Section 4.3.3

Initialize:

Existing lightpath information I

Set of traffic demands which have been provisioned lightpaths D

While: $T \neq \emptyset$ **do**

Set $T' \subset T$

Solve ILP problem with I for set of traffic demands T'

Provision lightpath for each traffic demand in T'

Update I

Remove T' from T

$(i, j) \in E$, and zero otherwise. The sets, parameters, and variables that are additionally introduced in the ILP problem are summarized in Table 4.8.

In the heuristic algorithm, the following ILP problem in (4.3a)–(4.3p) is solved for each T'.

$$\min F + \epsilon \left(\sum_{t \in T'} \left(\sum_{k \in K} \frac{\tau_{tk}}{k+1} + \sum_{q \in Q} \sum_{c \in C} \frac{c q x^t_{cq}}{|C||Q|} + \sum_{(i,j) \in E} \frac{e^t_{ij}}{|E|} + \frac{f_t}{|W|} + \sum_{w \in W} \frac{y^t_w}{|W|} \right) \right) \tag{4.3a}$$

$$f_t + \sum_{w \in W} y^t_w - 1 \leq F, \forall t \in T' \tag{4.3b}$$

$$\sum_{c \in C} \sum_{q \in Q} x^t_{cq} = 1, \forall t \in T' \tag{4.3c}$$

$$f_t - w \leq (1 - y^t_w)|W|, \forall t \in T', w \in W \tag{4.3d}$$

$$f_t + \sum_{w' \in W} y^t_{w'} - w \geq (y^t_w - 1)|W| + 1, \quad \forall t \in T', w \in W \tag{4.3e}$$

$$\sum_{j:(i,j) \in E} e^t_{ij} - \sum_{j:(j,i) \in E} e^t_{ji} = 1, \forall t \in T', i = s_t \tag{4.3f}$$

$$\sum_{j:(i,j) \in E} e^t_{ij} - \sum_{j:(j,i) \in E} e^t_{ji} = 0, \forall t \in T', i \in V \backslash \{s_t, d_t\} \tag{4.3g}$$

$$b_t \leq \eta_q \sum_{w \in W} y_w^t + A \left(1 - \sum_{c \in C} x_{cq}^t\right), \forall t \in T', q \in Q \tag{4.3h}$$

$$\sum_{(i,j) \in E} d_{ij} \left(\sum_{t' \in T' \setminus \{t\}} z_{wij}^{tt'} + \sum_{c \in C} \zeta_{cwij}^t \right) \leq \sum_{k \in K} \delta_k \tau_k^t, \quad \forall t \in T', w \in W \tag{4.3i}$$

$$L_w^{t_d} + \sum_{t \in T'} \sum_{c \in C} \sum_{(i,j) \in E} X_c^{t_d} Y_w^{t_d} E_{ij}^{t_d} d_{ij} \zeta_{cwij}^t \leq \Delta^{t_d}, \quad \forall t_d \in T_d, w \in W, \tag{4.3j}$$

$$\sum_{(i,j) \in E} d_{ij} e_{ij}^t \leq (r_{qk} - \Gamma) \left(\sum_{c \in C} x_{cq}^t + \tau_k^t - 1 \right) + \Gamma, \quad \forall t \in T', q \in Q, k \in K \tag{4.3k}$$

$$z_{wij}^{tt'} \geq \sum_{q \in Q} x_{cq}^t + \sum_{q' \in Q} x_{c'q'}^{t'} + y_w^t + y_w^{t'} + e_{ij}^t + e_{ij}^{t'} - 5, \quad \forall t \in T', t' \in T' \setminus \{t\}, (c, c') \in \alpha, w \in W, (i, j) \in E \tag{4.3l}$$

$$\zeta_{c'wij}^t \geq \sum_{q \in Q} x_{cq}^t + y_w^t + e_{ij}^t + \sum_{t_d \in T_d} X_{c'}^{t_d} Y_w^{t_d} E_{ij}^{t_d} - 3, \quad \forall t \in T', (c, c') \in \alpha, w \in W, (i, j) \in E \tag{4.3m}$$

$$\sum_{q \in Q} x_{cq}^t + \sum_{q' \in Q} x_{cq'}^{t'} + y_w^t + y_w^{t'} + e_{ij}^t + e_{ij}^{t'} \leq 5, \quad \forall t \in T', t' \in T' \setminus \{t\}, c \in C, w \in W, (i, j) \in E \tag{4.3n}$$

$$\sum_{q \in Q} x_{cq}^t + y_w^t + e_{ij}^t + \sum_{t_d \in T_d} X_{c'}^{t_d} Y_w^{t_d} E_{ij}^{t_d} \leq 3, \quad \forall t \in T', c \in C, w \in W, (i, j) \in E \tag{4.3o}$$

$$\sum_{k \in K} \tau_k^t = 1, \forall t \in T' \tag{4.3p}$$

The first term of (4.3a) represents the maximum allocated spectrum slot index. The second term of (4.3a) works for allocating the larger XT level, the core which has fewer neighboring cores, the modulation which has more capacity per spectrum slot, the route which has fewer hops, and the fewer spectrum slots which have lower indices, as possible. In the heuristic algorithm, lightpaths are iteratively provisioned for different T' until lightpaths are provisioned

for all traffic demands in T. The lightpaths for T' need to be provisioned so that the other lightpaths, which have not been provisioned, are provisioned as easily as possible. Minimizing the second term of (4.3a) aims to establish the lightpaths to keep the availability of spectrum resources as much as possible. Equations (4.3b)–(4.3h), (4.3k)–(4.3n), and (4.3p) correspond to (4.2b)–(4.2h), (4.2j)–(4.2l), and (4.2m), where T is replaced by T'. Equation (4.3i) estimates the XT level of lightpath $t \in T'$. The left side of (4.3i) computes the total length where the lightpath for traffic demand $t \in T'$ is adjacent to other lightpaths. Equation (4.3j) ensures that the adjacent length of existing lightpath for t_d does not exceed Δ^{t_d}. Equation (4.3o) ensures that traffic demand $t \in T'$ does not use the same spectrum slot that is used by existing lightpaths.

When $|T'| = 1$, (4.3a) is simplified by:

$$\min F + \epsilon \left(\sum_{t \in T'} \left(\sum_{k \in K} \frac{\tau_{tk}}{k+1} + \sum_{q \in Q} \sum_{c \in C} \frac{c x_{cq}^{t}}{|C|} + \sum_{(i,j) \in E} \frac{e_{ij}^{t}}{|E|} \right) \right). \tag{4.4}$$

Table 4.8: Summary of sets, parameters, and variables which are additionally introduced.

Sets	Description
T'	Set of traffic demands picked for provisioning lightpaths, where $T' \subset T$.
T_d	Set of allocated traffic demands whose lightpaths have been provisioned.
Parameters	**Description**
$L_w^{t_d}$	Adjacent length of existing lightpath for traffic demand $t_d \in T_d$ in the wth spectrum slot ($w \in W$) before allocating T'.
$X_c^{t_d}$	Binary parameter that equals one if traffic demand $t_d \in T_d$ uses core $c \in C$, and zero otherwise.
$Y_w^{t_d}$	Binary parameter that equals one if traffic demand $t_d \in T_d$ uses the wth spectrum slot ($w \in W$), and zero otherwise.
$E_{ij}^{t_d}$	Binary parameter that equals one if traffic demand $t_d \in T_d$ uses link $(i, j) \in E$, and zero otherwise.
Δ^{t_d}	Maximum length with which existing lightpath $t_d \in T_d$ can be adjacent to other active cores.
ϵ	Small value which is equal to or smaller than $\frac{1}{5\|T'\|+1}$.
Variables	**Description**
ζ_{cwij}^{t}	Binary variable that equals one if traffic demand $t \in T'$ is adjacent to an existing lightpath, which uses core $c \in C$ of link $(i, j) \in E$ in the wth spectrum slot ($w \in W$), and zero otherwise.

4.5 Evaluation

This section presents the performance evaluation environment followed by the numerical results of the proposed and benchmark models.

4.5.1 Evaluation environment

The proposed and benchmark models are evaluated in terms of the maximum allocated spectrum slot index and the computation time. Both proposed and benchmark models are evaluated with the ILP approach, which solves (4.2a)–(4.2m), and the heuristic algorithm presented in Section 4.4. The proposed and benchmark models allocate spectrum slots to traffic demands based on Tables 4.3 and 4.4, respectively.

The capacities of a single spectrum slot of BPSK, QPSK, 8QAM, and 16QAM are assumed to be 12.5, 25, 37.5, and 50 [Gbps], respectively [24]. The bandwidth of each spectrum slot is assumed to be 12.5 GHz [53]. The guard band for lightpaths is not considered [21]. MCF parameters can be considered by setting power-coupling coefficient, h, which is calculated by the mode-coupling coefficient, propagation constant, bending radius, and core pitch of MCF.

Intel Xeon E-2288G 3.70GHz 8-core CPU with 64GB memory is used throughout the evaluation in this chapter. The ILP problems are solved by CPLEX Optimization Studio 12.10 [65].

4.5.2 5-node network

Comparison of proposed and benchmark models

The ILP approach and the heuristic algorithm are used in a 5-node network, which is shown in Fig. 4.3. The MCF in the 5-node network is assumed to be 3-core fiber, as shown in Fig. 4.4. 50 different scenarios, each of which consists of 12 traffic demands, are generated. Each traffic demand consists of a source and destination pair, which is randomly selected from all nodes; the source and the destination nodes must be different. The transmission capacity requirement of each traffic demand is selected from uniform random values between 150 and

Table 4.9: Average and standard deviation of maximum index of allocated spectrum slots (5-node, $|T| = 12$). (©2022 IEEE.)

	Proposed						Benchmark					
$\|T'\|$	1	2	3	4	6	12	1	2	3	4	6	12
Average	8.92	8.3	8.18	7.94	7.38	6.06	9.14	8.98	8.64	8.64	8.12	7.20
Standard deviation	1.31	1.6	1.66	1.71	1.51	0.58	1.64	1.59	1.53	1.63	1.24	0.77

200 [Gbps], which are multiples of 10. The number of available spectrum slots in each core is set to 15. The power-coupling coefficient of the MCF, h, is set to 1.0×10^{-8}.

Table 4.9 shows the average and standard deviation of the maximum index of the allocated spectrum slots for 50 scenarios. When $|T'| = 12$, that is $|T'| = |T|$, we get a solution by the ILP approach. When $|T'| \neq 12$, we get a solution by the heuristic algorithm. Compared to the benchmark model, the proposed model reduces the maximum index of the allocated spectrum slots regardless of the value of $|T'|$. In the case of using the ILP approach (i.e., $|T'| = 12$), the proposed model reduces the average maximum slot index by 15.8%, compared to the benchmark model. In the case of using the heuristic algorithm with $|T'| = 1$, the proposed model reduces the average maximum slot index by 2.4%, compared to the benchmark model. The maximum index is reduced as $|T'|$ becomes large in the proposed and benchmark models.

Ten scenarios out of 50 scenarios are picked up randomly, and their results are shown in Table 4.10. In some cases of using the heuristic algorithm, e.g., scenario 6 in $|T'| = 1$, the maximum index of the proposed model is larger

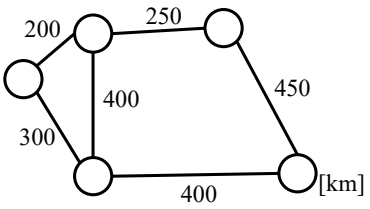

Figure 4.3: 5-node network. (©2022 IEEE.)

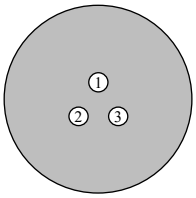

Figure 4.4: 3-core MCF. (©2022 IEEE.)

Table 4.10: Maximum index of allocated spectrum slots for ten scenarios picked up from 50 scenarios (5-node, $|T| = 12$). (©2022 IEEE.)

		Proposed						Benchmark					
	$\|T'\|$	1	2	3	4	6	12	1	2	3	4	6	12
Scenario	1	9	9	9	9	9	6	11	11	11	11	10	8
	2	9	9	9	9	9	6	10	10	10	10	8	7
	3	8	8	8	8	8	6	9	9	9	11	8	7
	4	8	8	8	8	8	5	9	9	9	9	9	7
	5	10	9	10	9	6	6	10	10	10	10	8	8
	6	9	10	7	7	6	6	8	8	7	8	7	7
	7	8	8	8	6	6	6	10	11	11	11	8	8
	8	10	10	10	8	8	6	10	10	10	10	9	8
	9	8	6	7	6	9	6	7	7	7	7	7	7
	10	9	9	9	9	7	6	10	11	10	10	8	8

Table 4.11: Average computation time in [sec] and standard deviation (5-node, $|T| = 12$). (©2022 IEEE.)

	Proposed						Benchmark					
$\|T'\|$	1	2	3	4	6	12	1	2	3	4	6	12
Average	1.53	4.93	10.65	24.65	118.70	4293.80	0.98	3.95	7.56	14.29	75.22	6433.23
Standard deviation	0.15	0.36	2.50	8.84	70.64	7942.50	0.11	0.22	0.72	5.44	49.01	10741.04

than that of the benchmark model. This is because when the proposed model uses a more spectrum-efficient modulation format, which is more sensitive to inter-core XT, than the benchmark model, the same spectrum slots in adjacent cores may be unavailable to another lightpath. If the effect of the occurrence of unavailable slots is significant in using the proposed model, the maximum index of the proposed model can be larger than that of the benchmark model. In the five cases out of the 50 cases, where the heuristic algorithm is used, the maximum index of the proposed model is larger than that of the benchmark model in this evaluation.

The average and standard deviation of the computation time for getting

results for 50 scenarios of the proposed and benchmark models are shown in Table 4.11. Since the size of each ILP problem in the heuristic algorithm or in the ILP approach becomes large as $|T'|$ becomes large, the average computation time and standard deviation become large. In the case of using the heuristic algorithm, the average computation time for getting results using the proposed model is larger than that using the benchmark model. In the case of using the ILP approach, the average computation time for getting results using the proposed model is smaller than that using the benchmark model.

The proposed and benchmark models with the heuristic algorithm are evaluated for a larger number of traffic demands ($|T| = 20$). 25 different scenarios, each of which consists of 20 traffic demands, are generated. $|T'|$ is set to be 1, 2, or 4.

Table 4.12 shows the average and standard deviation of the maximum index of the allocated spectrum slots for 25 scenarios. Compared to the benchmark model, the proposed model reduces the average of the maximum index of the allocated spectrum slots in all the examined settings of $|T'|$. The proposed model using the heuristic algorithm with $|T'| = 1$ reduces the average maximum slot index by 5.5% compared to the benchmark model using the heuristic algorithm with $|T'| = 1$. It is observed that the reduction ratio of $|T| = 20$ is larger than that of $|T| = 12$. As is the case of $|T| = 12$, the average maximum allocated slot index decreases as $|T'|$ becomes large in both proposed and benchmark models for $|T| = 20$.

Table 4.12: Average and standard deviation of maximum index of allocated spectrum slots (5-node, $|T| = 20$). (©2022 IEEE.)

	Proposed			Benchmark		
	$\|T'\|$ =1	$\|T'\| = 2$	$\|T'\| = 4$	$\|T'\|$ =1	$\|T'\| = 2$	$\|T'\| = 4$
Average	11.60	10.84	10.52	12.28	12.04	11.88
Standard deviation	2.06	1.43	0.98	1.04	0.82	0.91

$|T|$ dependence of ILP approach

Next, the proposed and benchmark models with the ILP approach are evaluated when the number of traffic demands $|T|$ is changed. Ten different scenarios

Table 4.13: Average and standard deviation of maximum index of allocated spectrum slots using ILP approach (5-node). (©2022 IEEE.)

	$\|T\|$	10	12	14	16
Average	Proposed	3.0	3.0	3.5	4.0
	Benchmark	3.6	4.0	4.0	4.1
	Reduction ratio [%]	16.7	25.0	12.5	2.4
Standard deviation	Proposed	0.0	0.0	0.5	0.0
	Benchmark	0.49	0.0	0.0	0.3

are generated for each $|T|$. The transmission capacity requirement of each traffic demand is selected from uniform random values between 75 and 100 [Gbps], which are multiples of five. The number of available spectrum slots in each core is set to 10. The power-coupling coefficient of the MCF, h, is set to 1.0×10^{-8}. $|T|$ is set to be 10, 12, 14, and 16.

Table 4.13 shows the average and standard deviation of the maximum index of the allocated spectrum slots. Compared to the benchmark model, the proposed model reduces the average of the maximum index of the allocated spectrum slots in all the examined settings of $|T|$. The reduction ratios of the average maximum index using the proposed model compared to that using the benchmark model are in the range of 2.4–25.0% in this evaluation. The trend of the reduction ratio depending on $|T|$ is not clearly observed.

Table 4.14 shows the average computation time in [sec] and its standard deviation. The computation times using the proposed and benchmark models increase as $|T|$ becomes large. As $|T|$ becomes large, the standard deviation of the average computation time becomes large. The ratio of the computation time using the proposed model to that using the benchmark model is between 0.98 and 1.75. The trend of the difference between the computation times using the proposed and benchmark models depending on $|T|$ is not clearly observed.

Table 4.14: Average computation time in [sec] and standard deviation using ILP approach (5-node). (©2022 IEEE.)

	$\|T\|$	10	12	14	16
Average	Proposed	126	333	1905	20561
	Benchmark	85.6	273	1944	11766
Standard deviation	Proposed	29.7	152.5	1250	28030
	Benchmark	54.1	93.4	2163	13015

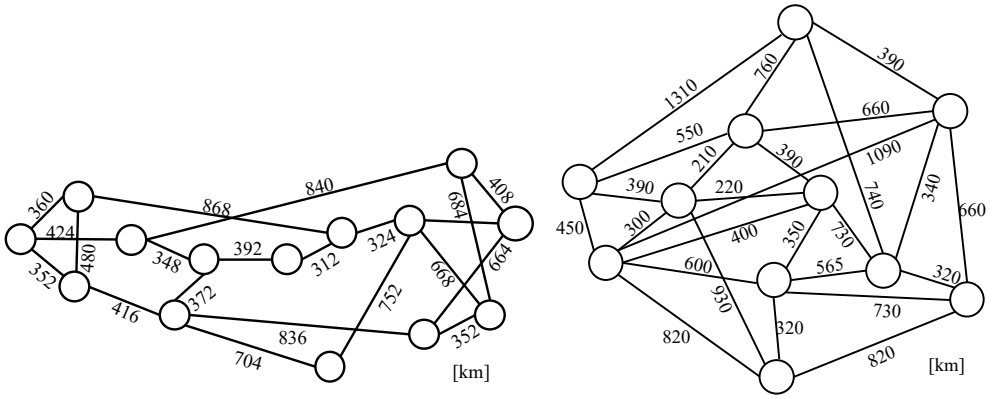

(a) NSFNET. (b) COST239 network.

Figure 4.5: Evaluation networks. (©2022 IEEE.)

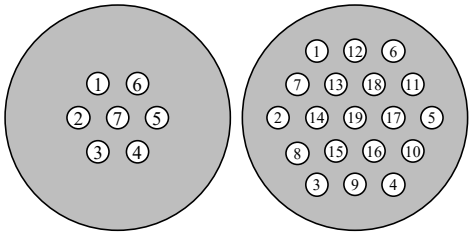

(a) 7-core MCF. (b) 19-core MCF.

Figure 4.6: Structure of MCFs. (©2022 IEEE.)

4.5.3 Larger networks

Comparison of proposed and benchmark models

Next, we consider two larger networks. We evaluate the proposed and benchmark models in NSFNET [71] and the COST239 network [63], which are shown in Fig. 4.5. The heuristic algorithm is used, where $|\boldsymbol{T}'|$ is set to one. NSFNET has 14 nodes and 42 directional links. The COST239 network has 11 nodes and 52 directional links. The MCF in a network is assumed to be 7-core fiber or 19-core fiber, whose cores are indexed, as shown in Fig. 4.6. We generate 500 traffic demands, each of which occurs between a source and destination node pair, which is randomly selected from all nodes. The transmission capacity requirement of each traffic demand is selected from uniform random

values between 100 and 500 [Gbps], which are multiples of 10. The number of available spectrum slots in each core is set to 320. We assume some scenarios in each network with each type of MCF, where the power-coupling coefficient of the MCF, h, is set to 1.0×10^{-7}, 2.0×10^{-8}, 5.0×10^{-8}, 1.0×10^{-8}, 2.0×10^{-9}, 5.0×10^{-9}, and 1.0×10^{-9}, respectively.

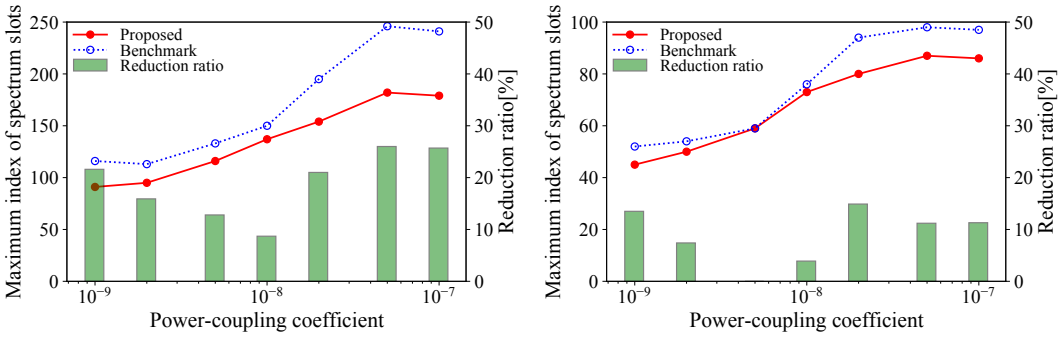

(a) NSFNET, 7-core MCF

(b) COST239, 7-core MCF

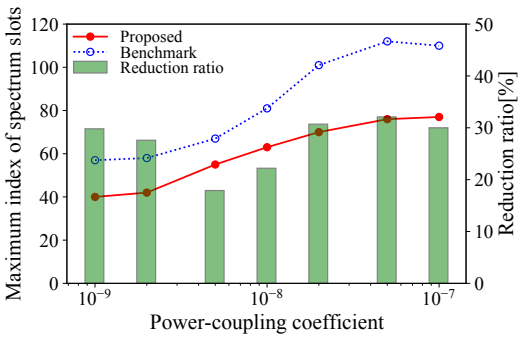

(c) NSFNET, 19-core MCF

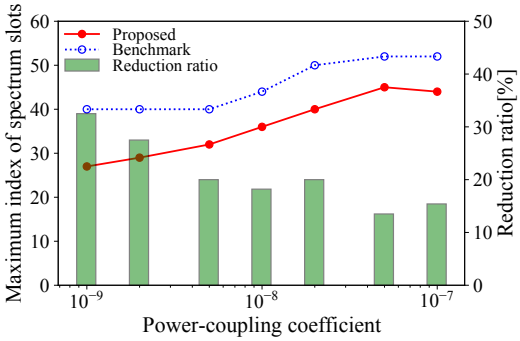

(d) COST239, 19-core MCF

Figure 4.7: Maximum index of spectrum slots in each value of power-coupling coefficient.

Fig. 4.7 shows the maximum index of the allocated spectrum slots for 500 traffic demands, including the reduction ratio of the proposed model, compared to the benchmark model. As well as in the 5-node network, the proposed model improves spectrum efficiency in NSFNET and the COST239 network. The proposed model reduces the maximum index of the allocated spectrum slots by at most 32.5% compared to the benchmark model. In each network with each power-coupling coefficient, the maximum index of the proposed model is equal

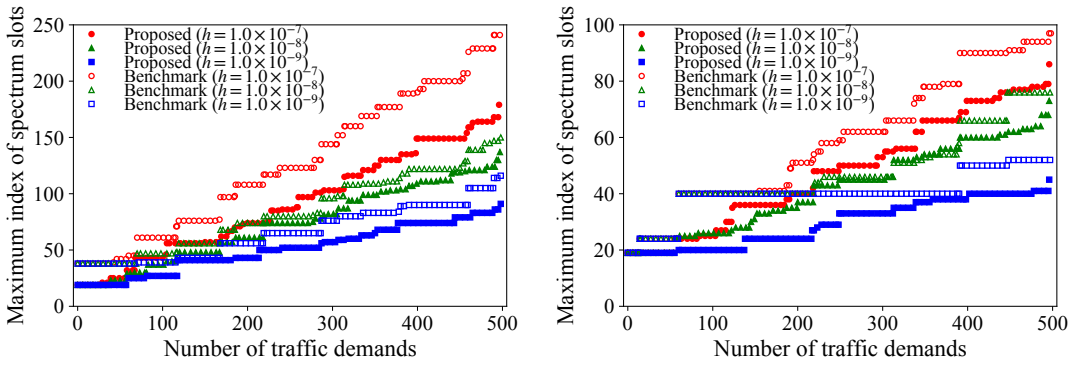

(a) NSFNET (b) COST239

Figure 4.8: Transition of maximum index of spectrum slots during running heuristic algorithm for 500 traffic demands (7-core MCF). (©2022 IEEE.)

to or less than that of the benchmark model. The maximum index of spectrum slots tends to become large as the power-coupling coefficient becomes large. This is because larger inter-core XT occurs as the power-coupling coefficient becomes large.

When h is around 1.0×10^{-9} and 1.0×10^{-7}, the reduction ratio tends to become large. Since inter-core XT becomes small as h becomes small, the effect of the proposed model that makes transmission reach longer by setting the strict XT threshold tends to appear. On the other hand, since inter-core XT becomes large as h becomes large, the effect of the proposed model that relaxes the XT threshold by making the reach shorter tends to appear.

When 19-core fiber is used, the maximum index is smaller than when the 7-core fiber is used, since more spectrum resources are available in the 19-core fiber than in the 7-core fiber. The reduction ratio of the proposed model in 19-core fiber is larger than that in the 7-core fiber. This is because it becomes easier to adjust the adjacent length as the number of cores becomes large, and the effectiveness of the proposed model due to relaxing the XT threshold and making transmission reach long clearly appears.

In the COST239 network, the maximum index is smaller than that in NSFNET. This is because the COST239 network has more links and more choices to detour a congested link than NSFNET.

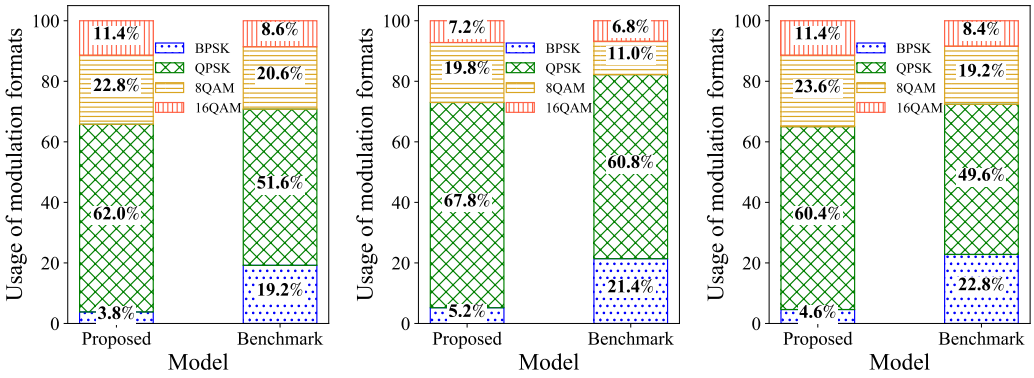

(a) $h = 1.0 \times 10^{-9}$ (b) $h = 1.0 \times 10^{-8}$ (c) $h = 1.0 \times 10^{-7}$

Figure 4.9: Usage of modulation formats (NSFNET, 7-core MCF). (©2022 IEEE.)

Fig. 4.8 shows the transition of the maximum index of the allocated spectrum slots while running the heuristic algorithm for 500 traffic demands, where the 7-core fiber is used. This shows that when the number of traffic demands is smaller than 500, the proposed model improves spectrum efficiency, compared to the benchmark model. The larger the number of traffic demands is, the higher the workload in the network is. In this evaluation, regardless of the workload in the network, the proposed model improves spectrum efficiency compared to the benchmark model.

Figs. 4.9–4.12 show the usage of modulation formats when $h = 1.0 \times 10^{-7}, 1.0 \times 10^{-8}$, and 1.0×10^{-9}. In the examined networks and the number of cores, regardless of the power-coupling coefficient, there are more opportunities in the proposed model to use spectrum-efficient modulation formats such as QPSK, 8QAM, and 16QAM than in the benchmark model. As a result, the proposed model uses fewer spectrum slots and suppresses the maximum index of the allocated spectrum slots compared to the benchmark model.

Comparing Fig. 4.9 and Fig. 4.10, and Fig. 4.11 and Fig. 4.12, we observe that there are more opportunities in the COST239 network to use spectrum-efficient modulation formats than in NSFNET. This also makes the maximum index in the COST239 network smaller than that in NSFNET.

Comparing Fig. 4.9 and Fig. 4.11, and Fig. 4.10 and Fig. 4.12, we ob-

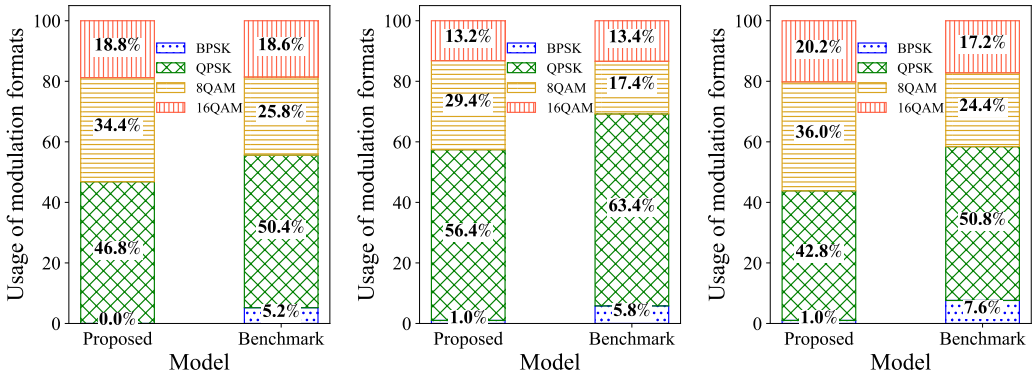

(a) $h = 1.0 \times 10^{-9}$ (b) $h = 1.0 \times 10^{-8}$ (c) $h = 1.0 \times 10^{-7}$

Figure 4.10: Usage of modulation formats (COST239 network, 7-core MCF). (©2022 IEEE.)

serve that when the 19-core fiber is used, there are more opportunities to use spectrum-efficient modulation formats than when the 7-core fiber is used. This also makes the maximum index when the 19-core fiber is used smaller than that when the 7-core fiber is used. The heuristic algorithms use the most efficient modulation format possible, so spectral slots are assigned to lightpaths to suppress adjacent lengths. Since when the 19-core fiber is used, it is easier to suppress the adjacent length than when the 7-core fiber is used, there are more opportunities to use spectrum-efficient modulation formats.

The computation time for running the heuristic algorithm is shown in Table 4.15. The difference between the computation times of the proposed and benchmark models is comparable, compared to the difference in the evaluation in the 5-node network. This is because the effect of the difference between the proposed and benchmark models, which comes from the fineness in the XT level setting, becomes small as the network and the number of traffic demands become large. When the 19-core fiber is used, it takes more computation time than when the 7-core fiber is used. This is because there are more decision variables in the ILP problem in the heuristic algorithm in the case of the 19-core fiber. The computation time in the COST239 network is larger than that in NSFNET.

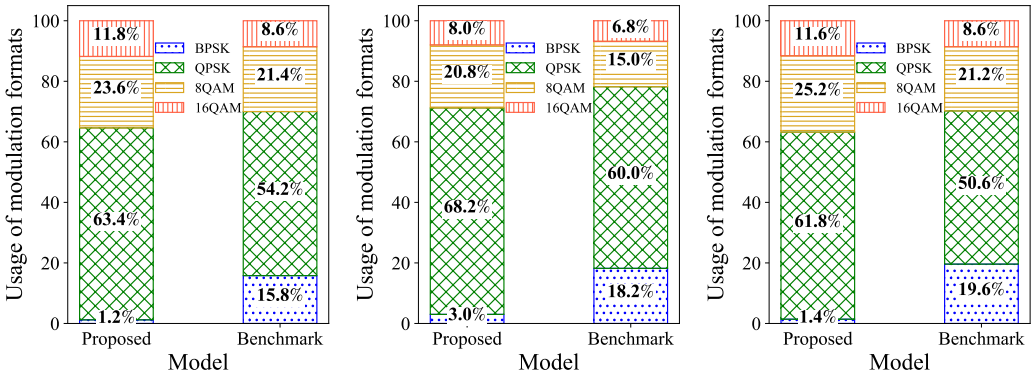

(a) $h = 1.0 \times 10^{-9}$ (b) $h = 1.0 \times 10^{-8}$ (c) $h = 1.0 \times 10^{-7}$

Figure 4.11: Usage of modulation formats (NSFNET, 19-core MCF). (©2022 IEEE.)

$|T'|$ dependence of heuristic algorithm

The proposed model with the heuristic algorithm is evaluated, where $|T'| = 2$ in NSFNET and the COST239 network. The MCF used in a network is assumed to be 7-core. The power-coupling coefficient of the MCF is assumed to be $1.0{\times}10^{-8}$. 400 and 500 traffic demands are given in NSFNET and the COST239 network, respectively. The other settings are the same as those in Section 4.5.3.

Fig. 4.13 shows the transition of the maximum index of the allocated spectrum slots using the proposed model with the heuristic algorithm with $|T'| = 1$ and 2. It is observed that the maximum indices of allocated spectrum slots are comparable for $|T'| = 1$ and $|T'| = 2$. When a spectrum-efficient modulation format, which is sensitive to inter-core XT, is used in the same spectrum slots in adjacent cores can be unavailable to another lightpath. If the effect of the occurrence of unavailable slots is significant using the algorithm with $|T'| = 2$, the maximum index can be larger than that with $|T'| = 1$. In a large network, the possibility that lightpaths for two traffic demands share a link is less; as the network becomes large, the advantage of simultaneously provisioning lightpaths for multiple traffic demands becomes smaller in this case. In this evaluation, the spectrum efficiency of the heuristic algorithm with $|T'| = 1$ and 2 is comparable.

Table 4.16 shows the computation time for the heuristic algorithm with

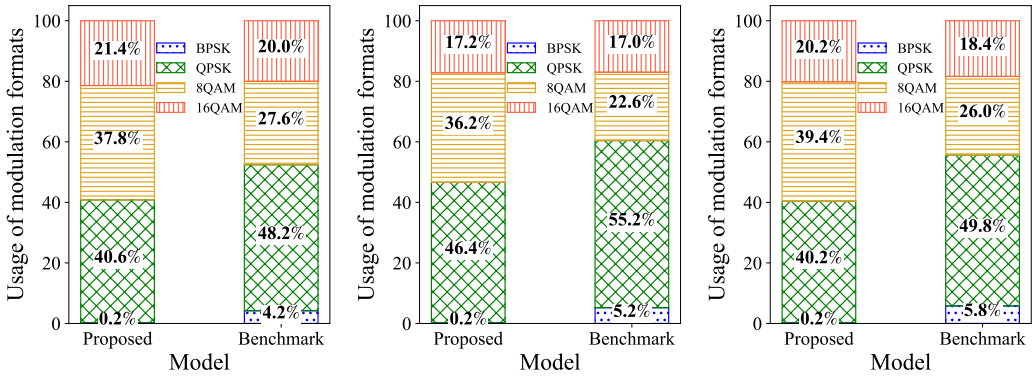

(a) $h = 1.0 \times 10^{-9}$ (b) $h = 1.0 \times 10^{-8}$ (c) $h = 1.0 \times 10^{-7}$

Figure 4.12: Usage of modulation formats (COST239 network, 19-core MCF). (©2022 IEEE.)

each $|T'|$. The computation time using the heuristic algorithm with $|T'| = 1$ is smaller than that with $|T'| = 2$. Therefore, the heuristic algorithm with $|T'| = 1$ is preferable for our evaluation.

4.6 Summary

This chapter proposed an RMSCA model, which jointly considers inter-core XT and intra-core PLIs for SS-EONs. In order to deal with inter-core XT and intra-core PLIs jointly, the proposed model considers the OSNR penalty. The proposed model sets multiple XT thresholds and their corresponding transmission reaches by considering the OSNR penalty due to XT. An optimization problem is presented and formulated as an ILP problem. A heuristic algorithm for the proposed model is introduced. The proposed model is evaluated with the ILP approach and the heuristic algorithm. In the case of using the ILP approach for 12 traffic demands in the 5-node network, it was observed that the proposed model reduces the average allocated maximum slot index by 15.8% compared to the benchmark model. Numerical results observed that the proposed model reduces the maximum index of the allocated spectrum slots by at most 32.5% in the evaluation scenarios compared to the benchmark model. It was observed that the proposed model uses a more spectrum-efficient

Table 4.15: Computation time [sec] for running heuristic algorithm. (©2022 IEEE.)

MCF	Network	Model	Power-coupling coefficient 1.0×10^{-9}	2.0×10^{-9}	5.0×10^{-9}	1.0×10^{-8}
7-core	NSFNET	Proposed	8398	8117	9929	9016
		Benchmark	9306	9688	10285	9597
	COST239	Proposed	5986	6089	6270	5993
		Benchmark	5577	5958	6141	5370
19-core	NSFNET	Proposed	12139	13083	14349	14894
		Benchmark	14190	14987	16838	14653
	COST239	Proposed	9490	9900	9681	9740
		Benchmark	8702	9024	9538	9317

MCF	Network	Model	Power-coupling coefficient 2.0×10^{-8}	5.0×10^{-8}	1.0×10^{-7}
7-core	NSFNET	Proposed	9189	7572	6703
		Benchmark	10602	9582	6993
	COST239	Proposed	5870	4881	4642
		Benchmark	5366	4727	4549
19-core	NSFNET	Proposed	12755	9776	9621
		Benchmark	14873	12987	9485
	COST239	Proposed	9143	8487	8386
		Benchmark	9790	8670	8204

modulation format than the benchmark model. The computation times of the proposed and benchmark models are comparable in the evaluation in NSFNET and the COST239 network.

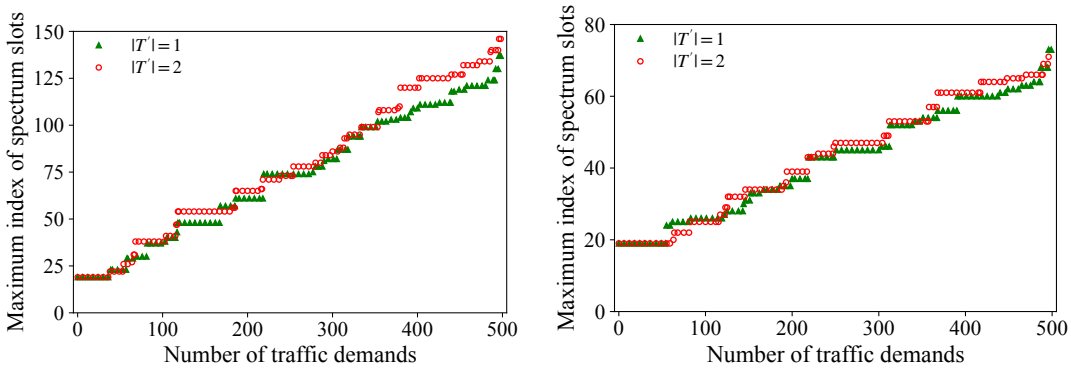

(a) NSFNET (b) COST239

Figure 4.13: Transition of maximum index of spectrum slots during running heuristic algorithm (7-core MCF). (©2022 IEEE.)

Table 4.16: Computation time [sec] for running heuristic algorithm using each $|\boldsymbol{T}'|$. (©2022 IEEE.)

Network	$\|\boldsymbol{T}'\|$	Computation time
NSFNET	1	5161
	2	1559×10^3
COST239	1	5993
	2	1784×10^3

Chapter 5

Lightpath provisioning model considering crosstalk-derived fragmentation in spectrally-spatially EONs

5.1 Fragmentation-aware model with XT-estimated approach

This section presents a fragmentation-aware model with the XT-estimated approach. The fragmentation-aware model estimates the XT value to satisfy the XT threshold and uses a fragmentation metric.

The XT-estimated approach is described in Section 1.2.1. This chapter discusses the XT-estimated approach with the WC-XT as the existing fragmentation-aware model with the XT-estimated approach [28].

To evaluate fragmentation in a network, several fragmentation metrics are introduced in [28]. One of them is the root mean square factor (RMSF). The fragmentation metric of each link is calculated using a metric. The fragmentation of a link is called link fragmentation. The RMSF accounts for the sizes of all vacant segments, the number of vacant segments, and the highest allocated slot index on each core. The RMSF decreases when (i) the highest slot

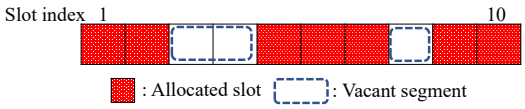

Figure 5.1: Example of allocated slots and vacant segments in a core of a link. (©2023 Elsevier.)

allocated in each core decreases, (ii) the number of vacant segments decreases on each core, and (iii) the size of larger segments increases at the cost of decreasing the size of smaller ones. The link fragmentation using the RMSF of link (i, j) is presented by:

$$\frac{1}{|C|}\sum_{c\in C}\frac{F_{cij}|\Xi_{cij}|}{\sqrt{\frac{\sum_{\xi\in\Xi_{cij}} Z_\xi^2}{|\Xi_{cij}|}}}, \tag{5.1}$$

where C is a set of cores, F_{cij} is the maximum index of allocated spectrum slots in core $c \in C$ of link (i, j), Ξ_{cij} is a set of vacant segments in core $c \in C$ of link (i, j), and Z_ξ is a size of vacant segment ξ. Fig. 5.1 shows an example of allocated slots and vacant segments in a core of a link. In this example, $F_{cij} = 10$ and $|\Xi_{cij}| = 2$. The whole network fragmentation is calculated as an average of link fragmentation [28].

5.2 Proposed model

The proposed model suppresses both fragmentation caused by allocating spectrum slots to lightpaths and due to inter-core XT. In the proposed model, vacant spectrum slots are classified into available vacant slots and unavailable vacant slots. The XT-estimated approach allocates spectrum slots to a lightpath so that the XT value of each lightpath does not exceed its XT threshold. If a lightpath cannot accept more XT than that currently accepted, the vacant spectrum slots adjacent to the lightpath become unavailable vacant slots.

The proposed model provisions a lightpath for a traffic demand under the existence of lightpaths that have already been provisioned. Since the transmission distance of an existing lightpath is constant, i.e., its route is not changed, the WC-XT value of the existing lightpath depends on the lightpath-adjacent

number. The maximum lightpath-adjacent number is called the acceptable lightpath-adjacent number, which is denoted by n_p. The XT threshold of an existing lightpath can be translated into the acceptable lightpath-adjacent number.

The fragmentation due to inter-core XT is explained using Fig. 5.2. Two lightpaths are provisioned in the network, as shown in Fig. 5.2(a). Each fiber in a network is assumed to be a 7-core MCF. Lightpath 1 is allocated to core 2 and lightpath 2 is allocated to core 1, as shown in Fig. 5.2b. Spectrum slots are allocated to each lightpath, as shown in Fig. 5.2c. The lightpath-adjacent numbers, N_w, of lightpaths 1 and 2 in slots 3 and 4 are one; those of other slots are zero. The power-coupling coefficient of the MCF, h, is assumed to be 1.0×10^{-8}. The transmission distance, L', of lightpaths 1 and 2 are assumed to be 1000 km. The XT thresholds of lightpaths 1 and 2 are assumed to be -20 dB and -15 dB, respectively. The acceptable lightpath-adjacent number, n_p, of lightpaths 1 and 2 can be calculated to be one and three, respectively, by (1.2). Since lightpath 1 is adjacent to lightpath 2 in core 1 at slots 3 and 4, cores 3 and 7 at slots 3 and 4 on links A-B and B-D cannot be used by any other lightpath. Therefore, slots 3 and 4 in cores 3 and 7 on links A-B and B-D are unavailable vacant slots. On the other hand, slots 1 and 2 are available in cores 1, 3, and 7, since there is no lightpath adjacent to lightpath 1 in slots 1 and 2. Since the acceptable lightpath-adjacent number of lightpath 2 is more than one, any spectrum slots do not become unavailable because of the XT threshold of lightpath 2. In this way, unavailable vacant slots arise due to inter-core XT.

Though vacant slots in core 3 are contiguous, available vacant slots 1 and 2 become fragmented slots due to the existence of unavailable vacant slots 3 and 4. This is why inter-core XT can cause fragmentation. In this thesis, it is called the fragmentation due to inter-core XT.

As described above, the proposed model considers the fragmentation due to inter-core XT. The proposed model classifies vacant slots into available ones and unavailable ones when calculating the metric, which is different from existing works that use a fragmentation metric that does not reflect fragmentation due to inter-core XT.

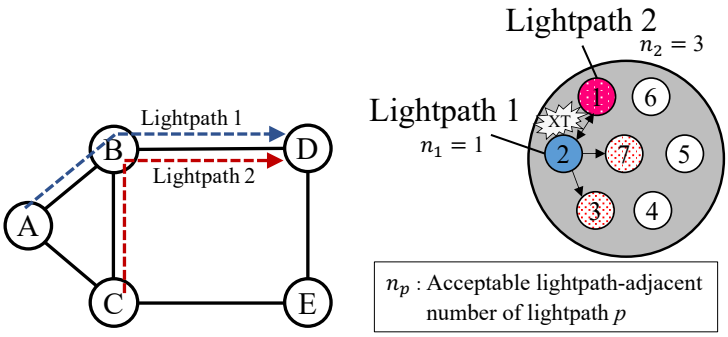

(a) Network and lightpaths.

(b) Core utilization in link B–D (Cores 3 and 7 become unavailable due to XT threshold of lightpath 1).

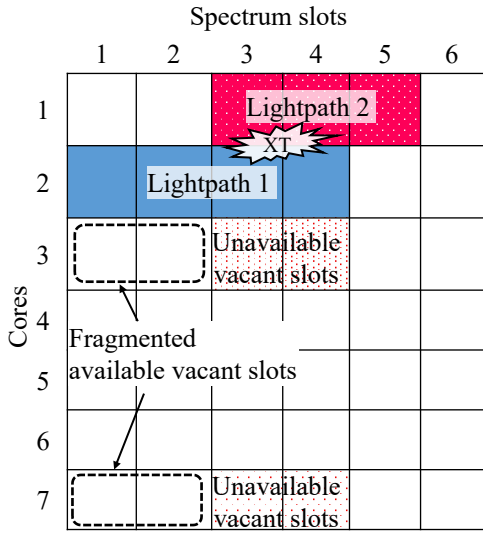

(c) Spectrum slot utilization in link B–D (Slots 3 and 4 in cores 3 and 7 become unavailable due to XT threshold of lightpath 1).

Figure 5.2: Unavailable vacant slots and fragmented slots due to inter-core XT. (©2023 Elsevier.)

5.3 Lightpath provisioning problem

5.3.1 Overview

This chapter presents a lightpath provisioning problem using the proposed model to suppress the fragmentation. The fragmentation in the lightpath provisioning problem is considered by classifying vacant spectrum slots into available vacant slots and unavailable vacant slots. A traffic demand, which consists of a transmission capacity and a source-destination node pair, is given. A lightpath for the traffic demand is provisioned by determining routing, modulation, spectrum, and core allocation in the problem. When a lightpath is provisioned, both XT threshold and transmission reach, which are different by each modulation format, need to be satisfied. The lightpath provisioning problem is formulated as an ILP problem that minimizes the weighted sum of three factors, which are the highest index of allocated or unavailable vacant slots, the number of available vacant segments, and the size of available vacant segments in each core of each link. The objective function aims to suppress the network fragmentation, which is presented in Section 5.1.

Each time a traffic demand arrives, the ILP problem for the traffic demand is solved to minimize the objective function at the time of arrival of the traffic demand. This process of provisioning lightpaths is called the ILP approach hereafter.

5.3.2 Assumption and notations

A traffic demand is given in an optical network (V, E), where V is a set of nodes and E is a set of MCF links. The lightpath for traffic demand is denoted by p_{new}, and RMSCA of p_{new} is decided in the optimization problem. In the network, there is a set of existing lightpaths P. When provisioning lightpath p_{new}, the RMSCA of existing lightpaths is not changed. The length of each link is denoted by d_{ij} for $(i, j) \in E$. It is assumed that each MCF link has the same number of cores, and their arrangement is identical. Let C denote a set of cores in each link and Φ denote a set of adjacent core pairs. The same number of spectrum slots is available in each core. W denotes a set of indices of the spectrum slots. A set of modulation formats is represented by Q.

The given parameters in the problem are described below. The traffic demand requires transmission capacity b and has source and destination node pair (s, d). The capacity per spectrum slot of modulation format $q \in Q$ is represented by η_q. The transmission reach of modulation format $q \in Q$ is represented by r_q. The XT threshold for modulation $q \in Q$ is represented by θ_q. The power-coupling coefficient of an MCF in the network is represented by h. When lightpath p_{new} is provisioned, information on existing lightpaths that have already been provisioned is given as parameters. The information includes the status of links, spectrum slots, and cores used for the existing lightpaths and the acceptable adjacent number of each lightpath. X_c^p is a binary parameter that equals one if lightpath $p \in P$ uses core $c \in C$, and zero otherwise. Y_w^p is a binary parameter that equals one if lightpath $p \in P$ uses the wth spectrum slot ($w \in W$), and zero otherwise. E_{ij}^p is a binary parameter that equals one if lightpath $p \in P$ uses link $(i, j) \in E$, and zero otherwise. A_{cwij} is a binary parameter that equals one if the wth spectrum slot ($w \in W$) in core $c \in C$ of link $(i, j) \in E$ is allocated slot, and zero otherwise. U_{cwij} is a binary parameter that equals one if the wth spectrum slot ($w \in W$) in core $c \in C$ of link $(i, j) \in E$ is unavailable vacant slot, and zero otherwise. N_w^p is an integer parameter that denotes the number of lightpaths that can be additionally adjacent to lightpath $p \in P$ in the wth spectrum slot ($w \in W$). N_w^p is calculated by the acceptable lightpath-adjacent number of p and the number of lightpath-adjacent cores of p in the wth spectrum slot ($w \in W$). The acceptable lightpath-adjacent number of p is calculated by (1.2) using the XT threshold of p. Γ_w^p is a binary parameter that equals one if $N_w^p = 1$, and zero otherwise. ϵ_1 is a fragmentation parameter of the maximum index of allocated or unavailable spectrum slots. ϵ_2 is a fragmentation parameter of the number of available vacant segments. ϵ_3 is a fragmentation parameter of the size of available vacant segments. ϵ_1, ϵ_2, and ϵ_3 are positive values; they are used in Section 5.3.3 as weights to deal with network fragmentation. Let α denote a value, which is larger than or equal to the required transmission capacity, i.e., $\alpha \geq b$. Let β denote a value, which is larger than or equal to the number of cores in a fiber, i.e., $\beta \geq |C|$. Let γ denote a value, which is larger than or equal to any lightpath length, i.e., $\gamma \geq r_q, \forall q \in Q$. Let δ denote a value, which is larger than or equal to the number of links in the network,

i.e., $\delta \geq |E|$.

The spectrum contiguity and continuity constraints are imposed in provisioning lightpaths. It is assumed that a switch in the network cannot change the core during transmission; the core continuity constraint is imposed. The modulation format is unchangeable over a lightpath.

When lightpath p_{new} is provisioned, the XT value of each existing lightpath is ensured not to exceed the acceptable XT value of each existing lightpath.

The following decision variables are considered in the lightpath provisioning problem. e_{ij} is a binary variable that is set to one if lightpath p_{new} uses link $(i, j) \in E$, and zero otherwise. x_c is a binary variable that is set to one if lightpath p_{new} uses core $c \in C$, and zero otherwise. y_w is a binary variable that is set to one if lightpath p_{new} uses the wth spectrum slot ($w \in W$), and zero otherwise. m_q is a binary variable that is set to one if lightpath p_{new} uses modulation format $q \in Q$, and zero otherwise. n is an integer variable that denotes the acceptable number of adjacent cores for lightpath p_{new}. ψ^p is a binary variable that equals one if lightpath p_{new} shares a link with lightpath $p \in P$, and zero otherwise. ζ^p is a binary variable that equals one if lightpath p_{new} is adjacent to lightpath $p \in P$ in any spectrum slot, and zero otherwise. a_{cw} is a binary variable that equals one if lightpath p_{new} is adjacent to an existing lightpath in the wth spectrum slot ($w \in W$) in core $c \in C$, and zero otherwise. u_{cw} is a binary variable that equals one if the wth spectrum slot ($w \in W$) in core $c \in C$ is an unavailable vacant slot due to the XT threshold of lightpath p_{new}, and zero otherwise. υ_{cwij} is a binary variable that equals one if the wth spectrum slot ($w \in W$) in core $c \in C$ of link $(i, j) \in E$ is an unavailable vacant slot by provisioning lightpath p_{new}, and zero otherwise. l_{ij} is an integer variable, which is equal to ne_{ij}. f is an integer variable that represents the starting spectrum slot index of lightpath p_{new}. s_{cwij} is a binary variable that equals one if the wth spectrum slot ($w \in W$) in core $c \in C$ of link $(i, j) \in E$ is used for a lightpath or unavailable, and zero otherwise. F_{cij} is an integer variable that represents the maximum index of allocated or unavailable spectrum slots in core $c \in C$ of link $(i, j) \in E$. B_{cij} is an integer variable that represents the number of available vacant segments in core $c \in C$ of link $(i, j) \in E$. z^k_{cwij} is a binary variable that equals one if $s_{cw'ij} = 0, \forall w' \in [w-k+1, w]$, in core $c \in C$ of link $(i, j) \in E$, and zero otherwise.

Table 5.1: Summary of sets in Chapter 5.

Sets	Description
V	Set of nodes.
E	Set of fiber links.
P	Set of existing lightpaths.
C	Set of cores in each fiber link.
Φ	Set of adjacent core pairs.
W	Set of spectrum slot indices.
Q	Set of modulation formats.

σ^k_{cwij} is a binary variable that equals one if $z^k_{cwij} = 1$ and $s_{c(w+1)ij} = 1$, and zero otherwise. Let $s_{c(|W|+1)ij}$ and s_{c0ij} equal one.

The sets, parameters, and variables used in this chapter are summarized in Tables 5.1–5.3, respectively.

Table 5.2: Summary of parameters in Chapter 5.

Parameters	Description
b	Required transmission capacity for the traffic demand.
d_{ij}	Length of fiber link $(i, j) \in E$.
η_q	Capacity of single spectrum slot of modulation $q \in Q$.
r_q	Transmission reach of modulation $q \in Q$.
θ_q	XT threshold value for modulation format $q \in Q$.
h	Power-coupling coefficient of the MCF in the network.
X^p_c	Binary parameter that equals one if lightpath $p \in P$ uses core $c \in C$, and zero otherwise.
Y^p_w	Binary parameter that equals one if lightpath $p \in P$ uses the wth spectrum slot ($w \in W$), and zero otherwise.
E^p_{ij}	Binary parameter that equals one if lightpath $p \in P$ uses link $(i, j) \in E$, and zero otherwise.

Parameters	Description
A_{cwij}	Binary parameter that equals one if the wth spectrum slot ($w \in W$) in core $c \in C$ of link $(i, j) \in E$ is allocated slot, and zero otherwise.
U_{cwij}	Binary parameter that equals one if the wth spectrum slot ($w \in W$) in core $c \in C$ of link $(i, j) \in E$ is unavailable vacant slot, and zero otherwise.
N_w^p	Integer parameter that denotes the number of lightpaths that can be additionally adjacent to lightpath $p \in P$ in the wth spectrum slot ($w \in W$).
Γ_w^p	Binary parameter that equals one if $N_w^p = 1$, and zero otherwise.
ϵ_1	Fragmentation parameter of the maximum index of allocated or unavailable spectrum slots.
ϵ_2	Fragmentation parameter of the number of available vacant segments.
ϵ_3	Fragmentation parameter of the size of available vacant segments.
α	Large value which is larger than or equal to the required transmission capacity, i.e., $\alpha \geq b$.
β	Large value which is larger than or equal to the number of cores in a fiber, i.e., $\beta \geq \|C\|$.
γ	Large value which is larger than or equal to any lightpath length, i.e., $\gamma \geq r_q, \forall q \in Q$.
δ	Large value which is larger than or equal to the number of links in the network, i.e., $\delta \geq \|E\|$.

Table 5.3: Summary of variables in Chapter 5.

Variables	Description
e_{ij}	Binary variable that is set to one if lightpath p_{new} uses link $(i, j) \in E$, and zero otherwise.

Variables	Description
x_c	Binary variable that is set to one if lightpath p_{new} uses core $c \in C$, and zero otherwise.
y_w	Binary variable that is set to one if lightpath p_{new} uses the wth spectrum slot ($w \in W$), and zero otherwise.
m_q	Binary variable that is set to one if lightpath p_{new} uses modulation format $q \in Q$, and zero otherwise.
n	Integer variable that denotes the acceptable lightpath-adjacent number of lightpath p_{new}.
ψ^p	Binary variable that equals one if lightpath p_{new} shares a link with lightpath $p \in P$, and zero otherwise.
ζ^p	Binary variable that equals one if lightpath p_{new} is adjacent to lightpath $p \in P$ in any spectrum slot, and zero otherwise.
a_{cw}	Binary variable that equals one if lightpath p_{new} is adjacent to an existing lightpath in the wth spectrum slot ($w \in W$) in core $c \in C$, and zero otherwise.
u_{cw}	Binary variable that equals one if the wth spectrum slot ($w \in W$) in core $c \in C$ is an unavailable vacant slot due to the XT threshold of lightpath p_{new}, and zero otherwise.
υ_{cwij}	Binary variable that equals one if the wth spectrum slot ($w \in W$) in core $c \in C$ of link (i, j) adjacent to an existing lightpath is an unavailable vacant slot by provisioning lightpath p_{new}, and zero otherwise.
l_{ij}	Integer variable, which is equal to ne_{ij}.
f	Integer variable that represents the starting spectrum slot index of lightpath p_{new}.
s_{cwij}	Binary variable that equals one if the wth spectrum slot ($w \in W$) in core $c \in C$ of link $(i, j) \in E$ is used for a lightpath or unavailable, and zero otherwise.
F_{cij}	Integer variable that represents the maximum index of allocated or unavailable spectrum slots in core $c \in C$ of link $(i, j) \in E$.

Variables	Description
B_{cij}	Integer variable that represents the number of available vacant segments in core $c \in C$ of link $(i,j) \in E$.
z^k_{cwij}	Binary variable that equals one if $s_{cw'ij} = 0, \forall w' \in [w-k+1, w]$ in core $c \in C$ of link $(i,j) \in E$, and zero otherwise.
σ^k_{cwij}	Binary variable that equals one if $z^k_{cwij} = 1$ and $s_{c(w+1)ij} = 1$, and zero otherwise.

5.3.3 Formulation

The lightpath provisioning problem for the proposed model is formulated as follows:

$$\min \sum_{c \in C} \sum_{(i,j) \in E} \left(\epsilon_1 F_{cij} + \epsilon_2 B_{cij} + \epsilon_3 \sum_{w \in W} \sum_{k=1}^{w} (-k^2 \sigma^k_{cwij}) \right), \tag{5.2a}$$

s.t.

$$\sum_{c \in C} x_c = 1, \tag{5.2b}$$

$$\sum_{q \in Q} m_q = 1, \tag{5.2c}$$

$$f - w \leq (1 - y_w)|W|, \forall w \in W, \tag{5.2d}$$

$$f + \sum_{w' \in W} y_{w'} - w \geq (y_w - 1)|W| + 1, \forall w \in W, \tag{5.2e}$$

$$\sum_{j:(i,j) \in E} e_{ij} - \sum_{j:(j,i) \in E} e_{ji} = 1, i = s, \tag{5.2f}$$

$$\sum_{j:(i,j) \in E} e_{ij} - \sum_{j:(j,i) \in E} e_{ji} = 0, \forall i \in V \backslash \{s, d\}, \tag{5.2g}$$

$$b \leq \eta_q \sum_{w \in W} y_w + \alpha(1 - m_q), \forall q \in Q, \tag{5.2h}$$

$$\sum_{(i,j) \in E} d_{ij} e_{ij} \leq (r_q - \gamma) m_q + \gamma, \forall q \in Q, \tag{5.2i}$$

$$\sum_{(i,j) \in E} E^p_{ij} e_{ij} \leq \delta \psi^p, \forall p \in P, \tag{5.2j}$$

$$\zeta^p \geq x_c + y_w + \psi^p - 2,$$

$$\forall p \in P, (c, c') \in \Phi, w \in W, \text{ if } X^p_{c'} Y^p_w = 1, \tag{5.2k}$$

$$\zeta^p + y_w \leq 1, \forall p \in P, w \in W, \text{ if } N^p_w = 0, \tag{5.2l}$$

$$\left(\frac{\theta_q}{h} - \gamma\right) m_q + \gamma \geq \sum_{(i,j) \in E} l_{ij} d_{ij}, \forall q \in Q, \tag{5.2m}$$

$$l_{ij} \geq n - \beta(1 - e_{ij}), \forall (i, j) \in E, \tag{5.2n}$$

$$l_{ij} \leq \beta e_{ij}, \forall w \in W, (i, j) \in E, \tag{5.2o}$$

$$n \geq \sum_{c \in C} a_{cw}, \forall w \in W, \tag{5.2p}$$

$$a_{c'w} \geq x_c + y_w + e_{ij} - 2,$$
$$\forall (c, c') \in \Phi, w \in W, (i, j) \in E, \text{ if } A_{cwij} = 1, \tag{5.2q}$$

$$x_c + y_w + e_{ij} \leq 3 - (A_{cwij} + U_{cwij}),$$
$$\forall c \in C, w \in W, (i, j) \in E, \tag{5.2r}$$

$$\beta(1 - u_{cw} + a_{cw}) \geq n - \sum_{c' \in C} a_{c'w}, \forall c \in C, w \in W, \tag{5.2s}$$

$$x_c - u_{c'w} - a_{c'w} \leq n - \sum_{c'' \in C} a_{c''w}, \forall (c, c') \in \Phi, w \in W, \tag{5.2t}$$

$$|P|(\upsilon_{cwij} - y_w + 1) \geq \sum_{p \in P} \Gamma^p_w X^p_{c'} Y^p_w E^p_{ij} \zeta^p,$$
$$\forall (c, c') \in \Phi, w \in W, (i, j) \in E, \tag{5.2u}$$

$$s_{cwij} \geq x_c + y_w + u_{cw} - 1,$$
$$\forall c \in C, w \in W, (i, j) \in E, \tag{5.2v}$$

$$|P| s_{cwij} \geq \upsilon_{cwij} + A_{cwij} + U_{cwij},$$
$$\forall c \in C, w \in W, (i, j) \in E, \tag{5.2w}$$

$$F_{cij} \geq w s_{cwij}, \forall c \in C, w \in W, (i, j) \in E, \tag{5.2x}$$

$$\sum_{w'=w-k+1}^{w} \left(1 - s_{cw'ij}\right) - k + 1 \leq z^k_{cwij},$$
$$\forall k \in [1, w], c \in C, w \in W, (i, j) \in E, \tag{5.2y}$$

$$z^k_{cwij} \leq \frac{\sum_{w'=w-k+1}^{w} \left(1 - s_{cw'ij}\right)}{k},$$
$$\forall k \in [1, w], c \in C, w \in W, (i, j) \in E, \tag{5.2z}$$

$$\sigma^k_{cwij} \geq z^k_{cwij} + s_{c(w+1)ij} + s_{c(w-k)ij} - 2,$$

$$\forall k \in [1, w], c \in C, w \in W, (i, j) \in E, \tag{5.2aa}$$

$$\sigma^k_{cwij} \leq z^k_{cwij}, \forall k \in [1, w], c \in C, w \in W, (i, j) \in E, \tag{5.2ab}$$

$$\sigma^k_{cwij} \leq s_{c(w+1)ij},$$

$$\forall k \in [1, w], c \in C, w \in [1, |W| - 1], (i, j) \in E, \tag{5.2ac}$$

$$\sigma^k_{cwij} \leq s_{c(w-k)ij},$$

$$\forall k \in [1, w - 1], c \in C, w \in W, (i, j) \in E, \tag{5.2ad}$$

$$B_{cij} \geq \sum_{w \in W} \sum_{k \in [1,w]} \sigma^k_{cwij}, \forall c \in C, (i, j) \in E, \tag{5.2ae}$$

$$e_{ij} \in \{0, 1\}, \forall (i, j) \in E, \tag{5.2af}$$

$$x_c \in \{0, 1\}, \forall c \in C, \tag{5.2ag}$$

$$m_q \in \{0, 1\}, \forall q \in Q, \tag{5.2ah}$$

$$y_w \in \{0, 1\}, \forall w \in W, \tag{5.2ai}$$

$$\psi^p, \zeta^p \in \{0, 1\}, \forall p \in P, \tag{5.2aj}$$

$$a_{cw}, u_{cw} \in \{0, 1\}, \forall c \in C, w \in W, \tag{5.2ak}$$

$$\upsilon_{cwij} \in \{0, 1\}, \forall c \in C, w \in W, (i, j) \in E, \tag{5.2al}$$

$$s_{cwij} \in \{0, 1\}, \forall c \in C, w \in W \cup \{0, |W| + 1\}, (i, j) \in E, \tag{5.2am}$$

$$z^k_{cwij}, \sigma^k_{cwij} \in \{0, 1\}, \forall k \in [1, w], c \in C, w \in W, (i, j) \in E, \tag{5.2an}$$

$$f \in W. \tag{5.2ao}$$

Equation (5.2a) is the objective function that minimizes the weighted sum of three factors; it aims to suppress network fragmentation. The first term indicates the highest index of allocated or unavailable vacant slots in each core of each link. The second term indicates the number of available vacant segments in each core of each link. The third term indicates the negative squared value of the size of available vacant segments in each core of each link. The first, second, and third terms are set to satisfy (i), (ii), and (iii) in Section 5.1, respectively. To show that the third term satisfies (iii), let us consider an example where two available vacant segments are generated by provisioning a lightpath. The total size of the two segments is constant and described as K. Each size of the two segments is described as k_1 and k_2 ($1 \leq k_1 \leq k_2 \leq K-1, k_2 = K-k_1$). In this example, the third term is calculated

as $-k_1^2 - k_2^2 = -k_1^2 - (K-k_1)^2 = -2k_1^2 + 2Kk_1 - K^2$. The third term is minimized by making $k_1 = 1$. As observed in this example, minimizing the third term makes the size of larger segments increase at the cost of decreasing the size of smaller ones.

The constraints are described as follows. Equations (5.2b) and (5.2c) represent that one core is determined for lightpath p_{new} and it is not changed over the lightpath. Equation (5.2c) represents that one modulation is determined for lightpath p_{new} and it is not changed over the lightpath. Equations (5.2d) and (5.2e) represent the spectrum contiguity constraint. The spectrum continuity constraint is ensured by the existence of y_w^t; $y_w^t = 1$ indicates that spectrum slot w is used consistently in the lightpath. Equations (5.2f) and (5.2g) represent the traffic flow constraint. Equation (5.2h) ensures that spectrum slots allocated to the lightpath provide at least the required transmission capacity b. Equation (5.2i) ensures that the length of the lightpath does not exceed the transmission reach corresponding to modulation format $q \in Q$ allocated to the lightpath. Equation (5.2j) ensures that ψ^p is one when lightpaths p_{new} and $p \in P$ share the same link. Equation (5.2k) ensures that ζ_w^p is one when lightpath p_{new} is adjacent to lightpath $p \in P$ in the wth spectrum slot ($w \in W$). Equation (5.2l) ensures that lightpath p_{new} is not adjacent to lightpath $p \in P$ in the wth spectrum slot ($w \in W$) if lightpath p cannot be adjacent to any other lightpath in the wth spectrum slot. Equations (5.2m)–(5.2q) ensure that lightpath p_{new} satisfies its XT threshold. Equation (5.2r) ensures that lightpath p_{new} use only the available vacant slots. Equations (5.2s) and (5.2t) ensure that $u_{c'w}$ is one when the lightpath p_{new} cannot be additionally adjacent to another lightpath in the wth spectrum slot ($w \in W$) in core $c' \in C$, and zero otherwise. Equation (5.2u) ensures that $\upsilon_{c'w}^p$ is one when the lightpath $p \in P$ cannot be additionally adjacent to another lightpath in the wth spectrum slot ($w \in W$) in core $c' \in C$ due to provisioning lightpath p_{new}, and zero otherwise. Equations (5.2v) and (5.2w) ensure that s_{cwij} is one if the wth spectrum slot ($w \in W$) in core $c \in C$ of link $(i,j) \in E$ is allocated to a lightpath or is an unavailable vacant slot. Equation (5.2x) calculates the maximum index of allocated or unavailable spectrum slots in core $c \in C$ of link $(i,j) \in E$. Equations (5.2y) and (5.2z) ensure that z_{cwij}^k equals one if $s_{cw'ij} = 0, \forall w' \in [w-k+1, w]$ in core $c \in C$ of link $(i,j) \in E$. Equations (5.2aa)–

(5.2ad) ensure that σ^{k}_{cwij} equals one if $z^{k}_{cwij} = 1$, $s_{c(w-k)ij} = 1$, and $s_{c(w+1)ij} = 1$, and zero otherwise. Equation (5.2ae) calculates the number of available vacant segments in core $c \in C$ of link $(i, j) \in E$. Equations (5.2af)–(5.2ao) define decision variables.

5.4 Lightpath provisioning algorithm

5.4.1 Overview

This section introduces a lightpath provisioning algorithm in the case that the ILP problem presented in Section 5.3.3 is not tractable. The heuristic algorithm divides the RMSCA problem into the routing problem and modulation, spectrum, and core allocation (MSCA) problem.

5.4.2 Assumption and notations

In addition to the assumption and notations presented in Section 5.3.2, the following assumptions and notations are introduced. Using the k-shortest path algorithm [72], a set of candidate routes is determined in advance, which is given as R_{a}. Route R is an element of R_{a}, i.e., $R \in R_{\mathrm{a}}$, which is a set of links. The distance of the route is presented as l_R. Information on existing lightpaths is given as $\mathcal{I}$. $\mathcal{I}$ includes the RSCA information on lightpath $p \in P$. $\mathcal{I}$ also includes the acceptable number of lightpaths that can be additionally adjacent to p: N^{p}_{w}. Let X^p denote the core allocated to p. Y^p denotes the set of spectrum slots allocated to p. E^p denotes the set of links, which are used to the route of p. The status of spectrum slots in the network is given as $\mathcal{S}$. $\mathcal{S}$ consists of S^{a}_{cij} and S^{u}_{cij}, each of which represents the status of spectrum slots of core $c \in C$ in link $(i, j) \in E$. S^{a}_{cij} is a set of indices of allocated spectrum slots of core $c \in C$ in link $(i, j) \in E$. S^{u}_{cij} is a set of indices of unavailable vacant spectrum slots of core $c \in C$ in link $(i, j) \in E$. Let C_c denote the set of cores adjacent to core $c \in C$.

Algorithm 2 Lightpath provisioning algorithm

Input: Network (V, E), C, Q, $\mathcal{I}$, $\mathcal{S}$,
traffic demand of p_{new}, and R_{a}.

Output: RMSCA for lightpath
p_{new}; $(X^{p_{\text{new}}}, Y^{p_{\text{new}}}, E^{p_{\text{new}}}, M^{p_{\text{new}}})$

Initialize:
Value of RMSF $\Omega \leftarrow \infty$
for all $R \in R_{\text{a}}$ **do**
  for all $c \in C$ **do**
    S_{Rc} = GetCandidateSegment$(R, c, \mathcal{S})$
    for all $q \in Q$ **do**
      if $r_q \geq l_R$ **then**
        $\varsigma \leftarrow \lceil b/\eta_q \rceil$
        for all $W_{Rc} \in S_{Rc}$ **do**
          if $|W_{Rc}| \geq \varsigma$ **then**
            Y', Ω' = AllocateSlot$(R, c, W_{Rc}, q, \varsigma, \mathcal{I})$
            if $\Omega > \Omega'$ **then**
              $X^{p_{\text{new}}} \leftarrow c, Y^{p_{\text{new}}} \leftarrow Y', E^{p_{\text{new}}} \leftarrow R, M^{p_{\text{new}}} \leftarrow q$
              $\Omega \leftarrow \Omega'$
if $\Omega = \infty$ **then**
  lightpath p_{new} is blocked

```
1: function GetCandidateSegment(R, c, 𝒮)
2:     A_s ← W, S_Rc ← {}, W_Rc ← {}
3:     for all (i, j) ∈ R do
4:         for all w ∈ A_s do
5:             if w ∈ S^a_cij ∪ S^u_cij then
6:                 Remove w from A_s
7:     pred ← Min(A_s) − 1
8:     for w ∈ A_s do
9:         if w ≠ pred + 1 then
10:            Add W_Rc in S_Rc
11:            W_Rc ← {}
12:        Add w in W_Rc
13:        pred = w
14:    Add W_Rc in S_Rc
15:    return S_Rc
```

function AllocateSlot($R, c, W_{Rc}, q, \varsigma, \mathcal{I}$)
  $n \leftarrow \lfloor \theta_q / h \rfloor$, $removed\_slot \leftarrow \{\}$, $\Omega \leftarrow \infty$, $f \leftarrow 0$
  for all $w \in W_{Rc}$ **do**
    for all $(i, j) \in R$ **do**
      $count \leftarrow 0$
      for all $c_a \in C_c$ **do**
        if $w \in S^a_{c_a ij}$ **then**
          $count \leftarrow count + 1$
      if $count \geq n + 1$ **then**
        Add w in $removed\_slot$
        break
  $W'_{Rc} \leftarrow W_{Rc} - removed\_slot$
  for all $w \in W'_{Rc} \setminus \{\text{Max}(W'_{Rc}) - \varsigma + 1, \cdots, \text{Max}(W'_{Rc})\}$ **do**
    if $\{w, \cdots, w + \varsigma - 1\} \subseteq W'_{Rc}$ **then**
      $\mathcal{S} \leftarrow$ UpdateSlotStatus$(R, c, w, \varsigma, n, \mathcal{S}, \mathcal{I})$
      Ω' = CalculateRMSF$(\mathcal{S})$
      if $\Omega > \Omega'$ **then**
        $\Omega \leftarrow \Omega'$
        $f \leftarrow w$
  if $f = 0$ **then**
    $Y^{p_{\text{new}}} \leftarrow \{\}$
  else
    $Y^{p_{\text{new}}} \leftarrow \{f, \cdots, f + \varsigma - 1\}$
  return $Y^{p_{\text{new}}}, \Omega$

1: **function** UPDATESLOTSTATUS($R, c, w, \varsigma, n, \mathcal{S}, \mathcal{I}$)
2: $P' \leftarrow \{\}$
3: **for all** $p \in P$ **do**
4: **if** $X^p \in C_c$ and $w' \in Y^p$ and $R \cap E^p \neq \emptyset$ **then**
5: Add p in P'
6: **for all** $(i, j) \in R$ **do**
7: Add $\{w, \cdots, w + n - 1\}$ in S^a_{cij}
8: **for** $w' = w, \ldots w + \varsigma - 1$ **do**
9: $\mathscr{C} \leftarrow \{\}$
10: **for all** $c' \in C_c$ **do**
11: **if** $w' \in S^a_{c'ij}$ **then**
12: Add c' in $\mathscr{C}$
13: **if** $|\mathscr{C}| = n$ **then**
14: **for all** $c' \in C_c \setminus \mathscr{C}$ **do**
15: **for all** $(i, j) \in R$ **do**
16: $S^u_{c'ij} \leftarrow S^u_{c'ij} \cup \{w'\}$
17: **for all** $p \in P'$ **do**
18: **if** $N^p_{w'} = 1$ **then**
19: **for all** $c_a \in C_{X^p} \setminus \{c\}$ **do**
20: **for all** $(i, j) \in R$ **do**
21: **if** $w' \notin S^a_{c'ij}$ **then**
22: $S^u_{c_aij} \leftarrow S^u_{c_aij} \cup \{w'\}$
23: **return** $\mathcal{S}$

1: **function** CALCULATERMSF($\mathcal{S}$)
2: $\Omega \leftarrow 0$
3: **for all** $(i, j) \in E$ **do**
4: **for all** $c \in C$ **do**
5: $A_s \leftarrow W \setminus \{S^a_{cij} \cup S^u_{cij}\}$
6: $F_{cij} \leftarrow \text{MAX}(\{S^a_{cij} \cup S^u_{cij}\})$
7: $W_{cij} \leftarrow \text{GETCANDIDATESEGMENT}(A_s)$
8: **if** $W_{cij} \neq \emptyset$ **then**
9: $\Xi \leftarrow 0$
10: **for all** $\xi \in W_{cij}$ **do**
11: $\Xi \leftarrow \Xi + |\xi|^2$
12: $\Omega \leftarrow \Omega + \frac{F_{cij}|W_{cij}|}{|C|\sqrt{\frac{\Xi}{|W_{cij}|}}}$
13: **return** Ω

5.4.3 Description of lightpath provisioning algorithm (Algorithm 2)

Algorithm 2 examines the allocation of spectrum slots to minimize RMSF for each route $R \in R_a$, core $c \in C$, and modulation format $q \in Q$, and provisions lightpath p_{new} by using the allocation with the lowest RMSF. Algorithm 2 runs as follows. Line 1 initializes Ω, which is a temporal value of RMSF, as ∞. Line 4 gets a set of candidate available vacant segments along $R \in R_a$ in $c \in C$ (GETCANDIDATESEGMENT). In lines 5–13, the slot allocation in R of c, whose RMSF is the lowest, is obtained for each $q \in Q$. If the reach of modulation q, r_q, is shorter than the distance of route R, l_R, modulation q is not available for lightpath p_{new}. Otherwise, the number of required slots, ς, is calculated in line 7. In lines 8–13, the slot allocation in R of c with q, whose RMSF is the lowest, is obtained (ALLOCATESLOT). If the size of vacant available segment W_{Rc} is less than ς, available vacant segment W_{Rc} is not available for lightpath p_{new}. Otherwise, the slot allocation is tried with available vacant segment W_{Rc} in line 10. If the slot allocation is successful and its RMSF is lower than the temporal RMSF Ω, Ω and RMSCA are updated in lines 11–13. If Ω is not

updated through the above process, lightpath p_{new} is blocked (lines 14 and 15).

5.4.4 Functions used in Algorithm 2

Function GetCandidateSegment gets the set of candidate available vacant segments along route R in core c. In lines 2–6, a set of slots, which are available along R in c is obtained as A_s. In lines 7–14, A_s is divided into a set of segments, each of which is spectrally contiguous.

Function AllocateSlot gets the slot allocation using available vacant segment W_{Rc}, whose RMSF is the minimum of route R in core c with modulation q. In line 2, lightpath-adjacent number n is calculated. In lines 3–12, vacant slots, which are not available because XT is more than the threshold of modulation q, are removed from W_{Rc}. Lines 13–19 get starting slot index f, where slots are allocated with the minimum RMSF in R of c with q. In line 13, $\{\text{Max}(W'_{Rc}) - \varsigma + 1, \cdots, \text{Max}(W'_{Rc})\}$ is the candidate starting slot index. Line 14 checks whether there are ς contiguous slots from the wth slot. Lines 15 and 16 get the slot status $\mathcal{S}$ and RMSF Ω', where wth to $(w+\varsigma-1)$th slots are allocated to lightpath p_{new}, respectively. In lines 17–19, if the RMSF gotten in line 16 Ω' is smaller than the temporal RMSF Ω, Ω and f are updated to Ω' and w, respectively. In lines 20–24, if $f = 0$, i.e., there is no allocation for lightpath p_{new} using W_{Rc}, R, c, and q, the RMSF is returned as ∞. Otherwise, the slot allocation and the RMSF are returned as $Y^{p_{\text{new}}}$ and Ω, respectively.

Function UpdateSlotStatus updates the slot status, where ς slots from the wth slot are allocated along route R of core c for lightpath p_{new}. In lines 2–5, a set of lightpaths, which are adjacent to p_{new}, is obtained as P'. In lines 6 and 7, allocated slots for p_{new} are added to S^a_{cij}. In lines 8–22, additional unavailable vacant slots are added to S^u_{cij}. Lines 10–12 get the set of lightpath adjacent core as $\mathscr{C}$ in w'th slot. In lines 13–16, if the lightpath adjacent number is equal to the acceptable lightpath-adjacent number in the w'th slot and the w'th slot is vacant along R of core c', the w'th slot along R of core c' is considered as an unavailable vacant slot. In lines 17–20, if the additional acceptable lightpath-adjacent number of existing lightpath $p \in P'$

in the w'th slot is equal to one, the vacant slots adjacent to lightpath p are considered as unavailable vacant slots.

Function CalculateRMSF calculates the value of RMSF of the network, whose slot status is $\mathcal{S}$. Line 5 gets the available vacant slots in link (i, j) of core c. Line 6 gets the maximum index of allocated or unavailable vacant slots. Line 7 gets the set of available vacant segments. Lines 8–12 add the value of RMSF in link (i, j) of core c to Ω.

5.4.5 Computational time complexity

The computational time complexity of Algorithm 2 is described as follows.

The computational time complexity of lines 3–6 and lines 8–13 of function GetCandidateSegment is $O(|E||W|^2)$ and $O(|W|)$, respectively. Therefore, the computational time complexity of function GetCandidateSegment is $O(|E||W|^2)$.

The computational time complexity of lines 3–5, lines 6 and 7, and lines 8–22 of function UpdateSlotStatus is $O(|P||C||E||W|)$, $O(|E|)$, and $O(|W|(|W||C|+|C||E|+|P||C||E||W|))$, respectively. Therefore, the computational time complexity of function UpdateSlotStatus is $O(|P||C||E||W|^2)$.

In consideration of the computational time complexity of function GetCandidateSegment, the computational time complexity of function CalculateRMSF is $O(|E||C|(|W|+|E||W|^2+|W|))$, i.e., $O(|C||E|^2|W|^2)$.

The computational time complexity of lines 3–11 of function AllocateSlot is $O(|W|^2|E||C|)$. With the computational time complexity of functions UpdateSlotStatus and CalculateRMSF, the computational time complexity of lines 13–23 of function AllocateSlot is $O(|W|^2(|P||C||E||W|^2+|C||E|^2|W|^2))$, i.e., $O(|C||E||W|^4(|P|+|E|))$. Therefore, the computational time complexity of function AllocateSlot is $O(|C||E||W|^4(|P|+|E|))$.

Finally, the computational time complexity of Algorithm 2 is $O(|R_a||C|(|E||W|^2+|Q||W|\times|C||E||W|^4(|P|+|E|)))$, i.e., $O(|R_a||Q||C||E||W|^5(|P|+|E|))$.

5.4.6 Computational space complexity

The computational space complexity of Algorithm 2 is described as follows. Algorithm 2 needs to store $\mathcal{S}$, which is the status of all spectrum slots in

each link of each core in the network. It also needs to store $\mathcal{I}$, which is the information on all existing lightpaths; a core, links, and spectrum slots are allocated to each existing lightpath. Therefore, the computational space complexity of Algorithm 2 is $O(|C||E||W|+|P||E||W|)$, i.e., $O((|C|+|P|)|E||W|)$.

5.5 Evaluation

This section presents a benchmark model and the performance evaluation environment followed by the numerical results of the proposed and benchmark models.

5.5.1 Benchmark model

To evaluate the proposed model, a benchmark model is introduced. The benchmark model calculates a metric without classifying vacant slots into available ones and unavailable ones. The difference between the proposed and benchmark models is whether vacant slots are classified when calculating the metric. The benchmark model is essentially the same as the proposed model, with the exception of the aforementioned point. The ILP approach and the algorithm of the benchmark model are based on those introduced in Section 5.3.3 and Section 5.4, respectively. Comparing the proposed and benchmark models, the influence of classifying vacant slots into available ones and unavailable ones can be observed.

5.5.2 Evaluation environment

The proposed and the benchmark models are evaluated in terms of the blocking probability.

The traffic demands are generated randomly based on a Poisson distribution process with the arrival rate of λ. The holding time of traffic demands, H, follows an exponential distribution. The traffic load is given in Erlang by $\rho = \lambda H$. The source-destination pair for each traffic demand is randomly generated. Each traffic demand is independent of the previous one.

The transmission is realized using super channels (Schs). A Sch consists of

optical careers, each of which consists of three slots (37.5 GHz). Four types of modulation formats, 16-QAM, 8-QAM, QPSK, and BPSK, are considered. The capacities of a Sch of 16-QAM, 8-QAM, QPSK, and BPSK are assumed to be 200, 150, 100, and 50 [Gbps], respectively [25]. Each transmission reaches is, 600, 1200, 3500, 6300 [km], respectively [73]. The XT thresholds of each modulation format is -25, -21, -18.5, -14 [dB], respectively [31,32,73]. The value of a XT threshold can be set depending on the bit error rate (BER) desired by a network operator. If BER is more strictly managed, more strict XT thresholds should be used as used in the evaluation of [33,34]. The other parameters, such as the number of slots in a link, the power-coupling coefficient, and the required transmission capacity of each traffic demand, are different for each evaluation, so they are described in the following section.

Results of blocking probability are obtained with a 95% confidence interval. The interval is not greater than 5% and 10% of the average blocking probability when the average blocking probability is more than 0.01 and otherwise, respectively.

In the evaluation, a specified blocking probability that the network operator guarantees is considered. The proposed and benchmark models are compared by the admissible traffic load within the guaranteed blocking probability. The guaranteed blocking probability is assumed to be 0.01.

The number of candidate routes in Algorithm 2 is set to three in the evaluation.

The ILP problems are solved by CPLEX Optimization Studio 20.1.0 [65].

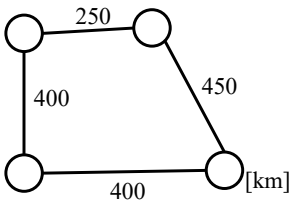

Figure 5.3: 4-node network. (©2023 Elsevier.)

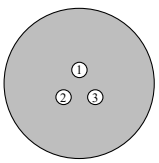

Figure 5.4: 3-core MCF. (©2023 Elsevier.)

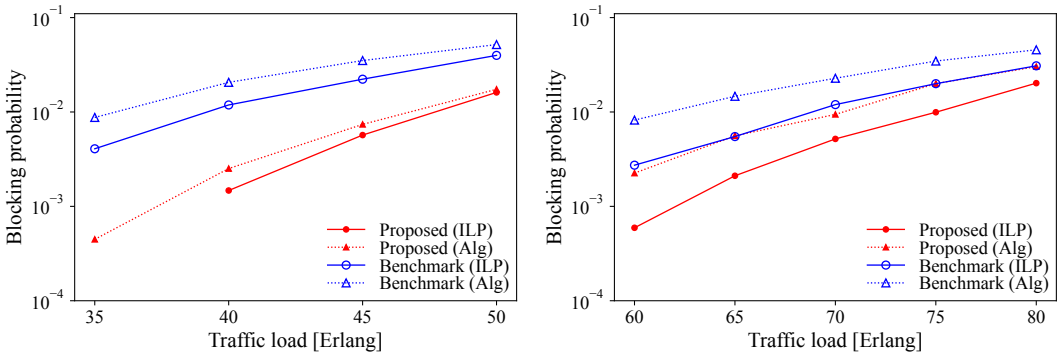

(a) $h = 1.0 \times 10^{-8}$ (b) $h = 5.0 \times 10^{-9}$

Figure 5.5: Blocking probability (4-node network). (©2023 Elsevier.)

5.5.3 4-node network

The proposed and benchmark models are evaluated using the ILP approach presented in Section 5.3.3 and the lightpath provisioning algorithm presented in Section 5.4 in a 4-node network, which is shown in Fig. 5.3. The 4-node network is used to evaluate the basic characteristics of the proposed model and the performance of the ILP approach. The network to which the ILP approach can apply is the 4-node network. The MCF in the 4-node network is assumed to be 3-core fiber, as shown in Fig. 5.4. The power-coupling coefficient, h, is set to 1.0×10^{-8} and 5.0×10^{-9}. The number of available slots is 30 in each core; ten Schs are available. The required transmission capacity for each traffic demand is selected from uniform random values between 100 and 200 [Gbps], which are multiples of 50. Only 16-QAM, 8-QAM, and QPSK are used in this evaluation. To reach the network steady state, initially, 1000 lightpaths are processed.

ϵ_1, ϵ_2, and ϵ_3 used in the ILP approach are set based on the number of Schs. In this evaluation, the values of ϵ_1, ϵ_2, and ϵ_3 are ten, ten, and one, respectively.

Fig. 5.5 shows the blocking probability of each model. For every h and traffic load in the evaluation, the blocking probability of the proposed model is less than that of the benchmark model. When the ILP approach is used and the blocking probability is 0.01, the proposed model accommodates 21.0% and

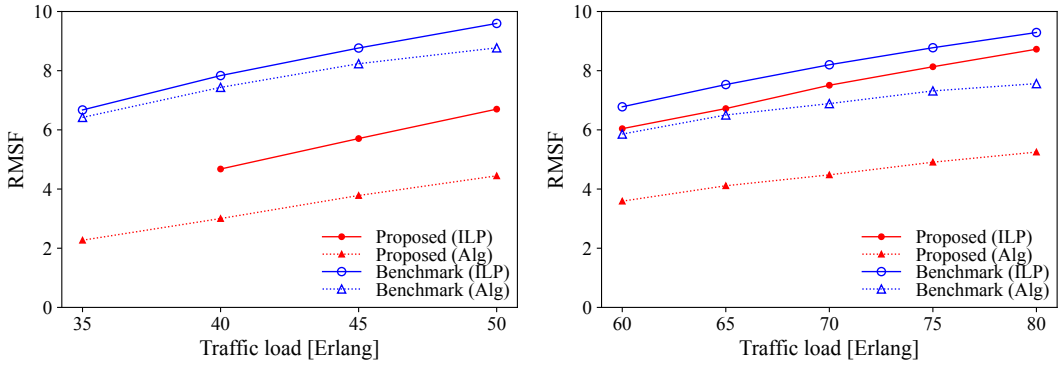

(a) $h = 1.0 \times 10^{-8}$ (b) $h = 5.0 \times 10^{-9}$

Figure 5.6: Average value of RMSF (4-node network). (©2023 Elsevier.)

8.2% more traffic than the benchmark model with $h = 1.0\times10^{-8}$ and 5.0×10^{-9}, respectively, as observed in Figs. 5.5(a) and (b). When the algorithm is used and the blocking probability is 0.01, the proposed model accommodates 26.2% and 8.9% more traffic than the benchmark model with $h = 1.0 \times 10^{-8}$ and 5.0×10^{-9}, respectively, as observed in Figs. 5.5(a) and (b).

In the comparison of Figs. 5.5(a) with (b), it is observed that the advantage of the proposed model for the benchmark model becomes large when h is large in the 4-node network. The advantage of considering the fragmentation due to inter-core XT becomes apparent in the 4-node network according to the increase of h, that is, when the amount of XT becomes large.

In comparison of the result of the ILP approach with that of the algorithm in Figs. 5.5(a) and (b), it is observed that the blocking probability of the ILP approach is less than that of the algorithm in each h. The main difference between the ILP approach and the algorithm is the metric aiming to minimize; The ILP minimizes (5.2a) and the algorithm minimizes (5.1). Since there are only two paths for any source and destination node pair in the 4-node network, all possible routes can be considered in the algorithm in the 4-node network. There is no difference between the ILP approach and the algorithm in terms of routing options. The difference between the result of the ILP approach and that of the algorithm comes from the difference in metrics between the ILP approach and the algorithm.

Fig. 5.6 shows the average RMSF considering unavailable vacant slots. When the lightpaths are provisioned in the same approach (ILP approach or algorithm), the average RMSF of the proposed model is less than that of the benchmark model. When the ILP approach is used, the proposed model reduces the average RMSF by at most 40.1% and 10.9% compared to the benchmark model with $h = 1.0 \times 10^{-8}$ and 5.0×10^{-9}, respectively, as observed in Figs. 5.6(a) and (b). When the algorithm is used, the proposed model reduces the average RMSF by at most 64.6% and 38.7% compared to the benchmark model with $h = 1.0 \times 10^{-8}$ and 5.0×10^{-9}, respectively, as observed in Figs. 5.6(a) and (b). Note that the average RMSF of the ILP approach is larger than that of the algorithm when the same model is used. Since the objective of the ILP problem, (5.2a), is not exactly the same as RMSF in (5.1), RMSF is not necessarily minimized in the ILP problem. The average RMSF of the ILP approach can be larger than that of the algorithm.

5.5.4 Larger networks

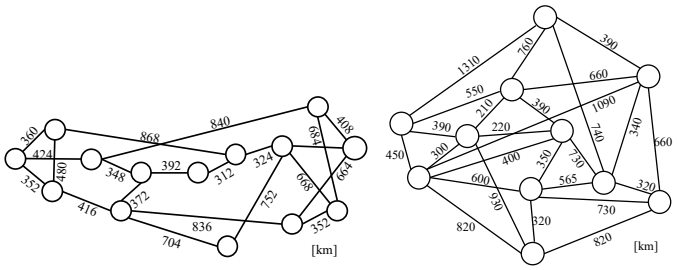

(a) NSFNET. (b) COST239 network.

Figure 5.7: Evaluation networks. (©2023 Elsevier.)

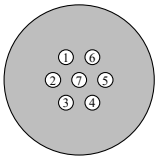

Figure 5.8: 7-core MCF. (©2023 Elsevier.)

Next, the proposed and benchmark models are evaluated in NSFNET [71] and COST239 network [63], which are shown in Fig. 5.7. NSFNET has 14 nodes and 42 directional links. COST239 network has 11 nodes and 52 directional links. The MCF in the networks is assumed to be 3-core fiber and 7-core fiber, as shown in Figs. 5.4 and 5.8, respectively. The power-coupling coefficient is set to 1.0×10^{-8} and 5.0×10^{-9}. In this evaluation, a 4 THz bandwidth is split into 320 slots, each of which is 12.5 GHz. The required

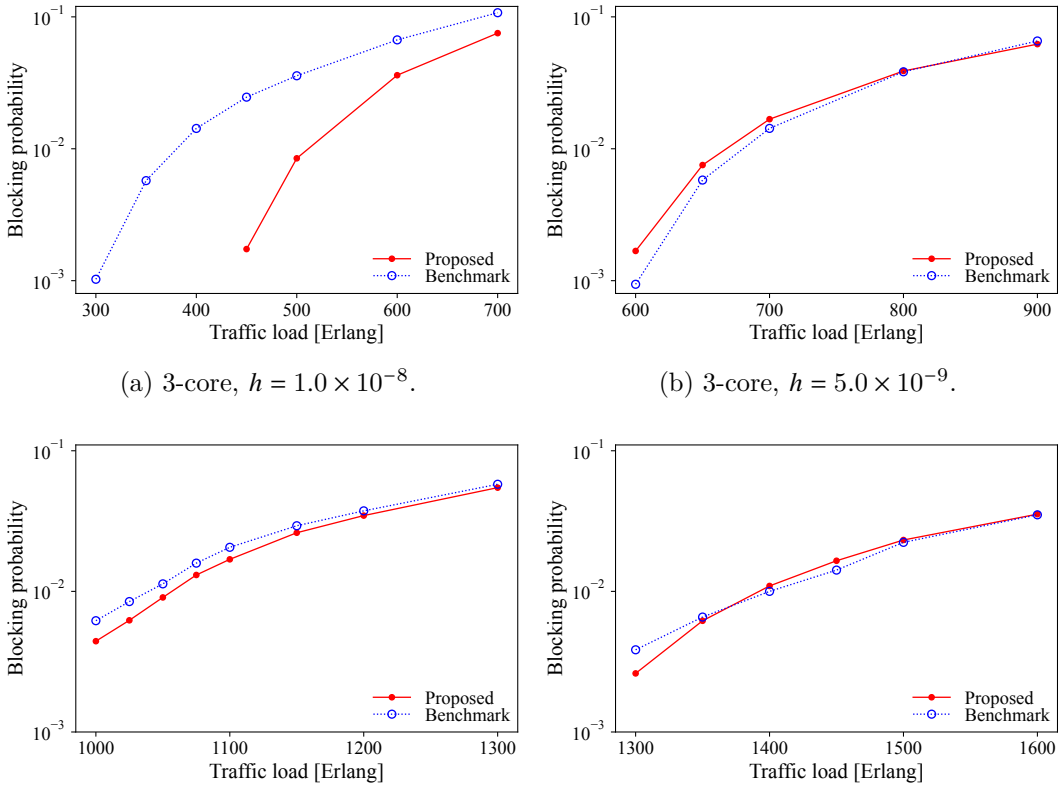

(a) 3-core, $h = 1.0 \times 10^{-8}$.

(b) 3-core, $h = 5.0 \times 10^{-9}$.

(c) 7-core, $h = 1.0 \times 10^{-8}$.

(d) 7-core, $h = 5.0 \times 10^{-9}$.

Figure 5.9: Blocking probability (NSFNET). (©2023 Elsevier.)

transmission capacity for each traffic demand is selected from uniform random values between 100 and 500 [Gbps], which are multiples of 50. To reach the network steady state, initially, 3000 lightpaths are processed.

Fig. 5.9 shows the blocking probability of the proposed and benchmark models in NSFNET with each power-coupling coefficient. Figs. 5.9(a) and (b) are the results where MCF in the network is 3-core fiber. Figs. 5.9(c) and (d) are the results where MCF in the network is 7-core fiber.

Figs. 5.9(a) and (c) show that the blocking probability of the proposed model is smaller than that of the benchmark model when $h = 1.0 \times 10^{-8}$ of each number of cores. When MCF is 3-core fiber and the blocking probability is 0.01, the proposed model accommodates 32.8% more traffic than the benchmark model, as observed in Fig. 5.9(a). When MCF is 7-core fiber and

the blocking probability is 0.01, the proposed model accommodates 1.4% more traffic than the benchmark model, as observed in Fig. 5.9(c).

Fig. 5.9(b) shows that the blocking probability of the proposed model is larger than that of the benchmark model in 600–700 Erlang when $h = 5.0\times10^{-9}$ of 3-core fiber. In 900 Erlang, the blocking probability of the proposed model is smaller than that of the benchmark model. When the blocking probability is 0.01, the proposed model accommodates 1.0% less traffic than the benchmark model. The proposed model tends to allocate slots not to generate unavailable vacant slots; it tends to avoid using the same spectrum slots of adjacent cores. It may lead to an increase in spectrum slots that are affected by inter-core XT and generate more unavailable vacant slots at the following lightpath provisioning. It can be considered that this phenomenon may be strongly apparent in this environment.

Fig. 5.9(d) shows that the blocking probability of the proposed model and that of the benchmark model are comparable when $h = 5.0 \times 10^{-9}$ of 7-core fiber.

In the comparison of Figs. 5.9(a) with (b) and (c) with (d), it is observed that the advantage of the proposed model for the benchmark model becomes large when h is large in NSFNET, as observed in the evaluation in the 4-node network in Section 5.5.3.

In the comparison of Figs. 5.9(a) with (c) and (b) with (d), it is observed that the difference between the proposed model and the benchmark model becomes large when the number of cores is small. Under the same h, the influence for adjacent cores becomes large as the number of cores becomes small. When a core is used in 3-core MCF, it is adjacent to all of the other cores, so the influence for adjacent cores is large. It can be considered that the difference of models tends to clearly appear in 3-core MCF than in 7-core MCF.

Fig. 5.10 shows the blocking probability of the proposed and benchmark models with each power-coupling coefficient in COST239 network. Figs. 5.10(a) and (b) are the results where MCF in the network is 3-core fiber. Figs. 5.10(c) and (d) are the results where MCF in the network is 7-core fiber.

Fig. 5.10(a) shows that the blocking probability of the proposed model is smaller than that of the benchmark model when $h = 1.0 \times 10^{-8}$ of 3-core

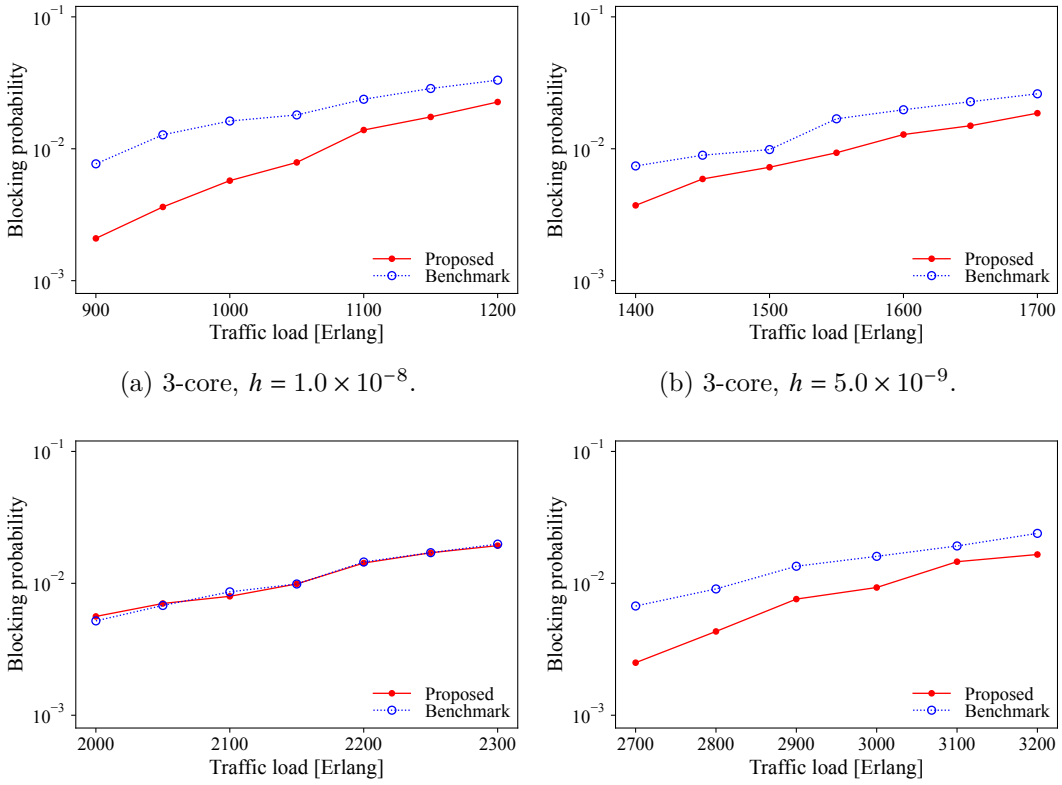

(a) 3-core, $h = 1.0 \times 10^{-8}$.

(b) 3-core, $h = 5.0 \times 10^{-9}$.

(c) 7-core, $h = 1.0 \times 10^{-8}$.

(d) 7-core, $h = 5.0 \times 10^{-9}$.

Figure 5.10: Blocking probability (COST239 network). (©2023 Elsevier.)

MCF. When MCF is 3-core fiber and the blocking probability is 0.01, the proposed model accommodates 12.4% more traffic than the benchmark model, as observed in Fig. 5.10(a). Fig. 5.10(c) shows that the blocking probability of the proposed model and that of the benchmark model is comparable when $h = 1.0 \times 10^{-8}$ of 7-core MCF.

Figs. 5.10(b) and (d) show that the blocking probability of the proposed model is smaller than that of the benchmark model when $h = 5.0 \times 10^{-9}$. When MCF is 3-core fiber and the blocking probability is 0.01, the proposed model accommodates 5.6% more traffic than the benchmark model, as observed in Fig. 5.10(b). When MCF is 7-core fiber and the blocking probability is 0.01, the proposed model accommodates 6.0% more traffic than the benchmark model, as observed in Fig. 5.10(d).

In the comparison of Figs. 5.10(a) with (b), it is observed that the advantage of the proposed model for the benchmark model becomes large when h is large in COST239 network with 3-core MCF, as observed in the evaluation in the 4-node network and NSFNET. In the comparison of Figs. 5.10(c) with (d), it is observed that the advantage of the proposed model for the benchmark model becomes small when h is large in COST239 network with 7-core MCF; this is a different trend from other network environments. From this observation, it can be considered that there is a range of values of h, where the advantage of the proposed model for the benchmark model becomes large, and the range is different by networks and the number of cores. In COST239 network with 7-core MCF, it can be considered that the value of h, where the advantage of the proposed model for the benchmark model becomes large, is smaller than that in the other networks.

In the comparison of Figs. 5.10(a) with (c), it is observed that the difference between the proposed model and the benchmark model becomes large when the number of cores is small, as observed in NSFNET. Figs. 5.10(b) and (d) observe the advantage of the proposed model for the benchmark model similarly in 3-core MCF and 7-core MCF, respectively.

5.6 Summary

This chapter proposed a fragmentation-aware lightpath provisioning model, which suppresses both fragmentation caused by allocating spectrum slots to lightpaths and due to inter-core XT. The proposed model classifies vacant spectrum slots into available vacant slots and unavailable vacant slots to suppress the fragmentation due to inter-core XT. To suppress the fragmentation, an optimization problem was presented, which is based on the proposed model. The optimization problem was formulated as an ILP problem. A heuristic algorithm for lightpath provisioning is presented in the case that the ILP problem is not tractable. The performance of the proposed model was evaluated in terms of the blocking probability and compared to the benchmark model. Numerical results observed that the proposed model suppresses the blocking probability better than the benchmark model. The proposed model could accommodate at most 26.2% more traffic than the benchmark model in a 4-node network

of the evaluation scenario. In the evaluation, it was observed that the proposed model can accommodate 6.0% more traffic than the benchmark model in COST239 network of 7-core MCF of $h = 5.0 \times 10^{-9}$.

Chapter 6

Conclusions

The rapid growth in worldwide communications and the rapid adoption of the Internet have led to a growth in the amount of communication traffic every year. An optical network has the potential to support the continuously increasing demands for communications. EON is one of the new technologies for high-speed, flexible, and scalable optical networks. This thesis studied three specific problems with lightpath provisioning in EONs.

Firstly, this thesis proposed the MPP scheme for fault tolerance to minimize required spectrum resources in EONs. The proposed scheme allows allocating different numbers of spectrum slots and different amounts of transmission capacity to each path to minimize the required spectrum resources. Two optimization problems in the proposed scheme were presented. One problem considers that the route of link-disjoint paths for a traffic demand is given, and the other determines the routes of link-disjoint paths and the number of spectrum slots allocated to each path simultaneously. The two optimization problems were formulated as the FSA-NPS model and the RFSA-NPS model. Numerical results revealed that the conventional scheme does not always minimize the required spectrum resources and showed that the proposed scheme reduces the required spectrum resources in several cases. It was also observed that the required spectrum resources can be reduced by considering the routing of link-disjoint paths in the proposed scheme at the expense of more computation time; the reduction effect especially becomes large in the case where the network has a large number of nodes and needs to tolerate with multiple

failures.

Secondly, this thesis proposed an RMSCA model, which jointly considers inter-core XT and intra-core PLIs for SS-EONs. In order to deal with inter-core XT and intra-core PLIs jointly, the proposed model considers the OSNR penalty. The proposed model sets multiple XT thresholds and their corresponding transmission reaches by considering the OSNR penalty due to XT. An optimization problem is presented and formulated as an ILP problem. A heuristic algorithm for the proposed model is introduced. The proposed model is evaluated with the ILP approach and the heuristic algorithm. Numerical results observed that the proposed model reduces the maximum index of the allocated spectrum slots compared to the benchmark model. It was observed that the proposed model uses a more spectrum-efficient modulation format than the benchmark model.

Thirdly, this thesis proposed a fragmentation-aware lightpath provisioning model, which suppresses both fragmentation caused by allocating spectrum slots to lightpaths and due to inter-core XT. The proposed model classifies vacant spectrum slots into available vacant slots and unavailable vacant slots to suppress the fragmentation due to inter-core XT. To suppress the fragmentation, an optimization problem was presented, which is based on the proposed model. The optimization problem was formulated as an ILP problem. The performance of the proposed model was evaluated in terms of the blocking probability and compared to the benchmark model. Numerical results observed that the proposed model suppresses the blocking probability better than the benchmark model. The proposed model could accommodate more traffic than the benchmark model.

The proposed scheme and models lead to improve spectrum efficiency in EONs. Since EONs will be used to support various network services, this thesis considers various scenarios in EONs. Lightpath provisioning is considered for both static and dynamic cases. A fault-tolerant EON is also considered. A network provider can use suitable scheme or models according to the network environment and specific requirements to achieve a reliable, high-capacity, or flexible optical network.

For future works, there can be three directions in lightpath provisioning in EONs. First, this thesis studies lightpath failures, PLIs, and fragmentation

separately. We should consider these three aspects at the same time. At that time, the classification of vacant slots into available and unavailable needs to be changed. The second direction is considering spectrum frequency conversion in a lightpath. This thesis imposes spectrum continuity constraint in lightpath provisioning; the same spectrum slots is used along a lightpath. Recently, a technique for spectrum conversion of optical signals without an electrical process has been studied. Using the spectrum conversion technique, we can eliminate the spectrum contiguity constraint. On the other hand, it needs to consider the signal degradation from spectrum conversion. The third direction is the consideration of a routing protocol of an optical network. Since intermediate nodes cannot catch the destination of an optical signal, the nodes route the optical signal by its frequency. When lightpaths are often provisioned and released in a network, the routing table of each optical node needs to be updated frequently. It needs to decide the routing of a lightpath and update the routing table immediately. It needs to develop a responsive routing protocol, which can suppress fragmentation and use spectrum efficiency.

Bibliography

[1] M. Jinno, B. Kozicki, H. Takara, A. Watanabe, Y. Sone, T. Tanaka, and A. Hirano, "Distance-adaptive spectrum resource allocation in spectrum-sliced elastic optical path network [topics in optical communications]," *IEEE Commun. Mag.*, vol. 48, no. 8, pp. 138–145, 2010.

[2] M. Jinno, "Elastic optical networking: roles and benefits in beyond 100-Gb/s era," *J. Lightw. Technol.*, vol. 35, no. 5, pp. 1116–1124, 2017.

[3] B. C. Chatterjee, N. Sarma, and E. Oki, "Routing and spectrum allocation in elastic optical networks: A tutorial," *IEEE Commun. Surveys Tuts.*, vol. 17, no. 3, pp. 1776–1800, 2015.

[4] J. Zhao, H. Wymeersch, and E. Agrell, "Nonlinear impairment-aware static resource allocation in elastic optical networks," *J. Lightw. Technol.*, vol. 33, no. 22, pp. 4554–4564, 2015.

[5] S. Behera, A. Deb, G. Das, and B. Mukherjee, "Impairment aware routing, bit loading, and spectrum allocation in elastic optical networks," *J. Lightw. Technol.*, vol. 37, no. 13, pp. 3009–3020, 2019.

[6] M. Klinkowski, "An evolutionary algorithm approach for dedicated path protection problem in elastic optical networks," *Cybernetics and Systems*, vol. 44, no. 6-7, pp. 589–605, 2013.

[7] S. Huang, B. Guo, X. Li, J. Zhang, Y. Zhao, and W. Gu, "Pre-configured polyhedron based protection against multi-link failures in optical mesh networks," *Optics express*, vol. 22, no. 3, pp. 2386–2402, 2014.

[8] L. Ruan and N. Xiao, "Survivable multipath routing and spectrum allocation in OFDM-based flexible optical networks," *J. Opt. Commun. Netw.*, vol. 5, no. 3, pp. 172–182, 2013.

[9] A. A. Jose, A. H. Al Muktadir, and E. Oki, "Network coding aware instantaneous recovery scheme based on optimal traffic splitting," *IEICE Commun. Express*, vol. 1, no. 1, pp. 28–32, 2012.

[10] A. H. Al Muktadir and E. Oki, "Differential delay aware instantaneous recovery scheme with traffic splitting," *Int. J. Commun. Systems*, vol. 30, no. 5, p. e3075, 2017.

[11] S. Yin, S. Huang, B. Guo, Y. Zhou, H. Huang, M. Zhang, Y. Zhao, J. Zhang, and W. Gu, "Shared-protection survivable multipath scheme in flexible-grid optical networks against multiple failures," *J. Lightw. Technol.*, vol. 35, no. 2, pp. 201–211, 2017.

[12] Y. Kishi, N. Kitsuwan, H. Ito, B. C. Chatterjee, and E. Oki, "Modulation-adaptive link-disjoint path selection model for 1+1 protected elastic optical networks," *IEEE Access*, vol. 7, pp. 25 422–25 437, 2019.

[13] B. C. Chatterjee, S. Ba, and E. Oki, "Fragmentation problems and management approaches in elastic optical networks: a survey," *IEEE Commun. Surveys Tuts.*, vol. 20, no. 1, pp. 183–210, 2017.

[14] M. S. Johnstone and P. R. Wilson, "The memory fragmentation problem: Solved?" *ACM Sigplan Notices*, vol. 34, no. 3, pp. 26–36, 1998.

[15] P. Wright, M. C. Parker, and A. Lord, "Simulation results of shannon entropy based flexgrid routing and spectrum assignment on a real network topology," in *2013 Europ. Conf. Opt. Commun. (ECOC)*. IET, 2013, pp. 1–3.

[16] ——, "Minimum-and maximum-entropy routing and spectrum assignment for flexgrid elastic optical networking," *J. Opt. Commun. Netw.*, vol. 7, no. 1, pp. A66–A72, 2015.

[17] G. M. Saridis, D. Alexandropoulos, G. Zervas, and D. Simeonidou, "Survey and evaluation of space division multiplexing: From technologies to optical networks," *IEEE Commun. Surveys Tuts.*, vol. 17, no. 4, pp. 2136–2156, 2015.

[18] M. N. Dharmaweera, L. Yan, M. Karlsson, and E. Agrell, "Nonlinear-impairments- and crosstalk-aware resource allocation schemes for multicore-fiber-based flexgrid networks," in *2016 Europ. Conf. Opt. Commun. (ECOC)*. VDE, 2016, pp. 1–3.

[19] M. Klinkowski, P. Lechowicz, and K. Walkowiak, "A study on the impact of inter-core crosstalk on SDM network performance," in *2018 Int. Conf. Comput. Netw. Commun. (ICNC)*. IEEE, 2018, pp. 404–408.

[20] F. Tang, Y. Yan, L. Peng, S. K. Bose, and G. Shen, "Crosstalk-aware counter-propagating core assignment to reduce inter-core crosstalk and capacity wastage in multi-core fiber optical networks," *J. Lightw. Technol.*, vol. 37, no. 19, pp. 5010–5027, 2019.

[21] A. Muhammad, G. Zervas, D. Simeonidou, and R. Forchheimer, "Routing, spectrum and core allocation in flexgrid SDM networks with multi-core fibers," in *2014 Int. Conf. Opt. Netw. Des. Model. (ONDM)*. IEEE, 2014, pp. 192–197.

[22] M. Yang, Y. Zhang, and Q. Wu, "Routing, spectrum, and core assignment in SDM-EONs with MCF: node-arc ILP/MILP methods and an efficient XT-aware heuristic algorithm," *J. Lightw. Technol.*, vol. 10, no. 3, pp. 195–208, 2018.

[23] A. Sano, H. Takara, T. Kobayashi, and Y. Miyamoto, "Crosstalk-managed high capacity long haul multicore fiber transmission with propagation-direction interleaving," *J. Lightw. Technol.*, vol. 32, no. 16, pp. 2771–2779, 2014.

[24] H. M. Oliveira and N. L. Da Fonseca, "Protection, routing, modulation, core, and spectrum allocation in SDM elastic optical networks," *IEEE Commun. Lett.*, vol. 22, no. 9, pp. 1806–1809, 2018.

[25] M. Klinkowski and G. Zalewski, "Dynamic crosstalk-aware lightpath provisioning in spectrally-spatially flexible optical networks," *J. Lightw. Technol.*, vol. 11, no. 5, pp. 213–225, 2019.

[26] T. Hayashi, T. Taru, O. Shimakawa, T. Sasaki, and E. Sasaoka, "Design and fabrication of ultra-low crosstalk and low-loss multi-core fiber," *Opt. Exp.*, vol. 19, no. 17, pp. 16 576–16 592, 2011.

[27] J. Strand and A. Chiu, "Impairments and Other Constraints on Optical Layer Routing," RFC 4054 (Informational), Internet Engineering Task Force, May 2005. [Online]. Available: http://www.ietf.org/rfc/rfc4054.txt

[28] P. Lechowicz, M. Tornatore, A. Włodarczyk, and K. Walkowiak, "Fragmentation metrics and fragmentation-aware algorithm for spectrally/spatially flexible optical networks," *J. Opt. Commun. Netw.*, vol. 12, no. 5, pp. 133–145, 2020.

[29] S. Trindade and N. L. da Fonseca, "Proactive fragmentation-aware routing, modulation format, core, and spectrum allocation in EON-SDM," in *2019 IEEE Int. Conf. Commun. (ICC)*. IEEE, 2019, pp. 1–6.

[30] F. Yousefi and A. G. Rahbar, "Novel crosstalk, fragmentation-aware algorithms in space division multiplexed-Elastic Optical Networks (SDM-EON) with considering physical layer security," *Optical Switching and Networking*, vol. 37, p. 100566, 2020.

[31] J. Zhang, B. Bao, Q. Yao, D. Ren, J. Hu, and J. Zhao, "3D fragmentation metric and RCSA scheme for space division multiplexing elastic optical networks," *IEEE Access*, vol. 8, pp. 201 595–201 605, 2020.

[32] Y. Chen, N. Feng, Y. Zhou, D. Ren, and J. Zhao, "Crosstalk classification based on synthetically consider crosstalk and fragmentation RMCSA in multi-core fiber-based EONs," in *Photonics*, vol. 10, no. 3. MDPI, 2023, p. 340.

[33] M. Jafari-Beyrami, A. G. Rahbar, and S. Hosseini, "On-demand fragmentation-aware spectrum allocation in space division multiplexed

elastic optical networks with minimized crosstalk and multipath routing," *Computer Networks*, vol. 181, p. 107531, 2020.

[34] H. Yang, Q. Yao, B. Bao, A. Yu, J. Zhang, and A. V. Vasilakos, "Multi-associated parameters aggregation-based routing and resources allocation in multi-core elastic optical networks," *IEEE/ACM Trans. Netw.*, vol. 30, no. 5, pp. 2145–2157, 2022.

[35] Y. Khorasani, A. G. Rahbar, and M. Jafari-Beyrami, "A novel two-dimensional metric for fragmentation evaluation in elastic optical networks," *Computer Networks*, vol. 216, p. 109275, 2022.

[36] L. Ruan and Y. Zheng, "Dynamic survivable multipath routing and spectrum allocation in OFDM-based flexible optical networks," *J. Opt. Commun. Netw.*, vol. 6, no. 1, pp. 77–85, 2014.

[37] X. Chen, S. Zhu, D. Chen, S. Hu, C. Li, and Z. Zhu, "On efficient protection design for dynamic multipath provisioning in elastic optical networks," in *2015 Intl. Conf. Opt. Netw. Des. Model. (ONDM)*. IEEE, 2015, pp. 251–256.

[38] G. Shen, H. Guo, and S. K. Bose, "Survivable elastic optical networks: survey and perspective," *Photon. Netw. Commun.*, vol. 31, no. 1, pp. 71–87, 2016.

[39] R. Goscien, K. Walkowiak, M. Klinkowski, and J. Rak, "Protection in elastic optical networks," *IEEE Netw.*, vol. 29, no. 6, pp. 88–96, 2015.

[40] Y. Sone, A. Watanabe, W. Imajuku, Y. Tsukishima, B. Kozicki, H. Takara, and M. Jinno, "Bandwidth squeezed restoration in spectrum-sliced elastic optical path networks (SLICE)," *J. Opt. Commun. Netw.*, vol. 3, no. 3, pp. 223–233, 2011.

[41] K. Walkowiak and M. Klinkowski, "Shared backup path protection in elastic optical networks: Modeling and optimization," in *2013 Intl. Conf. on the Des. Reliable Commun. Netw. (DRCN)*. IEEE, 2013, pp. 187–194.

[42] G. Shen, Y. Wei, and S. K. Bose, "Optimal design for shared backup path protected elastic optical networks under single-link failure," *J. Opt. Commun. Netw.*, vol. 6, no. 7, pp. 649–659, 2014.

[43] C. Wang, G. Shen, and S. K. Bose, "Distance adaptive dynamic routing and spectrum allocation in elastic optical networks with shared backup path protection," *J. Lightw. Technol.*, vol. 33, no. 14, pp. 2955–2964, 2015.

[44] M. Jinno, H. Takara, B. Kozicki, Y. Tsukishima, Y. Sone, and S. Matsuoka, "Spectrum-efficient and scalable elastic optical path network: architecture, benefits, and enabling technologies," *IEEE Commun. Mag.*, vol. 47, no. 11, pp. 66–73, 2009.

[45] S. K. Singh, T. Das, and A. Jukan, "A survey on internet multipath routing and provisioning," *IEEE Commun. Surveys Tuts.*, vol. 17, no. 4, pp. 2157–2175, 2015.

[46] A. H. Al Muktadir and E. Oki, "Differential delay aware instantaneous recovery scheme with traffic splitting," *Intl. J. Commun. Sys.*, vol. 30, no. 5, p. e3075, 2017.

[47] S. Huang, C. U. Martel, and B. Mukherjee, "Survivable multipath provisioning with differential delay constraint in telecom mesh networks," *IEEE/ACM Trans. Netw.*, vol. 19, no. 3, pp. 657–669, 2010.

[48] K. Takenaga, Y. Arakawa, S. Tanigawa, N. Guan, S. Matsuo, K. Saitoh, and M. Koshiba, "Reduction of crosstalk by trench-assisted multi-core fiber," in *Opt. Fiber Commun. Conf.* OSA, 2011, p. OWJ4.

[49] J. Sakaguchi, W. Klaus, B. J. Puttnam, J. M. D. Mendinueta, Y. Awaji, N. Wada, Y. Tsuchida, K. Maeda, M. Tadakuma, K. Imamura *et al.*, "19-core MCF transmission system using EDFA with shared core pumping coupled via free-space optics," *Opt. Exp.*, vol. 22, no. 1, pp. 90–95, 2014.

[50] S. Fujii, Y. Hirota, H. Tode, and K. Murakami, "On-demand spectrum and core allocation for multi-core fibers in elastic optical network," in *Opt. Fiber Commun. Conf.* OSA, 2013, pp. 1–3.

[51] H. Tode and Y. Hirota, "Routing, spectrum and core assignment for space division multiplexing elastic optical networks," in *2014 Int. Telecommun. Netw. Strategy Planning Symp. (Netw.)*. IEEE, 2014, pp. 1–7.

[52] G. Savva, G. Ellinas, B. Shariati, and I. Tomkos, "Physical layer-aware routing, spectrum, and core allocation in spectrally-spatially flexible optical networks with multicore fibers," in *2018 IEEE Int. Conf. Commun. (ICC)*. IEEE, 2018, pp. 1–6.

[53] K. Walkowiak, M. Klinkowski, and P. Lechowicz, "Dynamic routing in spectrally spatially flexible optical networks with back-to-back regeneration," *J. Opt. Commun. Netw.*, vol. 10, no. 5, pp. 523–534, 2018.

[54] P. Johannisson and E. Agrell, "Modeling of nonlinear signal distortion in fiber-optic networks," *J. Lightw. Technol.*, vol. 32, no. 23, pp. 4544–4552, 2014.

[55] A. Carena, V. Curri, G. Bosco, P. Poggiolini, and F. Forghieri, "Modeling of the impact of nonlinear propagation effects in uncompensated optical coherent transmission links," *J. Lightw. Technol.*, vol. 30, no. 10, pp. 1524–1539, 2012.

[56] A. A. Beyragh, A. G. Rahbar, S.-M. H. Ghazvini, and M. Nickray, "IF-RSCA: intelligent fragmentation-aware method for routing, spectrum and core assignment in space division multiplexing elastic optical networks (SDM-EON)," *Opt. Fiber Technol.*, vol. 50, pp. 284–301, 2019.

[57] S. Trindade and N. L. da Fonseca, "Core and spectrum allocation for avoidance of spectrum fragmentation in EON-SDM," in *2020 IEEE Int. Conf. Commun. (ICC)*. IEEE, 2020, pp. 1–6.

[58] J. Comellas, J. Perelló, J. Solé-Pareta, and G. Junyent, "Spatial partitioning for proactive spectrum fragmentation avoidance in flex-grid/SDM dynamic optical core networks," *Photon. Netw. Commun.*, vol. 40, no. 2, pp. 59–67, 2020.

[59] Q. Yao, H. Yang, B. Bao, A. Yu, J. Zhang, and M. Cheriet, "Core and spectrum allocation based on association rules mining in spectrally and

spatially elastic optical networks," *IEEE Trans. Commun.*, vol. 69, no. 8, pp. 5299–5311, 2021.

[60] B. Shariati, A. Mastropaolo, N.-P. Diamantopoulos, J. M. Rivas-Moscoso, D. Klonidis, and I. Tomkos, "Physical-layer-aware performance evaluation of SDM networks based on SMF bundles, MCFs, and FMFs," *J. Opt. Commun. Netw.*, vol. 10, no. 9, pp. 712–722, 2018.

[61] A. Bocoi, M. Schuster, F. Rambach, M. Kiese, C.-A. Bunge, and B. Spinnler, "Reach-dependent capacity in optical networks enabled by OFDM," in *2009 Conf. Opt. Fiber Commun. (OFC)*. IEEE, 2009, pp. 1–3.

[62] R. Bhandari, "Optimal physical diversity algorithms and survivable networks," in *Second IEEE Symp. Comp. Commun.* IEEE, 1997, pp. 433–441.

[63] M. Liu, M. Tornatore, and B. Mukherjee, "New strategies for connection protection in mixed-line-rate optical WDM networks," *J. Opt. Commun. Netw.*, vol. 3, no. 9, pp. 641–650, 2011.

[64] X. Chen, F. Ji, and Z. Zhu, "Service availability oriented p-cycle protection design in elastic optical networks," *J. Opt. Commun. Netw.*, vol. 6, no. 10, pp. 901–910, 2014.

[65] "IBM ILOG CPLEX Optimization Studio," https://www.ibm.com/products/ilog-cplex-optimization-studio, (Accessed: 11-Oct.-2023).

[66] P. Rajalakshmi and A. Jhunjhunwala, "Routing wavelength and timeslot reassignment algorithms for TDM based optical WDM networks-multi rate traffic demands," in *2006 IEEE Intl. Conf. Netw.*, vol. 2. IEEE, 2006, pp. 1–6.

[67] V. López, L. Velasco *et al.*, "Elastic optical networks," *Arch. Technol. Control, Switzerland: Springer Int. Publishing*, 2016.

[68] C. Pavan, R. M. Morais, J. R. F. da Rocha, and A. N. Pinto, "Generating realistic optical transport network topologies," *J. Opt. Commun. Netw.*, vol. 2, no. 1, pp. 80–90, 2010.

[69] T. Hayashi, T. Sasaki, and E. Sasaoka, "Behavior of inter-core crosstalk as a noise and its effect on Q-factor in multi-core fiber," *IEICE Trans. Commun.*, vol. 97, no. 5, pp. 936–944, 2014.

[70] I. Chlamtac, A. Ganz, and G. Karmi, "Lightpath communications: An approach to high bandwidth optical WAN's," *IEEE Trans. Commun.*, vol. 40, no. 7, pp. 1171–1182, 1992.

[71] Y. Sheng, Y. Zhang, H. Guo, S. K. Bose, and G. Shen, "Benefits of unidirectional design based on decoupled transmitters and receivers in tackling traffic asymmetry for elastic optical networks," *J. Lightw. Technol.*, vol. 10, no. 8, pp. C1–C14, 2018.

[72] J. Y. Yen, "Finding the k shortest loopless paths in a network," *management Science*, vol. 17, no. 11, pp. 712–716, 1971.

[73] E. E. Moghaddam, H. Beyranvand, and J. A. Salehi, "Crosstalk-aware resource allocation in survivable space-division-multiplexed elastic optical networks supporting hybrid dedicated and shared path protection," *J. Lightw. Technol.*, vol. 38, no. 6, pp. 1095–1102, 2019.

Publication List

Journal Papers

1. K. Takeda, T. Sato, R. Shinkuma, and E. Oki, "Multipath Provisioning Scheme for Fault Tolerance to Minimize Required Spectrum Resources in Elastic Optical Networks," Elsevier Computer Networks, vol. 188, p. 107895, 2021.

2. K. Takeda, T. Sato, B. C. Chatterjee, and E. Oki, "Joint Inter-Core Crosstalk- and Intra-Core Impairment-Aware Lightpath Provisioning Model in Space-Division Multiplexing Elastic Optical Networks," IEEE Transactions on Network and Service Management, vol. 19, no. 4, pp. 4323–4337, 2022.

3. K. Takeda, T. Sato, B. C. Chatterjee, and E. Oki, "Lightpath Provisioning Model Considering Crosstalk-Derived Fragmentation in Spectrally-Spatially Elastic Optical Networks," Elsevier Computer Networks, vol. 237, p. 110099, 2023.

International Conference Papers

1. K. Takeda, T. Sato, R. Shinkuma, and E. Oki, "Fault-tolerant multipath provisioning in elastic optical networks," in 2019 OptoElectronics and Communications Conference (OECC) and 2019 International Conference on Photonics in Switching and Computing (PSC), 2019, pp. 1–3.

2. K. Takeda, T. Sato, B. C. Chatterjee, and E. Oki, "Jointly inter-core XT and impairment aware lightpath provisioning in elastic optical networks,"

in 2021 IEEE International Conference on Communications (ICC), IEEE, 2021, pp. 1–6.

3. K. Takeda, T. Sato, B. C. Chatterjee, and E. Oki, "Crosstalk-derived fragmentation-aware lightpath provisioning model in spectrally-spatially elastic optical networks," in 2023 OptoElectronics and Communications Conference (OECC), 2023, pp. 1–6.

Technical Reports and Local Conference Papers

1. K. Takeda, T. Sato, R. Shinkuma, and E. Oki, "エラスティック光ネットワークにおける使用スペクトル資源を最小化する耐故障マルチパス設定方式," IEICE Technical Report, vol. 118, no. 505, PN2018-96, pp. 77–83, March 2019.

2. K. Takeda, T. Sato, R. Shinkuma, and E. Oki, "エラスティック光ネットワークにおけるマルチパス設定のための経路およびスペクトルスロット割り当てモデルの性能評価," IEICE Technical Report, vol. 119, no. 402, PN2019-50, pp. 97–102, January 2020.

3. 竹田 健太, 佐藤 丈博, 新熊 亮一, 大木 英司, "エラスティック光ネットワークにおけるマルチパス設定のための経路最適化効果の検証," IEICE 関西支部第 25 回学生会研究発表講演会, A3-2, March 2020.

4. K. Takeda, T. Sato, R. Shinkuma, and E. Oki, "Multipath Provisioning Scheme to Minimize Required Spectrum Resources in Elastic Optical Networks," International Symposium on Creation of Advanced Photonic and Electronic Devices 2020, March 2020.

5. 竹田 健太, 佐藤 丈博, B. C. Chatterjee, 大木 英司, "空間分割多重型エラスティック光ネットワークにおけるコア間クロストークとコア内信号劣化を同時に考慮した資源割り当てモデル," IEICE Technical Report, vol. 120, no. 388, PN2020-62, pp. 116-122, March 2021.

6. K. Takeda, T. Sato, B. C. Chatterjee, and E. Oki, "Performance of Lightpath Provisioning Model in Space-division Multiplexing-based Elastic

Optical Networks," International Symposium on Creation of Advanced Photonic and Electronic Devices 2021, March 2021.

7. 竹田 健太, 佐藤 丈博, B. C. Chatterjee, 大木 英司, "エラスティック光ネットワークにおけるコア間クロストークとコア内信号劣化を考慮した光パス設定モデルの性能評価", IEICE Technical Report, vol. 121, no. 350, PN2021-37, pp. 23-30, January 2022.

8. K. Takeda, T. Sato, B. C. Chatterjee, and E. Oki, "Crosstalk-Aware Lightpath Provisioning in Elastic Optical Networks," International Symposium on Creation of Advanced Photonic and Electronic Devices 2022, March 2022.

9. K. Takeda, T. Sato, B. C. Chatterjee, and E. Oki, "Performance of Crosstalk-Aware Lightpath Provisioning Model in Elastic Optical Networks," International Symposium on Creation of Advanced Photonic and Electronic Devices 2023, March 2023.

Awards

1. IEICE 関西支部第 25 回学生会研究発表講演会 支部長賞 奨励賞, March 2020.

2. IEEE ComSoc Student Grant at 2021 IEEE International Conference on Communications (ICC), June 2021.

3. 第 19 回 IEEE 関西支部学生研究奨励賞, March 2023.